Construction and commissioning of a novel dual fluidised bed reactor for biomass fast pyrolysis

Jonathan Reynders

CVD 800

2022-02-11

Construction and Commissioning of a Novel Dual Fluidised Bed Reactor for Biomass Fast Pyrolysis

by

Jonathan Reynders

A dissertation submitted in partial fulfilment
of the requirements for the degree

Masters in Engineering (Chemical Engineering)

in the

Faculty of Engineering, the Built Environment and Information Technology

University of Pretoria
Pretoria

2022-02-11

Construction and Commissioning of a Novel Dual Fluidised Bed Reactor for Biomass Fast Pyrolysis

Synopsis

The CRIPS 2 dual fluidised bed pyrolysis unit at the University of Pretoria was successfully constructed and subsequently commissioned through eight experimental runs. The scope of the investigation involved determining the mass and energy balances around the unit, the thermal efficiency during operation, and the pyrolysis capabilities.

The lignocellulosic biomass chosen for the experimental runs was *Eucalyptus grandis* wood chips with an average diameter of 448 to 489 µm. The products generated from the pyrolysis of lignocellulosic biomass are bio-oil, biochar, and non-condensable gases (NCG). The optimal experimental run involved the highest feed rate of biomass (5 kg/h) with a reduced NCG recycle flow-rate (140 l/ min) to produce a bio-oil with an HHV of 7.29 MJ/kg. The lower HHV and higher water content in the bio-oil was caused by oxygen transfer between the combustion bed and the pyrolysis unit. Nevertheless, the unit is very capable of processing higher biomass throughputs than the previous generation CRIPS unit. Residues found in the condensation unit and the bio-oil collection container were found to have an HHV of 22.11 MJ/kg, therefore confirming the pyrolysis potential of the unit. The biochar produced from the optimal run conditions had an HHV of 26.54 MJ/kg which can find a use in various heating applications. The BET surface area results for the collected biochar were very low. However, the wood feedstock was oversized to allow it to remain in the unit to produce additional combustion energy. As a result, the surface areas are not representative of the total biochar produced.

Mass balances were performed with an error of under one percent and confirmed that pyrolysis was taking place. However, energy balances indicated that 35 % of the heat was unaccounted for. This discrepancy was discovered due to thermal soaking of the unit, whereby the large thermal mass was still consuming the heat during operations and was not at a thermal-steady state. Nevertheless, analysis of the thermal conservation abilities could still be calculated, indicating that the operation of the unit was very close to its design values. The insulation and integrated combustion unit reduced the radial heat losses by 82 % during the experimental runs and by 40 % (theoretical) at full design capacity compared to the CRIPS 1 unit. The integrated APH (air preheater) also reduced the LPG flow rate requirements by 49 % and operated very close to the design values.

The recommendations for future work include various operational changes and unit modifications:

- Reduce the oxygen transfer through operation and unit modifications.
- Change the biomass screw conveyor delivery arrangement.
- Add cyclones in series for better biochar recovery.
- Increase the cyclone capacity.
- Add pilot burner and flame detection unit.
- Add a separate distribution manifold for recycled NCG.
- Provide additional insulation for the top of the unit.

Keywords: fast pyrolysis, dual fluidised bed, commissioning, performance analysis

Acknowledgements

I would like to thank Professor Mike Heydenrych for his guidance, patience and continued support, especially during lockdown due to the coronavirus pandemic. Thank you for always being available to listen and to help wherever you could. Your kindness and care have not gone unnoticed!

Thanks are due to Paul Sonnendecker and Peet Kruger for all their advice and continuous assistance in the workshop required to get the unit up and running. Thanks also to Gerrie Claassen and Isbe van der Westhuizen for their unstinting help in the laboratories and in organising pretty much anything.

Thank you Dr Ryan Merkel for your unwavering support, and encouragement and for introducing me to Korean cuisine.

Thanks are due to Bruce Sithole from the CSIR, his assistance in sample analysis is very much appreciated.

Thank you Yun-Wen Wu for always lending a helping hand throughout the implementation of the unit and for being an incredible friend.

I would also like to thank my friends and my family for their constant encouragement and moral support when times got tough. Finally, I would like to thank God for blessing me with this opportunity and for guiding me through the years.

Contents

List of Figures

List of Tables

Glossary of Abbreviations

APH	Air preheater
ASTM	American Society for Testing and Materials
CRIPS	Combustion reduction integrated pyrolysis system
CU	Combustion unit
d.b.	Dry basis
FCC	Fluid catalytic cracking
GHG	Greenhouse gases
HHV	Higher heating value
LDH	Layered double hydroxides
LPG	Liquefied petroleum gas
NCG	Non-condensable gases
P&ID	Process and instrumentation diagram
PD	Positive displacement
PFD	Process flow diagram
PU	Pyrolysis unit
SCADA	Supervisory control and data acquisition
SGV	Superficial gas velocity
TGA	Thermogravimetric analysis
VFD	Variable frequency drive

Nomenclature

β	Coefficient of volume expansion	1/K
ΔT	Temperature difference	K
ΔT_{LM}	Log mean temperature difference	K
$\dot{E}$	Energy flow	kW
$\dot{m}_{\text{in}}$	Mass flow rate in	kg/h
$\dot{m}_{\text{out}}$	Mass flow rate out	kg/h
$\dot{Q}_{\text{rad}}$	Heat transfer due to radiation	kW
ϵ	Bed voidage	-
ϵ_{rad}	Thermal radiation emissivity	-
λ	Latent heat of evapouration	kJ/kg
HHV_i	Higher heating value of component i	MJ/kg
μ	Viscosity	Pas
ν	Kinematic viscosity	m^2/s
ρ_f	Density of the fluid	kg/m^3
ρ_p	Density of the solid	kg/m^3
ρ_s	Density of the particle	kg/m^3
σ	Stefan-Boltzmann constant	$\text{W}/(\text{m}^2\text{k}^4)$
A_s	Surface area	m^2
Ar	Archimedes number	-
c_p	Heat capacity	kJ/(kgK)
$c_{p_{i_x}}$	Heat capacity of component i with x denoting in/out	kJ/(kgK)
$E_{i_{\text{in}}}$	Internal energy in of component i	kW
$E_{i_{\text{out}}}$	Internal energy out of component i	kW
g	Gravitational acceleration	m/s^2

h	Convection coefficient	$W/(m^2K)$
k_x	Thermal conductivity with specifiers denoted by x	W/(mK)
L	Length	m
L_c	Characteristic length	m
m	Mass	kg
Nu	Nusselt number	-
Pr	Prandtl number	-
Q_{loss}	Heat lost to environment	kW
Q_{rxn}	Heat generated by chemical reaction	kW
R	Thermal resistance with specifiers denoted by the subscript	K/W
r_x	Radius with x denoting the location	m
$R_{\text{Ins.}}$	Thermal resistance of the insulation	K/W
$R_{\text{Refr.}}$	Thermal resistance of the refractory	K/W
Ra_L	Rayleigh number	-
Re_{mf}	Reynolds number at minimum fluidisation	-
T	Temperature	°C or K
t	Time	s
T_s	Surface temperature	°C or K
T_∞	Temperature of surroundings sufficiently far away	°C or K
T_{ref}	Reference temperature	°C or K
T_{i_x}	Temperature of component i with x denoting in/out	°C or K
u_{mf}	Velocity of minimum fluidisation	m/s
W	Work	kW
x_p	Harmonic mean particle diameter	m
x_{sv}	Sauter mean diameter/Surface diameter	m
x_i	Mass fraction of component i	kg_i/kg

1 Introduction

1.1 Background

Fossil fuels have become synonymous with the chemical engineering industry. The implementation of cleverly engineered operating unit has created one of the biggest and longest-lasting sectors in the world. Unfortunately, the world's resources are scarce and our impact on the earth are becoming alarmingly more apparent. The engineering sectors are turning their gaze towards more environmentally friendly operations and sustainable feedstocks to fuel the resource-consuming world that we live in.

First-generation biofuels such as biodiesel have made a remarkable impact on the world's view of sustainable resources, but biofuels generally depend on the resources currently used by the food industry. The infringement on agriculture is also a difficult issue as it affects the supply and demand for crops, which in turn causes issues with food security. Thus second-generation biofuels have arisen in order to alleviate the pressures on other industries with lignocellulosic biomass as the feedstock of choice. Agricultural, silvicultural, municipal and industrial wastes in the form of lignocellulosic biomass can find their place as a viable feed for the second-generation biofuels.

One of the most frequently studied second-generation biofuel production techniques is pyrolysis. In this method biomass is heated very rapidly to form pyrolysis products in the absence of oxygen. These products consist of liquid, solid, and gaseous phases namely bio-oil, biochar, and non-condensable gases (NCG). Research has been done in various pyrolysis projects at the University of Pretoria, focusing on reactor designs and commissioning. The project discussed here focuses on the construction and commissioning of the CRIPS 2 (Combustion and Reduction Integrated Pyrolysis System 2) unit with additional analysis and determination plant performance.

1.2 Problem statement

Renewable resources are showing promise in the world of chemicals and biofuels with new unit operations at the forefront of research. The novel second-generation pyrolysis unit, designed and fabricated by de la Rey (2015), requires construction, commissioning and validation. The performance of the unit needs to be evaluated against the design values to fully realise its use in a scaled-up operation.

1.3 Method

1.3.1 Commissioning

The commissioning of the CRIPS 2 unit is not currently standardised, therefore one of the goals of the project was to standardise the commissioning procedures.

1.3.2 Performance analysis

The performance of the CRIPS 2 unit was determined with the use of mass and energy balances. All solid and liquid products were weighed following the trials and used in conjunction with the analytical results to close the loop of the mass balances. The energy balances consisted of accurate heat transfer calculations and literature data for the components entering and exiting the system. The values from the mass and energy balance were compared to those of the previous iterations of the CRIPS research.

1.3.3 Sample analysis

Sample analysis was carried out using well known methods in literature and standards such as ASTM. This ensured that the results would be reproducible and accurate.

1.4 Deliverables

The deliverables for this project are the following:

- Construction of a dual fluidised bed reactor for biomass fast pyrolysis.
- Achievement of the safe and reliable operation of the pilot plant.
- Optimised parameters for the start up and running of the system (stable control).
- Analysis of the feedstock and its products generated from the pilot plant.
- Energy and mass balances to validate the effectiveness of the CRIPS 2 design.

1.5 Report structure

This thesis is split up into the following six sections:

1. **Introduction:** This section outlines the project and the goals it attempted to achieve.
2. **Literature review:** Background research on the subject of biomass and its role in second-generation biofuels with the emphasis on pyrolysis.
3. **Combustion Reduction Integrated Pyrolysis System:** The novel pyrolysis unit used for the pyrolysis of biomass is described.
4. **Process operation and experimental work:** This section discusses the methods and calculations undertaken to achieve accurate and consistent results.
5. **Results and discussion:** The results of the commissioning, experimental, and analytical work are summarised in this section.
6. **Conclusions and recommendation:** This section gives a summary of the entire project with a list of recommendations for future work on the CRIPS 2 unit.

2 Literature review

2.1 Biorefineries

Humans have been refining many things in their surroundings since time immemorial, from languages, to art, to war, to food, to water and fuels. Our desire for improvement is insatiable, even if it leaves damage in its wake. In the chemicals, energy, and fuel industries, the biggest players are the petrochemical refineries. They take hydrocarbons in their many forms and converted them into incredibly pure products that power our vehicles, surface our roads, and even keep our groceries fresher for longer. Unfortunately, as the feedstock for the petrochemical industry is non-renewable, the carbon dioxide sent to the atmosphere through processing and combustion of petrochemical products outweighs the uptake ability of organisms that perform photosynthesis. It has been scientifically proven that the increase in greenhouse gases (GHG) is due to human activity. Furthermore, over the past ten years, the transport sector's rates of GHG emissions have grown more than those of any other sector thanks to of fossil fuel production (Cherubini, 2010). Petrochemical refineries have given us incredible technologies, but now it's time to shift our focus to a sustainable type of refinery – the biorefinery.

Biorefineries, like their petrochemical counterparts, select a feedstock and upgrade its value using various chemical and physical processes. The main difference is that biorefineries use biomass as a feedstock with the aim of processing it sustainably. The IEA Bioenergy Task 42 group have defined the term biorefinery as "the sustainable processing of biomass into a spectrum of marketable products and energy" (A Pandey *et al*, 2015). Not only does this concept affect how we look at chemical plants, but also how we look at industries such as forestry and farming. Figure 1 illustrates the opportunities that the biorefinery concept provides.

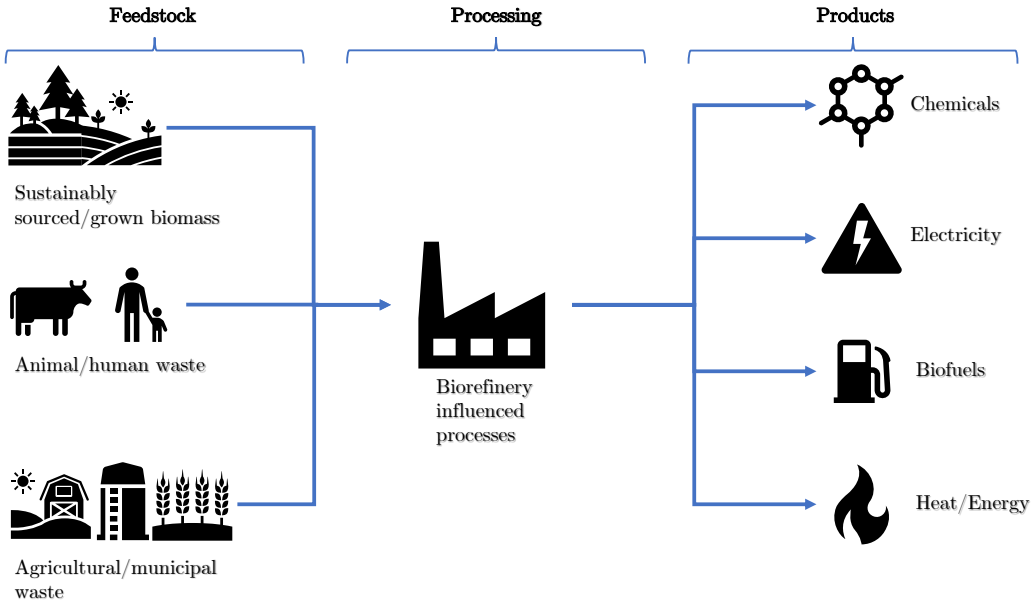

Figure 1: The biorefinery concept

Fuel is the most important product as up to 87 % of a barrel of crude oil will be refined into fuel (EIA, 2018). The consumption of crude oil is predicted to increase by around 38 % over the next ten years (Cherubini, 2010). Therefore, the biorefinery's main focus is on biofuels as it is imperative to switch over to more sustainable fuels. Biofuels are separated into two categories, namely first and second-generation biofuels. First-generation biofuels consist of bioethanol and biodiesel from the agricultural sector, while second-generation biofuels are generated from non-food feedstocks. Unfortunately, as the production of first-generation biofuels can compete with food production, the focus has shifted to feedstocks that do not encroach on our food security (Dhyani & Bhaskar, 2018). Production of second-generation biofuels only accounts for 0.2 % of the total output of the biofuel industry which goes to show how young the industry is (Gollakota, Kishore & Gu, 2018). Processes such as pyrolysis, hydrothermal liquefaction, and gasification to name a few have emerged as thermochemical routes competing with the petroleum industry. Furthermore, processes such as fast pyrolysis aimed at the production of liquid fuels have only gained attention in the past 30 years (Bridgwater, 2012). Compared to the 160 years of research that the petroleum industry has invested into their products, pyrolysis is still in its infancy.

2.2 Biomass feedstock

2.2.1 Background

The limited reserves of petroleum and the overwhelming evidence that global warming is a threat to the survival of the planet has forced society to think differently about how it looks at fuels, energy, and chemicals. Carbon dioxide (CO_2) emissions have increased by around 50 % in the past 30 years, which has worsened due to the lack of carbon sequestration from non-renewable resources (United Nations, 2020). This has lead to the use of biomass as a replacement for petroleum-based products. The key advantage of using biomass is that the CO_2 produced in the processing or combustion of the product is re-absorbed by living biomass, i.e. photosynthesis, which mitigates the large CO_2 emissions that we are experiencing today (Gupta & Demirbas, 2010). Carbon sequestration due to the use of biomass as a feedstock is illustrated in Figure 2

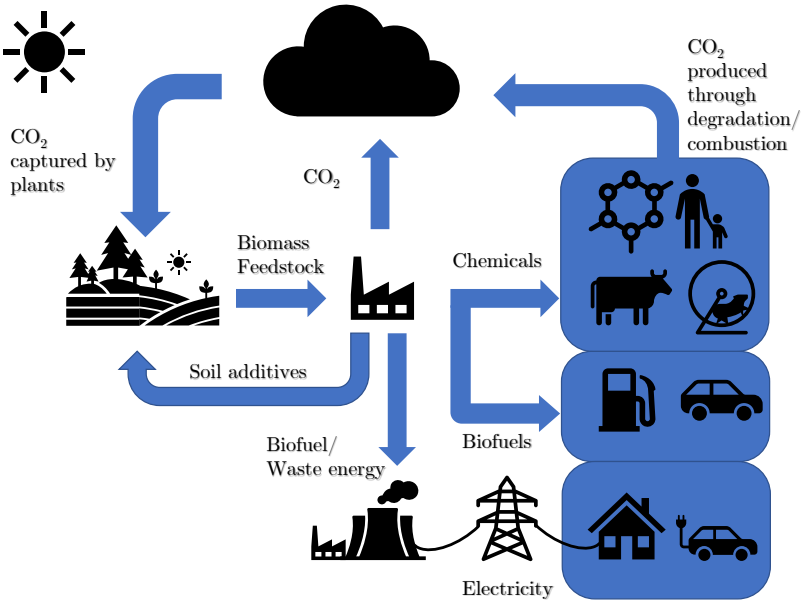

Figure 2: The carbon cycle in the biorefinery concept

The typical feedstocks for a petroleum refinery seem very discrete with gas, liquid, and solid resources entering in the form of natural gas, crude oil, and coal respectively. However, in reality, they form more of a spectrum with differing chemical makeups and properties. The same approach can be used for biomass feedstocks. J Singh & Trivedi (2018) summarise the sources of biomass feedstocks as agricultural, forest, industrial waste, urban wastes, and aquatic plants. These categories can be subdivided into more distinct

sources such as the petroleum industry. Each source has its own advantages and disadvantages. The accumulation of viable feedstocks and processes will allow sustainable synthesis of carbon-based products in the emerging biorefinery sector. This thesis focuses on the use of lignocellulosic biomass as a sustainable source of carbon.

Lignocellulosic biomass consists of varying combinations of three components: cellulose, hemicellulose, and lignin. Cellulose is a fibrous polysaccharide consisting of glucose chains that provide mechanical strength to the plant due to its crystalline structure. Hemicellulose is a much simpler polymer as it is amorphous and shorter in length. It forms a mesh around the cellulose to secure the fibres to the lignin – one can think of it as a mat that surrounds the cellulose fibres with the lignin as the binder. Finally, the lignin is the "glue" that binds everything together through large networks of aromatic compounds (Dhyani & Bhaskar, 2018). Figure 3 shows the molecular structure of these compounds and their location in lignocellulosic biomass.

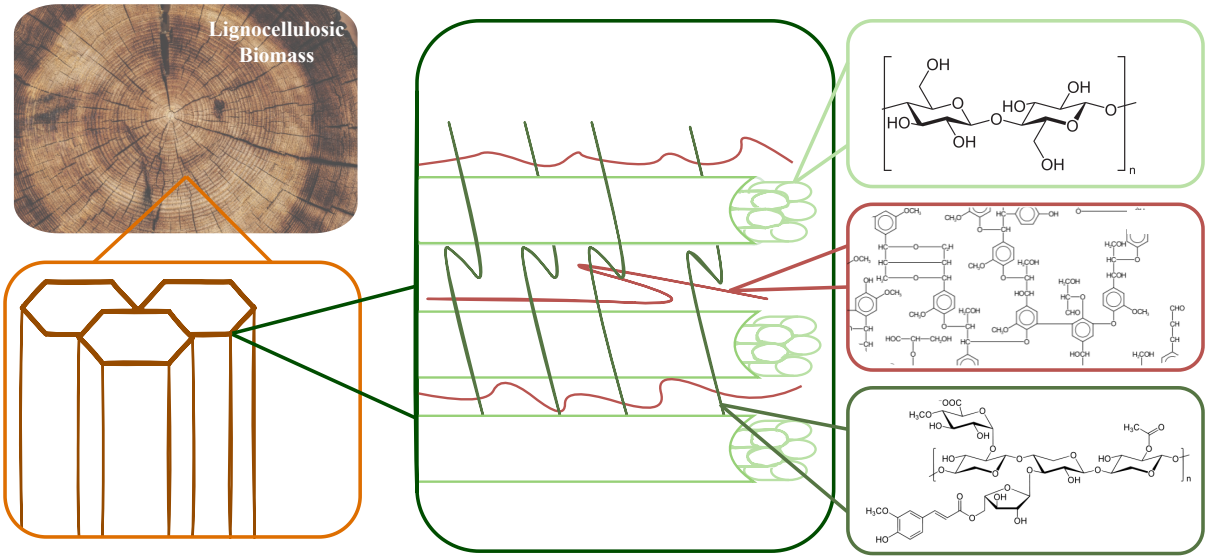

Figure 3: An illustration of the chemical makeup of lignocellulosic biomass (based off the illustration by Alonso, Wettstein & Dumesic (2012))

2.2.2 Woody biomass

Lignocellulosic biomass in the form of wood and forestry residues shows great promise in the bio-energy sector as plantations are typically distant from urban areas on land that would not be used for anything else. Forestry plantations rely on the climate and rainfall of the environs to maintain growth without the need for fertilisers. Trees are not resource-intensive yet their slow growth rate requires extensive planning if fully implemented in the biorefinery sectors. A study by Perlack *et al* (2005) was conducted on the viability of using agricultural and forestry residues as sources for fuel in the US. The study found that

1.3×10^9 t of biomass residues could supplement 30 % of the fuel used in the transport sector. Another study by Beringer, Lucht & Schaphoff (2011) found that 15 to 25 % of the global energy demand could be supplemented by 2050 by the use of biomass. Through sustainable farming and care, trees will not only be producing the air we breathe, but will supplement our energy and chemical sectors.

Like all other biological organisms, trees are composed of very complex structures and compounds. Understanding the nature of such a feedstock will allow one to design better-engineered processes in terms of chemistry and mechanical properties. Woody biomass can be split up into two main categories, but in reality, the diversity of the constituents is more of a spectrum than a binary one. Trees are considered as either softwood or hardwood. The main constituents of wood are cellulose, hemicellulose, lignin, and small quantities of extractives. The amounts of these constituents vary between soft and hardwoods as shown in Table 1. Note that arabinoglucuronoxylans and galactoglucomannans are the hemicellulose components in softwoods and glucuronoxylans and glucomannans are the hemicellulose components in hardwoods. The higher lignin content in softwoods (as noted in Table 1) could assist in the recovery of larger quantities of aromatic compounds which are sought after in the chemicals industry.

Table 1: Mass percentages of the main components in wood (on a dry basis) (Ek, Gellerstedt & Henriksson, 2009)

Component	Softwood (wt%)	Hardwood (wt%)
Cellulose	37 – 43	39 – 45
Hemicellulose	20 – 30	17 – 35
Lignin	25 – 33	20 – 25
Extractives	2 – 5	2 – 4

The characteristic data of various woody feedstocks waere compiled and summarised in Table 2. The HHV (higher heating value) is included in the analysis as it indicates the energy quality of a substance and is a good benchmark for fuel quality analysis. The standard deviation of the moisture and ash data is relatively high indicating that woody biomass is quite inconsistent with its physical characteristics (proximate analysis). However, the elemental analysis (ultimate analysis) is very consistent which is good for a process as it allows some margin in feedstock variation.

Table 2: Fibre, proximate, and ultimate analysis of woody biomass (based on data from Dhyani & Bhaskar (2018))

Property	Mean value
Fibre Analysis	
Cellulose (wt%)	40.84 ± 9.73
Hemicellulose (wt%)	28.61 ± 9.37
Lignin (wt%)	25.48 ± 5.16
Proximate analysis	
Moisture (wt%)	7.46 ± 3.02
Volatiles (wt%)	78.54 ± 7.03
Fixed Carbon (wt%)	19.07 ± 7.45
Ash (wt%)	1.19 ± 0.90
Ultimate analysis	
Carbon (wt%)	48.20 ± 2.30
Hydrogen (wt%)	5.92 ± 0.29
Oxygen (wt%)	44.50 ± 2.50
Nitrogen (wt%)	0.27 ± 0.15
Sulphur (wt%)	1.58 ± 1.21
Energy content	
HHV (MJ/kg)	18.51 ± 1.65

2.2.3 Agricultural residues

Excess biomass in the agricultural sector is commonplace and processing the excess will assist in waste management. Biochar production has shown promise in the agricultural sector as it can be added to fertiliser to aid in soil remediation. Zanzi, Sjöström & Björnbom (1996) investigated the yields of biochar from various feedstocks and found that straw would be more appropriate for char production than woody biomass. This is a remarkable discovery as the use of agricultural waste as a method of soil remediation will help to sustain our ever-growing food requirements. Several issues arise with the use of agricultural residues as a feedstock source. Firstly, transporting biomass from several farms to a central processing plant is not feasible as the bulk density of residues is very low and the variation of the feedstocks would be an issue. Secondly, supply would be controlled by the agricultural sector and this could lead to issues in terms of politics and consistent sourcing (Hood, Nelson & Powell, 2011). A way to resolve this concern is the use of smaller units at the source of the feedstock, which would allow farmers to control

their char production. Additionally, as the crude pyrolysis oil is already synthesised at the source, it could be transported more easily to a processing facility in another location.

The analysis of various agricultural residues is summarised in Table 3. The variation in the chemical and physical characteristics of these residues is much higher than that of woody biomass, which could become a problem when processing a combination of various feedstocks.

Table 3: Fibre, proximate, and ultimate analysis of agricultural residues (based on data from Dhyani & Bhaskar (2018))

Property	Mean value (wt%)
Fibre Analysis	
Cellulose (wt%)	36.96 ± 14.32
Hemicellulose (wt%)	24.59 ± 7.84
Lignin (wt%)	24.05 ± 12.56
Proximate analysis (wt%)	
Moisture (wt%)	10.97 ± 11.48
Volatiles (wt%)	73.24 ± 16.01
Fixed Carbon (wt%)	15.78 ± 7.17
Ash (wt%)	6.43 ± 5.64
Ultimate analysis	
Carbon (wt%)	46.09 ± 4.98
Hydrogen (wt%)	5.90 ± 0.60
Oxygen (wt%)	41.90 ± 6.45
Nitrogen (wt%)	1.34 ± 1.59
Sulphur (wt%)	1.65 ± 2.89
Energy content	
HHV (MJ/kg)	17.29 ± 2.93

2.2.4 Energy crops

Another source of biomass could potentially be from energy crops. Unlike in the agricultural industry, they could be used solely for biofuel production without hindering food security. Grasses are of special interest as energy crops – they can be planted in soils with low nutrient levels while retaining high yields with little fertiliser utilisation as noted by Parrish & Fike (2005). The typical composition of grass feedstocks is shown in Table 4. Compared to woody feedstocks, the hemicellulose content of grasses is higher.

Table 4: Composition of grasses (Prasad, Singh & Joshi, 2007)

Component	Composition (%)
Cellulose	25 – 40
Hemicellulose	35 – 50
Lignin	10 – 30

Sorghum has also been investigated as an energy crop even though it has been used in the agricultural sector. However, its drought resistance and low nutrient requirements make it a suitable candidate for second-generation biofuels. Combining the bioethanol production of the sugar constituent and pyrolysis of the bagasse was investigated by Zhao *et al* (2009) and further progression of such a setup was regarded as promising.

The analysis of various energy crops is summarised in Table 5. The variation in the physical characteristics of the energy crops is similar to that of woody biomass however, the high ash content (4.76 %) can become a problem in thermochemical processing as noted in Section 2.5.1.

Table 5: Fibre, proximate, and ultimate analysis of energy crop biomass (based on data from Dhyani & Bhaskar (2018))

Property	Mean value (wt%)
Fibre Analysis	
Cellulose (wt%)	33.05 ± 9.28
Hemicellulose (wt%)	33.11 ± 8.10
Lignin (wt%)	17.83 ± 7.81
Proximate analysis	
Moisture (wt%)	5.89 ± 2.46
Volatiles (wt%)	78.00 ± 6.60
Fixed carbon (wt%)	14.96 ± 1.86
Ash (wt%)	4.76 ± 1.55
Ultimate analysis	
Carbon (wt%)	47.72 ± 3.41
Hydrogen (wt%)	6.03 ± 0.54
Oxygen (wt%)	40.66 ± 4.93
Nitrogen (wt%)	0.72 ± 0.48
Sulphur (wt%)	0.11 ± 0.10
Energy content	
HHV (MJ/kg)	19.06 ± 2.63

2.3 Biomass pretreatment

2.3.1 Background

Biomass feedstocks require varying degrees of pretreatment due to their chemical complexity and unpredictable qualities. Firstly, pretreating the biomass is crucial to ensure that a homogeneous feedstock enters the thermochemical processes, i.e. fast pyrolysis, with predictable characteristics. Secondly, the pretreatment of biomass can also ensure higher process efficiencies and better product qualities (Lødeng *et al*, 2013). In the production of biofuels, the pretreatment process contributes around 20 % of the cost of the entire process (Gandia, Arzamedi & Dieguez, 2013). Thus, it is vital to research all available pretreatment routes as their significance in the future of biorefineries could be just as important as the processing. Each process has its advantages and disadvantages concerning the type of feedstock, the desired bioprocessing routes, and energy/chemical costs (LK Singh & Chaudhary, 2017).

2.3.2 Physical pretreatment

Physical pretreatments of biomass are well-understood processes that assist in homogenising the feedstock before pyrolysis through densification and particle size reduction. Additionally, different biomass feedstocks can be combined to further homogenise large feed stockpiles and maintain a predictable pyrolysis product (Carpenter *et al*, 2014)

Lignocellulosic biomass has a very low heat transfer coefficient and pyrolysis mechanisms, especially fast pyrolysis, require sufficient heat transfer to crack long-chain hydrocarbons. Milling or grinding of the biomass before the processing will increase the heat transfer due to the smaller particle diameter leading to greater temperature uniformity inside the particle (Zou *et al*, 2010; Williams & Besler, 1996).

Shen *et al* (2009) tested the effects of particle size on bio-oil yields from oil mallee woody biomass pyrolysis. It was found that increasing the particle size from 0.3 to 1.5 mm decreased the yield of oil. However, increasing the particle size from 1.5 to 5.6 mm had very little effect on oil yields. This information is valuable for the operation of a pyrolysis plant as particle size reduction is costly and excessive milling and grinding could prove to be too expensive (Kan, Strezov & Evans, 2016).

Milling and grinding are very efficient ways to decrease the particle size of large quantities of feedstock. Unfortunately, the particles do require screening if the process requires a consistent particle size. Extrusion or pelletisation processes offer a solution to this concern

by homogenising the size and thus the energy density of the feed while removing moisture from the biomass (Kan *et al*, 2016).

2.3.3 Thermal pretreatment

Drying can serve an important role in the production of pyrolysis oils as it removes water from the biomass thus reducing water content in the fuel. The thermal treatment is characterised by three categories: non-reactive drying (50 to 100 °C), reactive drying (120 to 150 °C), and torrefaction (200 to 300 °C) (Carpenter *et al*, 2014).

Non-reactive drying removes water from the biomass through evaporation. This process causes shrinkage as water escapes the cells causing the porosity to decrease as well. At slightly elevated temperatures (120 – 150 °C) the lignin begins to soften and melt, which allows processes such as pelletisation to make use of softer, drier wood. Reactive drying produces CO_2, water, formic and acetic acid as intermolecular bonds begin to break down. A long enough exposure to reactive drying will see char formation (Carpenter *et al*, 2014).

Torrefaction is the highest level of drying possible before pyrolysis takes place. It removes water from the biomass and has shown to reduce oxygen content as well (Uslu, Faaij & Bergman, 2008). As it is a harsher process, around 30 % of the energy content is lost due to the volatilisation of biomass however, the energy density can be increased up to 40 %. The higher energy density makes it ideal for transport, storage, and feeding into the reactor. Storage is also improved through decreased hygroscopicity (Carpenter *et al*, 2014). The bio-oils produced have also shown lower acidity levels which aid in production storage (A Boateng & Mullen, 2013). Westover *et al* (2013) studied the effects of torrefaction pretreatment on the pyrolysis of southern pine. It was found that up to four times less energy was required to grind torrefied feed. However, the oil production dropped by up to 51 % at temperatures of 270 °C; similar findings were also published by A Boateng & Mullen (2013). Therefore the sacrifice of the production rate to obtain a purer product needs to be balanced by the cost, location, and scale requirements of specific applications.

All drying methods rely on heating and this heat can be provided by the pyrolysis process, which is also known as autothermal processing (Chai & Saffron, 2016; Isaksson, Åsblad & Berntsson, 2013). Chai & Saffron (2016) note that if the correct supply chains are set up, the combination of torrefaction, pelletisation, and pyrolysis will be profitable and thus a feasible alternative to fossil fuels.

2.4 Pyrolysis

Various methods are available to process biomass with the ultimate goal of increasing energy density. Whether this is for fuel, energy, chemicals, or a combination thereof, it is important to understand the advantages and disadvantages of the various processing routes. Pyrolysis is categorised as a thermochemical process in bioprocessing. Other processes include gasification, hydrothermal liquefaction, and torrefaction to name a few. However, the other processes are outside the scope of this dissertation and will therefore not be discussed.

2.4.1 Background

Pyrolysis is simply the process of heating a feedstock, in this case, lignocellulosic biomass, in the absence of oxygen. At temperatures ranging from 300 to 1000 °C, the biomass thermally decomposes and forms gaseous, liquid, and solid products through depolymerisation reactions (Dhyani & Bhaskar, 2018; Roy & Dias, 2017). The names of these products are not standardised but shall be referred to as non-condensable gases (NCG), bio-oils, and biochars respectively.

There are three categories for biomass pyrolysis which are characterised by the heating rates at which the feedstock is processed. These categories have been dubbed fast/flash, intermediate, and slow pyrolysis. The heating rates alter the yields of solid, liquid, and gaseous products. Furthermore, the particle sizes used in the reactors must be taken into consideration as the heating rate of the solid feedstock is inversely proportional to the particle size. The parameters that define the process such as the heating rates and temperatures at which the reactions take place are shown in Table 6.

Table 6: Typical parameters and characteristics of pyrolysis processes (Roy & Dias, 2017)

Process Type	Temperature Range (°C)	Heating Rate (°C/s)	Residence Time
Slow Pyrolysis	300 – 550	0.1 – 0.8	5 min – 35 h
Intermediate Pyrolysis	300 – 450	3 – 5	10 min
Fast/Flash Pyrolysis	300 – 1000	10 – 1000	<2 s

The product yields of the pyrolysis techniques are shown in Table 7.

Table 7: Typical product yields for pyrolysis processes (Roy & Dias, 2017)

Process Type	Biochar Yield (%)	Bio-oil Yield (%)	NCG Yield (%)
Slow Pyrolysis	25 – 35	20 – 50	20 – 50
Intermediate Pyrolysis	25 – 40	35 – 50	20 – 30
Fast/Flash Pyrolysis	10 – 25	60 – 75	10 – 30

2.4.2 Fast pyrolysis

Fast and flash pyrolysis methods are geared toward maximum liquid yields, whereas the slower pyrolysis yields are focused more on the production of biochar which is not ideal for the liquid fuel industry. The biochar produced from fast pyrolysis is predominantly carbon due to the hydrocarbons produced in the vapour phase (LK Singh & Chaudhary, 2017). Unlike the slower pyrolysis methods, fast pyrolysis requires very high heating rates, incredibly short residence times, and quick cooling to achieve high oil production rates. The residence time in the reactor must be minimised to reduce further cracking of the uncondensed pyrolysis oils. Furthermore, the hot vapour stream should be separated from the biochar to reduce cracking as the char has a high surface area which in turn catalyses such reactions. Finally, the vapours should be quenched to stop secondary reactions (Luque *et al*, 2016).

The reactor configurations for fast pyrolysis have been categorised as follows: screw/auger, ablative, rotating cone, bubbling fluidised bed, and circulating fluidised bed reactors Bridgwater, 2013. The fluidised bed reactor is the most well-understood reactor in fast pyrolysis research and it has also been proven to be the most successful reactor configuration (F Agblevor, Besler & Wiselogel, 1996). Furthermore, the scale-up of fluidised bed reactors is the easiest compared to the other fast pyrolysis processes (Kan *et al*, 2016). They come in two configurations: bubbling and circulating fluidised bed reactors. The general fluidised bed reactor uses a fluidised bed of sand and/or catalyst to transfer heat into the feedstock through conduction. The addition of catalysts in the bed will also assist in speeding up reactions – ideally the desired reactions. Furthermore, incredibly high heating rates can be achieved in this process. The carbohydrates of the biomass are cracked and the vapours and gases produced are cooled to condense the oils.

In the case of bubbling fluidised bed (BFB) reactors, the sand remains in the pyrolysis zone while biochar and vapours are transported out of the unit via the flow of inert gas. Before cooling, the char must be separated from the vapour and gas stream – cyclones are employed to effectively separate the solids from the uncondensed product stream (Dhyani & Bhaskar, 2018). Unfortunately, not all the vapours can be collected

efficiently and methods such as electrostatic precipitation can aid in collecting all the liquid product (Bridgwater, 2012). The circulating fluidised bed (CFB) reactor differs from BFB setups as the fluidising gas velocity is high enough to transport the biochar, vapours, and bed material out of the reactor. Two cyclones are employed to separate the solids from the vapour stream (as noted above). Following this, the bio-oils are condensed in the typical fashion. However, the bed material and biochar enter another unit where air is added to combust the biochar, in turn, heating up and decoking the bed material (Duong, Prasertcharoensuk & Phan, 2019). The drawback of the high gas velocities is the ineffective separation of biochar from the pyrolysis vapours leading to high solids content in the oil. A typical fluidised bed reactor is illustrated in Figure 4.

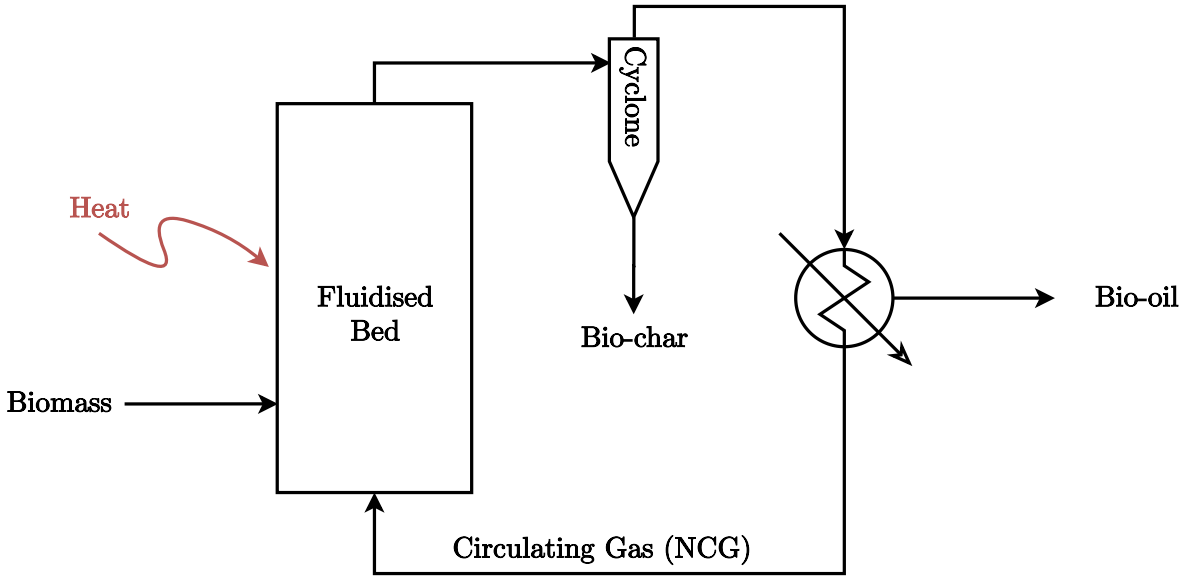

Figure 4: The typical setup for a fluidised bed for fast pyrolysis

Bridgwater (2013) summarises the key features of a fast pyrolysis process:

1. The heating rates and the heat transfer for the pyrolysis process must be very high (see Table 6).
2. Particle size is important: biomass particles must be less than 3 mm in size (noted as the smallest dimension).
3. The temperature must be closely controlled to 500 °C
4. The vapour residence time must be below 2 s to reduce secondary reactions.
5. The biochar must be removed from the product stream to reduce carbonisation reactions.

6. Finally, the pyrolysis vapours must be cooled rapidly to yield the bio-oil.

Guedes, Luna & Torres (2018) compiled the data from 2394 pyrolysis experiments to analyse the direction of the research. It was found that a majority of the pyrolysis research (including intermediate and slow pyrolysis) was focused on the yield of the process. Very little research has been done on the compositions of the bio-oils and their subsequent properties. For instance, 73 % of the research papers reported on how temperature impacts bio-oil yields, yet only 23 % reported on the water content of the bio-oil process, a crucial downside of the pyrolysis process. It is therefore imperative to fully characterise the process, feedstock, and products of pyrolysis to assist in the realisation of a successful future in the biorefinery industry.

2.5 Products of fast pyrolysis

2.5.1 Bio-oil

Pyrolysis oil, colloquially termed bio-oil, is the condensate of the pyrolysis of biomass. It is a dark brown/red liquid reminiscent of crude oil however, its composition is very similar to that of biomass feedstock. As noted in Table 6, the yield of pyrolysis oil reaches a maximum of 75 % for fast pyrolysis of woody biomass and its typical higher heating values are around 17 MJ/kg. To put this into context, the typical higher heating value of crude oil is 42.1 MJ/kg (Culp, 1991). The relatively low heating values are largely attributed to the high water content (roughly 25 %) and the myriad of oxygenated compounds (Bridgwater, 2013). The main oxygenated compounds in the pyrolysis oil are carboxylic acids, alcohols, aldehydes, ketones, ethers, esters, furans, carbohydrates, and phenolic groups (Meier, Oasmaa & Peacocke, 1997; Rezaei, Shafaghat & Daud, 2014). The chemical composition and characteristics of fast pyrolysis bio-oils are described in Table 8.

Table 8: Typical values for bio-oil produced from fast pyrolysis of wood summarised by Bridgwater (2013)

Property	Value
Water content (%)	25
pH	2.5
Specific gravity (SG)	1.2
HHV (MJ/kg)	17 – 18
Viscosity (MPa s)	40 – 100
Solid impurities (%)	0.10
Elemental analysis	
Carbon (%)	56
Hydrogen (%)	6
Oxygen (%)	38
Nitrogen (%)	0 – 0.1

The properties of the bio-oils produced from the feedstocks compiled in Tables 2, 3, and 5 are summarised in Table 9. The variation in the chemical and physical characteristics demonstrates the increased variability in the product caused by the variability of the feed. The most consistent feedstock, woody biomass, has produced bio-oil with the lowest variability where agricultural residues are very inconsistent with an HHV ranging from 5 to 40 MJ/kg. The HHV of bio-oil produced from energy crops is very high compared the HHVs of bio-oil originating from to woody and agricultural sources and thus deserves attention in the pyrolysis field. Unfortunately, the characteristics of bio-oil heavily depend on the processing conditions as well, and therefore standardisation of the bio-oil production would be crucial in the choice of appropriate feedstocks.

Table 9: Properties of bio-oil from the fast pyrolysis of lignocellulosic biomass compiled from data by Dhyani & Bhaskar (2018)

Property	Woody biomass Average value	Agricultural residue Average value	Energy crops Average value
Moisture (%)	21.10 ± 5.58	29.55 ± 21.28	25.07 ± 8.37
Ash (%)	0.09 ± 0.07	0.24 ± 0.22	0.35 ± 0.42
Ultimate analysis			
Carbon (%)	45.48 ± 4.76	45.83 ± 20.13	50.18 ± 15.39
Hydrogen (%)	6.75 ± 1.73	8.41 ± 1.66	8.71 ± 1.67
Oxygen (%)	45.29 ± 10.90	44.19 ± 21.62	39.11 ± 15.50
Nitrogen (%)	0.37 ± 0.61	1.39 ± 1.55	0.59 ± 0.47
Sulphur (%)	0.02 ± 0.03	0.09 ± 0.12	0.10 ± 0.10
Energy content			
HHV (MJ/kg)	17.63 ± 1.71	19.76 ± 10.90	24.55 ± 7.28

One might suspect that with their lower heating values and high oxygen content, there would be no use for pyrolysis oils. To some extent this is true as you cannot put bio-oil into a diesel engine, but raw bio-oil has its place as an energy carrier. Bridgwater (2013) notes that the densification of biomass in the form of bio-oil reduces transport costs by 87 %. This liquid can subsequently be processed at a separate facility to further refine and process the oil. It has also been found that as bio-oil burns with a stable and self-sustaining flame it could find applications in boilers, kilns, and turbines (Wornat, Porter & Yang, 1994). A lot of research is currently being done on catalysts and the upgrading of bio-oil to a more stable product comparable to petroleum. High-value chemicals could also be produced from the pyrolysis process as noted by Bridgwater (2013). The products of fast pyrolysis and their uses are illustrated by Figure 5.

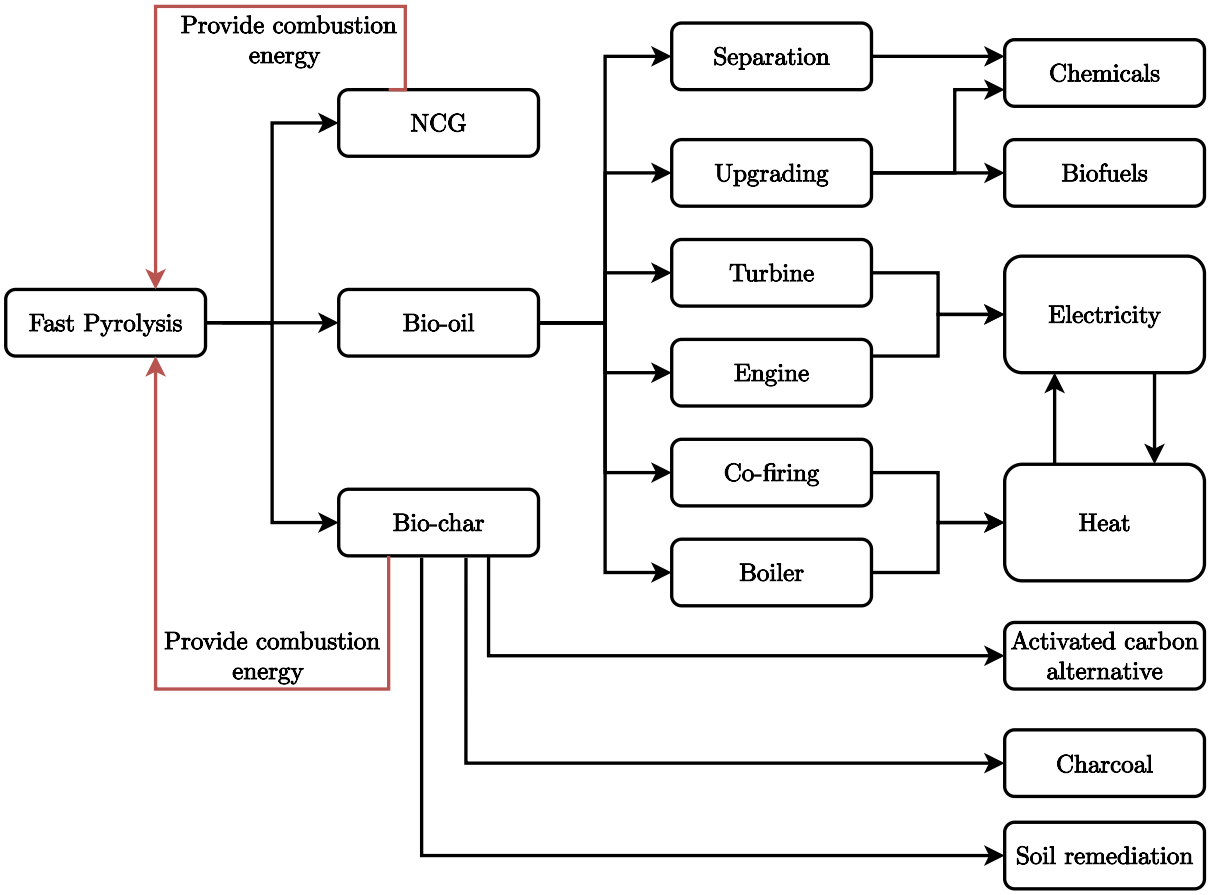

Figure 5: The uses of the products of fast pyrolysis (adapted from Bridgwater (2013))

2.5.2 Biochar

The solid product of fast pyrolysis resembling charcoal is dubbed biochar, which contains around a quarter of the energy of the parent biomass (Bridgwater, 2013). Research has shown biochar to have incredible soil conditioning properties and the ability to capture and store carbon. Additionally, it has been shown that introducing biochar into the soil can create a carbon-negative process for the pyrolysis industry. Storing the biochar in the soil prevents carbon dioxide production (which inevitably happens with decaying biomass or combustion) (Lehmann, Czimczik, *et al*, 2009). Calculations have predicted a decrease in carbon dioxide emissions by 0.5 billion tons or around 1.5 % of the total emissions (Windeatt *et al*, 2014). Wang *et al* (2013) also states that nitrous oxide emissions from plant growth can be reduced by up to 80 % with the use of biochar and good soil management practices. Around 67 % of the nitrous oxide emissions are due to the agricultural industry's excessive use of fertilisers (Cayuela *et al*, 2014). Biochar's proved entrapment of nitrogen could not only help with nutrient runoffs but increase the efficiency of farming practices. Furthermore, the biochar serves as a habitable medium for microbial species (Lehmann, Rillig, *et al*, 2011). Zhang *et al* (2017) did experiments on

soils tainted with heavy metals, specifically cadmium, by applying biochar to the soil with an optimal biochar-in-soil mass percentage of 2.5 %. It was found that microbiota was able to flourish as an increase in biodiversity was recorded.

Other notable uses of biochar include the removal of pollutants from aqueous and gaseous streams. Oliveira *et al* (2017) reviewed the research on biochar and pollution removal and found that an increase in pyrolysis temperatures (greater than 500 °C) created a biochar with an affinity for organic pollutants. The opposite is also true where lower pyrolysis temperatures (below 500 °C) yields a biochar product that has an affinity for inorganic pollutants. Beckinghausen *et al* (2020) investigated the ability of biochars to effectively remove nitrogen from wastewater using various pretreament methods. The steam activation of black wattle biochar more than doubled the BET surface area of the biochar and increased the ammonia adsorption capacity approximately ten-fold. In conclusion, the process of pretreating black wattle biochar yielded a lower energy consumption for ammonia fixation than producing ammonia through the Haber-Bosch process. This showed very promising results by demonstrating the sustainable and renewable uses of this byproduct of pyrolysis.

An analysis of the biochar characteristics derived from various feedstocks is compiled in Table 10. Higher heating values vary from 14 to 34 MJ/kg and it can be noted that the biomass with high ash content inevitably has lower HHVs. Again, the high ash content is usually associated with non-woody feedstocks. The table also illustrates how varied the biochar compositions can be with similar feedstocks which shows the importance of the standardisation of products for a pyrolysis based industry.

Table 10: Composition of biochars adapted from data by Dhyani & Bhaskar (2018)

Property	Mean value (wt%)
Ash (wt%)	11.69 ± 10.82
Ultimate analysis	
Carbon (wt%)	71.49 ± 13.00
Hydrogen (wt%)	2.47 ± 0.96
Oxygen (wt%)	13.56 ± 7.06
Nitrogen (wt%)	1.01 ± 0.94
Sulphur (wt%)	0.27 ± 0.27
Energy content	
HHV (MJ/kg)	25.40 ± 5.25

2.5.3 Non-condensable gases

The non-condensable products of fast pyrolysis contain about 5 % of the energy from the original feedstock. The composition of the gas phase includes carbon dioxide, carbon monoxide, hydrogen, and methane with trace elements of short-chain hydrocarbons. Due to the low yield and energy density, the gaseous phase is usually recirculated as an inert atmosphere and doubles up as a fluidisation medium for fluidised bed reactors (Bridgwater, 2013). Mante *et al* (2012) found that the recycling of non-condensable gases increased the liquid yield and decreased the yield of char. It was discovered from further analysis that more aromatic compounds were generated by converting oxygenated compounds such as the methoxy, acidic, and carbohydrate groups. Dhyani & Bhaskar (2018) state that using NCG as the fluidisation medium increases the final bio-oil's pH and increases the higher heating values, both of which are probably linked to decreased oxygen in the final liquid product. Park *et al* (2012) analysed the non-condensable gases produced from the pyrolysis of wild reed and found that carbon dioxide accounted for 56 % and carbon monoxide accounted for 29 %. This justifies the low heating value of around 11 MJ/kg.

2.6 Upgrading the pyrolysis products

Bio-oils produced from fast pyrolysis, as noted in Section 2.5.1, are highly oxygenated with high moisture contents. The upgrading of bio-oils is in the best interests of the biorefinery sector as it allows the oils to be used in the well-defined petrochemical refinery processes.

2.6.1 Physical upgrading

The bio-crude formed in pyrolysis reactions is exactly that, a crude oil. Like any traditional method of oil refining, physical upgrading like the simple act of filtering can greatly increase the value of the oil. However, Bridgwater (2012) notes that the high pressures required to filter oils and the types of filters required could be impractical. Hot vapour filtration is currently the most widely used physical upgrading method used in pyrolysis. Virtually char-free oil can be produced and FA Agblevor & Besler (1996) note that the yield of condensate did not change with hot vapour filtration of switchgrass pyrolysis. However, the work of Chen *et al* (2011) shows a decrease in oil yield with an increase in the higher heating value.

2.6.2 Hydrotreating

Hydrotreating is a commonly used process in the petroleum industry. It makes use of pure hydrogen and reacts it with a hydrocarbon stream, which in turn upgrades the product by removing sulphur and oxygen compounds while increasing the carbon to hydrogen ratio (Schaschke, 2014). This process can also be applied to the upgrading of pyrolysis oil. The reaction of typical pyrolysis oil with hydrogen is shown in Equation 1 (Bridgwater, 2012).

$$CH_{1.33}O_{0.43} + 0.77\,H_2 \longrightarrow CH_2 + 0.43\,H_2O \tag{1}$$

Unfortunately, the catalysts used in the typical hydrotreating process of a petroleum refinery battled with the large quantities of water inherently produced in the pyrolysis process. Furthermore, the use of hydrogen in upgrading bio-oil is very inefficient even though it yields good results (Bridgwater, 2012).

2.6.3 Upgrading with acid catalysts

HZSM-5 catalysts are universally applied to increase the aromaticity and hydrocarbon content of the bio-oil (Adjaye & Bakhshi, 1995). Zeolites have been proved to remove the high oxygen content of the bio-oil through CO_2 production. A conceptual reaction is shown in Equation 2 (Bridgwater, 2012).

$$CH_{1.33}O_{0.43} + 0.26\,O_2 \longrightarrow 0.65\,CH_{1.2} + 0.34\,CO_2 + 0.27\,H_{20} \tag{2}$$

It should be noted that the ZSM-5 catalysts are coked easily and form byproducts that require extra treatment to remove such as water and CO_2 (Bridgwater, 2012). The inclusion of FCC (fluid catalytic cracking) in the upgrading of fast pyrolysis oil has been investigated with promising results. Co-feeding vacuum gasoil and pyrolysis oil to an FCC unit proved successful even though the bio-oil was highly oxygenated (Pinho *et al*, 2017).

2.6.4 Upgrading with basic catalysts

Basic catalysts are not as well researched as traditional zeolite counterparts. They have proven to crack the cellulose and hemicellulose products more than the lignin-based prod-

ucts in *ex situ* upgrading. Furthermore, basic catalysts do not experience the intensity of coking that the acid catalysts have to deal with. These catalysts include ZnO, Zn and Mg variants of LDH (layered double hydroxides) (Bridgwater, 2012). Due to the low coking of basic catalysts, the production of PAHs (polycyclic aromatic hydrocarbons) is less common. In terms of *in situ* upgrading, it has been shown that the lignin in woody biomass pyrolysis takes part in hydrocracking and hydrodeoxygenation reactions when a basic catalyst is present (MP Pandey & Kim, 2011).

3 Combustion Reduction Integrated Pyrolysis System

The Combustion Reduction Integrated Pyrolysis System (CRIPS) has, excuse the pun, been in the pipeline at the University of Pretoria since the work of Swart (2012). It has gone through many design and implementation iterations. Ultimately, it has created opportunities for many researchers to explore the merging of biorefinery and process engineering.

3.1 Previous iterations and research

3.1.1 CRIPS 1 process overview

The CRIPS 1 pilot unit was designed and constructed by Swart (2012). The commissioning, troubleshooting and, operation of the plant was later performed by Grobler (2014). The CRIPS 1 pilot plant consisted of two separate fluidised bed units, namely the combustion and the pyrolysis units. The combustion unit provided the energy required for pyrolysis by heating up the bed material, in this case, silica sand. While the combustion bed fluidises and heats up the sand, the bed material falls through a z-valve into the pyrolysis unit where *Eucalyptus grandis* wood chips undergo pyrolysis reactions to form gaseous vapours and biochar. The bed material is also continually removed in a controlled manner from the pyrolysis unit via a screw feeder and returned to the combustion unit where the sand is be reheated and any coke formation is removed via combustion. The pyrolysis products exit the pyrolysis unit through a cyclone where the biochar is separated from the vapours. The vapours then travel into a condensation loop where the recirculating cooled product is mixed with the vapours following the biochar removal. Bio-oil is thus condensed and the remaining NCG is recirculated to the pyrolysis unit as the fluidisation medium. As additional NCG is formed from the continuous input of biomass, a portion of the NCG stream is purged to the combustion unit to provide additional combustible energy to the systems. The P&ID (process/piping and instrumentation diagram) for the CRIPS 1 unit is shown in Appendix A.1

3.1.2 CRIPS 1 design and operation

The work of Grobler (2014) and Swart (2012) demonstrates the contrast between design and real-world testing. The CRIPS 1 unit had many drawbacks, with energy loss being the ultimate issue. The modelled and laboratory operating conditions for the combustion unit are compared in Table 11. Note that n.d. stands for not determined.

Table 11: Operating parameters for the combustion unit in the CRIPS 1 system

Parameter	Modelled value[a]	Experimental value[b]
Bed temperature (°C)	900	670 – 700
Flue gas exit temperature (°C)	n.d.	450 – 500
Air flow (l/min)	n.d.	300
SGV (m/s)	1	0.4
LPG flow (l/min)	n.d.	15
NCG purge flow (l/min)	n.d.	4

[a] Swart (2012)
[b] Grobler (2014)

The modelled and experimental operating conditions for the pyrolysis unit are compared in Table 12.

Table 12: Operating parameters for the pyrolysis unit in the CRIPS 1 system

Parameter	Modelled value[a]	Experimental value[b]
Bed temperature (°C)	500	500
Vapour outlet temperature (°C)	500	195
SGV (m/s)	0.28	0.45
VRT (s)	10	4
Sawdust feed rate (kg/h)	20	2
Silica transfer rate (kg/h)	96	50

[a] Swart (2012)
[b] Grobler (2014)

Note that the flow rate of the biomass into the reactor was much less than the designed flow rate of 20 kg/h. The system failed to produce the desired quantity of the product and this was attributed to energy losses which are shown in Table 13.

Table 13: Experimental mass and energy values for the CRIPS 1 pilot plant

Parameter	Modelled value[a]	Experimental value[b]
Bio-oil (%)	64	36.3
Biochar (%)	n.d.	49.7
NCG (%)	n.d.	14

[a] Swart (2012)
[b] Grobler (2014)

Grobler (2014) recommended that extra insulation should be used for the reactors and the oil condensation unit. A large portion of this energy loss was also due to the hot flue gas leaving the unit. It was calculated that the setup could be operated at 5 to 10 times the feed rate if heat losses were mitigated. Furthermore, the high-pressure drop over the condensation unit hindered the velocity of the pyrolysis vapour stream exiting the reactor. Another issue was that the solvent used in starting the condensation process, ethylene glycol, would skew the product results and therefore a solution was required.

3.1.3 CRIPS 2 design

CRIPS 2 was designed and its components fabricated by de la Rey (2015) with this project reporting on the construction, commissioning, troubleshooting, and operation of the plant. The new design draws inspiration from the dual fluidised bed system used in the CRIPS 1 unit however, the two units have been combined into a single vessel. Secondly, a large portion of the combustion energy is recovered using a combustion air preheater (APH). The specifics of the process are outlined in Section 3.2.

The designed values for the combustion unit operation are summarised in Table 14. The flow rates of the combustion unit are significantly higher than those of the CRIPS 1 system due to the fact that the higher biomass throughput requires more energy. The flue gas exit temperature is also lower because of the APH, which translates into less fuel required per mass of biomass pyrolysed.

Table 14: Modelled operating parameters for the combustion unit in the CRIPS 2 system (de la Rey, 2015)

Parameter	Modelled value
Bed temperature (°C)	900
Flue gas exit temperature (°C)	433
Air flow (kg/h)	65.1
SGV (m/s)	1.2
LPG flow rate (kg/h)	1.9
NCG purge flow (kg/h)	5.2

The design operating parameters of the pyrolysis unit are summarised in Table 15. The parameters other than the biomass feed rate are similar to those of the CRIPS 1 unit.

Table 15: Modelled operating parameters for the pyrolysis unit in the CRIPS 2 system (de la Rey, 2015)

Parameter	Modelled value
Bed temperature (°C)	500
Vapour exit temperature (°C)	500
SGV (m/s)	0.9
VRT (s)	1.3
Biomass feed rate (kg/h)	26.1
Silica transfer rate (kg/h)	158

The product yields for the CRIPS 2 unit are listed in Table 16 with significantly higher predicted bio-oil yields compared to the CRIPS 1 unit.

Table 16: Modelled yields for the CRIPS 2 unit (de la Rey, 2015)

Component	CRIPS 2 yield (%)
Bio-oil	62.07
Biochar	18.01
NCG	19.92

3.1.4 CRIPS 2 novelty

The novelty of the CRIPS 2 system lies in its energy and mass conservation. The novelty modifications are summarised as follows:

- Recycled NCG (non-condensable gas) is purged to the combustion unit as a fuel source.
- Annular pyrolysis unit surrounding the cylindrical combustion unit.
- APH (air preheater) installed above the combustion unit.

The NCG produced from the pyrolysis reactions is used to add energy to the process by being purged into the combustion unit as the gas is of very low quality, i.e. it is not a valuable product. The annular arrangement of the pyrolysis unit also utilises all the waste heat from the combustion zone (in the radial direction). Furthermore, the integrated heat exchanger preheats the combustion air with waste heat from the hot flue gas.

The commonly implemented reactor setup is the circulating fluidised bed unit which comes with a few drawbacks. The biochar is combusted to heat the bed material, which is wasteful as the solid residue has many uses in soil remediation and carbon sequestration (as discussed in Section 2.5.2). The unit can operate with both a low biochar yield which means less LPG will be required to heat the combustion unit, or with a higher biochar yield where additional LPG is used to supplement the energy requirements. This can be done with varying feedstock sizes and NCG recycle flow rates, and by modifying the cyclone unit.

3.2 CRIPS 2 Process overview

3.2.1 Overview

The CRIPS 2 pilot plant utilises a dual fluidised bed setup much like the previous CRIPS 1 pilot plant (see the brief description in Section 3.1.1). However, the key difference with the new setup is that the combustion and pyrolysis units are integrated into a single unit as opposed to being two stand-alone units. This is achieved with an annular pyrolysis unit surrounding a central cylindrical combustion unit. The two units are separated with a cylindrical refractory wall as shown in Figure 6. Furthermore, multiple angled overflow holes were incorporated into the refractory material to allow for a better distribution

of hot bed material for the pyrolysis zone and the smaller size of the holes limits the interaction between the gases in combustion and pyrolysis zones. This design differs from that in the CRIPS 1 setup as only one overflow hole was utilised. An angled skirting was also integrated into the refractory to mimic a spouted bed reactor setup. As NCG exits the distributor, the velocity of the gas is very high due to a small outlet area. This forces the bed material to fluidise at low NCG flow rates and encourages more thorough mixing. Finally, as the NCG moves through the bed, the area of distribution increases via the skirting and the gas velocity decreases to the SGV (superficial gas velocities) values as per the design by de la Rey (2015).

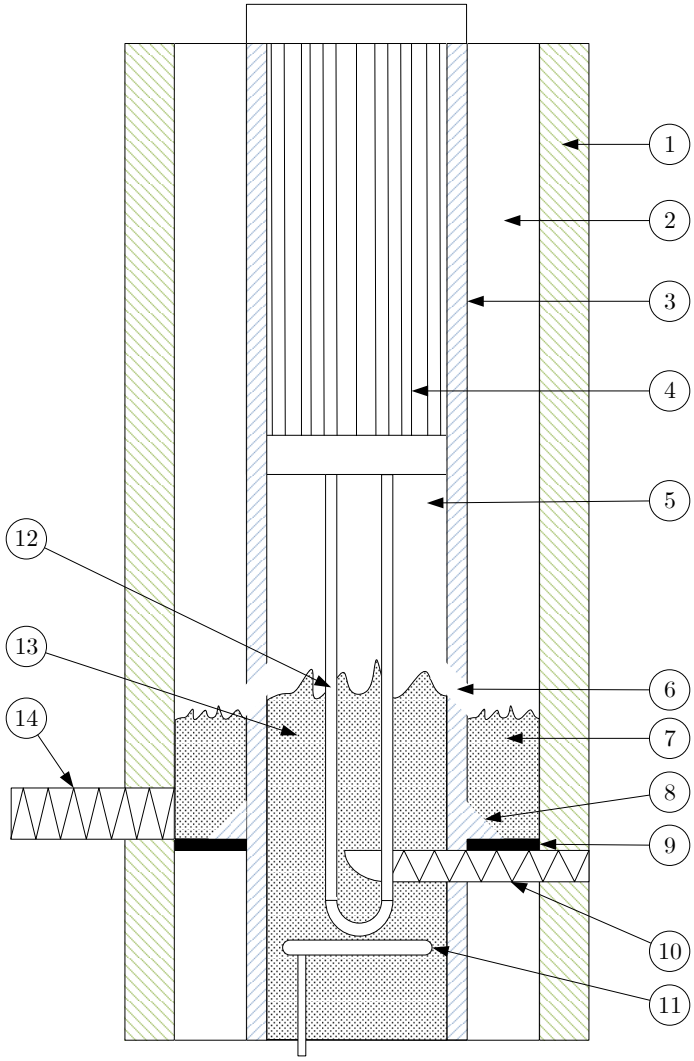

1	Outer insulation
2	Pyrolysis unit freeboard
3	Refractory material
4	APH
5	Combustion unit freeboard
6	Bed material overflow holes
7	Pyrolysis fluidised bed
8	Refractory skirting
9	NCG distributor
10	Bed material transfer screw
11	LPG distributor
12	Combustion air distributor
13	Combustion fluidised bed
14	Biomass screw conveyor

Figure 6: CRIPS 2 reactor setup

The bed material is heated in the combustion unit with a combination of air, LPG (liquefied petroleum gas), and residual biomass (in the form of biochar). The fluidisation

of the combustion bed material causes it to overflow through six angled holes in the refractory leading to the pyrolysis unit. The sand in the pyrolysis unit is fluidised using a gas distribution ring which also rotates the fluidised bed material with its angled nozzles. This setup ensures that the pyrolysis bed is well mixed and that the bed is constantly rotating clockwise around the unit towards a dead-zone. The dead-zone is an opening where the bed material falls into a controlled return screw feeder. From here, it is transported from the pyrolysis unit back to the combustion unit where it is reheated and decoked. The fluidisation gas in the pyrolysis unit is the recycled NCG formed from pyrolysis reactions and is recycled through the condensation loop.

Biomass is fed perpendicular to the pyrolysis unit where it interacts with the hot fluidised bed material to form pyrolysis products namely, bio-oil, biochar, and NCG. These products leave the unit directly above the screw conveyor where they enter a cyclone which removes the biochar. The gaseous vapours then flow into a condensation loop where cold bio-oil is mixed with the vapours to condense the bio-oil. The remaining NCG is recirculated to the pyrolysis distributor.

The flue gas produced from the combustion of LPG, residual biomass, and air leaves the combustion unit and enters the APH. The flue gas travels through the shell side of a modified shell and tube heat exchanger where its heat is exchanged with the incoming combustion air flowing through the tube side. Finally, The flue gas flows through a cyclone to separate any ash or sand fines before leaving the vicinity via an extraction unit.

3.2.2 Biomass feeder unit

The biomass feeder unit consists of a hopper (H-201), a frame, three load-cells (WT-201, WT-202, and WT-203), an agitator (M-203), an eccentric motor (M-204), a screw feeder coupled to a geared motor (S-201 and M-201), and a screw conveyor coupled to a standard motor (S-202 and M-202). A basic schematic of the biomass feeder unit is shown in Figure 7 (note that cooling water is abbreviated as CW).

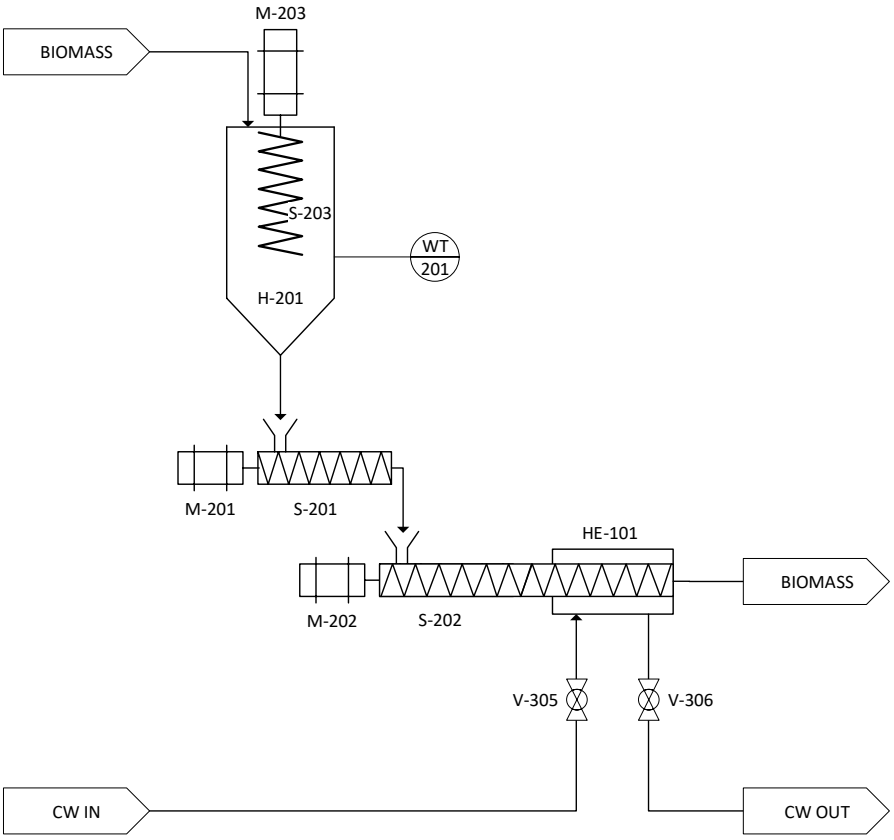

Figure 7: CRIPS 2 biomass feeder unit

Biomass in the form of wood chips is loaded into a sealed hopper before the start-up of the CRIPS 2 system. The mass of biomass charged to the pyrolysis process is determined by a calibrated set of three load-cells that hold the hopper to a frame. As wood chips are well known for their tendency to clump up and their stubbornness in cylindrical hoppers, a steel agitator was installed inside the hopper which loosens the chips. Additionally, an eccentric motor is attached to the base bracket of the hopper to induce vibrations through the chips for a continuous flow. The chips fall onto a screw feeder driven by a geared motor (M-201) which is powered and controlled via a VFD (variable frequency drive). The wood chips are moved by the screw feeder at a controlled rate and, via gravity, fall onto a screw conveyor where they are quickly transported to the pyrolysis bed. A flexible hose connects the outlet of the screw feeder to the inlet of the screw conveyor to ensure that the system is sealed. The flexible hose connection also means that the mass of the hopper is not affected by any of the process connections and therefore any change in the weight measured by the load-cells is due to the biomass in the hopper.

3.2.3 Combustion unit

The combustion unit consists of a cylindrical reactor (R-101) surrounded by refractory, LPG gas distribution manifold, two pressure detection tubes with relevant pressure transducers (PT-104 and PT-107), three thermocouples for bed and flue temperatures (TT-101, TT-102, and TT-107 respectively), and a modified shell and tube heat exchanger with a viewing port (HE-101). The pyrolysis unit consists of an annular reactor with the refractory as the inner wall and the stainless steel shell as the outer wall (R-102), an NCG distribution ring manifold, a biochar collection cyclone (C-102), five thermocouples (TT-103, TT-104, TT-105, and TT-306), two pressure transducers (PT-103 and PT-108), and a sand return screw feeder system (S-101 and M-101). A basic schematic of the pyrolysis unit is shown in Figure 8.

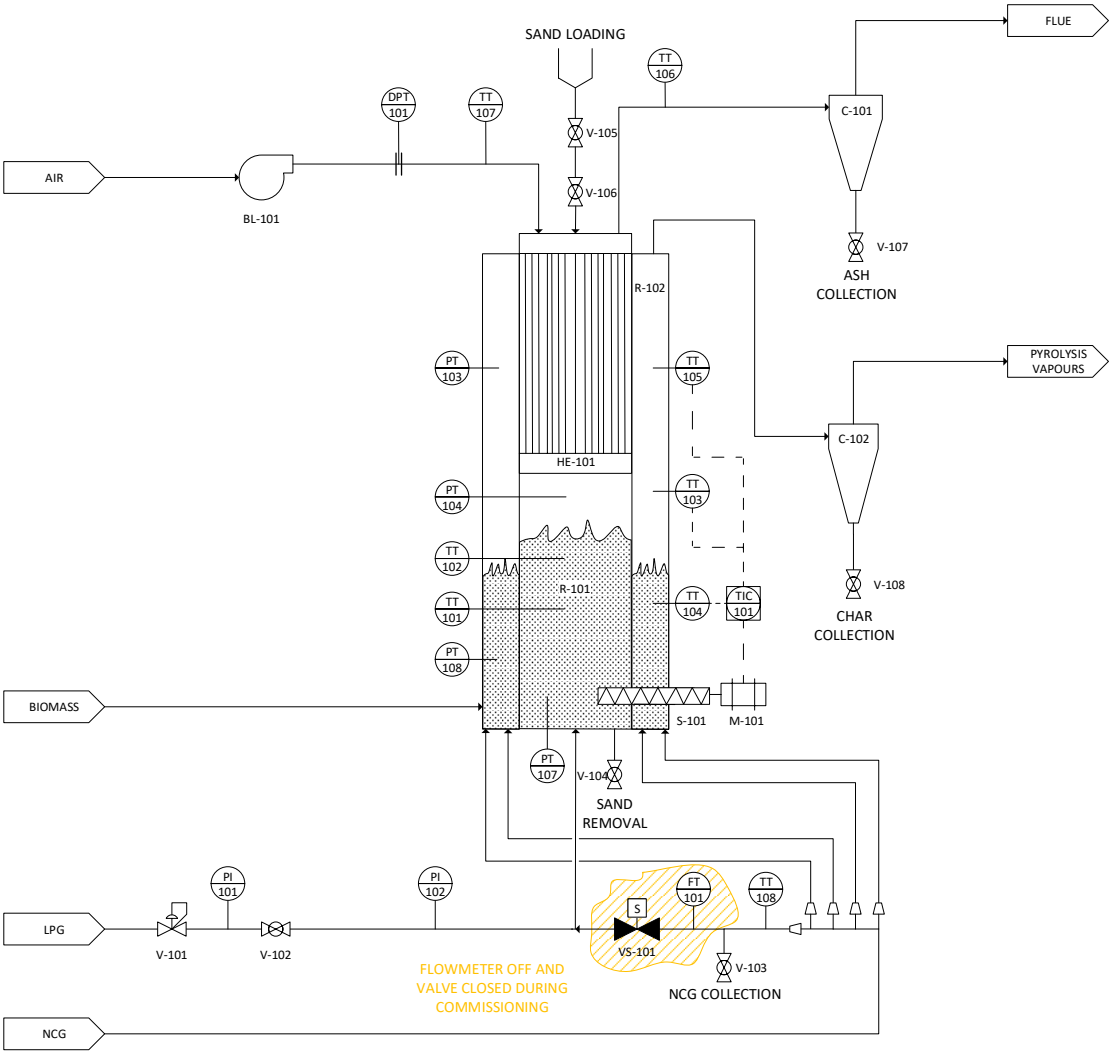

Figure 8: CRIPS 2 unit

Combustion starts with the suction of atmospheric air into a blower (BL-101) which is powered and controlled with a VFD. The velocity of the air is calculated using a differential pressure transducer (PDT-101) in conjunction with an in-line orifice plate. Following the orifice plate, the air travels through a flexible steel hose into the APH heat exchanger, where it is distributed into 48 tubes as it exchanges heat with exiting flue gases. The preheated air exits the tubes and flows into two U-shaped manifolds where it exits through nozzles at the base of the manifold. The distributed air fluidises the bed material while simultaneously combusting the LPG. The LPG enters the reactor from an external gas cylinder situated close to the operator allowing, easy shut-off and control. The flow rate of the LPG is manually controlled via a gas regulator where it flows through a shut-off valve and finally into the gas distribution manifold.

The combustion flue gas travels through the shell side of the APH heat exchanger past thirteen baffles for optimal heat transfer. A thermocouple, TT-107, measures the exit flue gas temperature before the cyclone. Following the cyclone, the flue gas is monitored via a handheld flue gas analyser that is used to assist the mass balance and give an indication of the efficiency of combustion.

Hot sand from the combustion unit enters the pyrolysis unit through the overflow orifices. Once inside the pyrolysis unit, the sand is fluidised by recycled NCG entering from the distribution ring. The NCG is recycled from the condenser unit via a VFD driven blower (BL-301). The flow rate is determined with an orifice plate using a DP cell (DPT-301) and its temperature is measured with a thermocouple (TT-306). The nozzles of the distribution ring (where the NCG exits the distributor) are angled at 12° to rotate the bed in a clockwise direction while fluidising it. Biomass enters the pyrolysis unit via the screw conveyor and immediately begins pyrolysing when in contact with the hot bed material. The products of pyrolysis (bio-oil, biochar, and NCG) leave the reactor and enter a cyclone which removes biochar and any residual fines (ash/sand particulates). The pyrolysis vapours exit the top of cyclone and travel to the condenser unit.

The temperature at which the pyrolysis occurs is constantly monitored and controlled to achieve optimal product formation ($\approx 500\,^{\circ}\mathrm{C}$). The monitoring is achieved by using three thermocouples situated in the bed at 120° from each other. Sand in the pyrolysis unit rotates around the reactor until it reaches a dead zone where it falls into the screw feeder and is transported back to the combustion unit. Sand from the combustion unit stops entering the pyrolysis unit when sufficient sand has entered the unit and the overflow orifices are blocked. Due to the endothermicity of the reaction, the sand will lose energy and thus cool down. By removing sand from the pyrolysis unit through the screw feeder, the bed will decrease in height, allowing sand to overflow from the combustion unit. The rate at which the screw recycles the sand will be proportional to the biomass feed rate

and energy losses to the surroundings through the sides and the top of the pyrolysis unit. The flow rate of the sand return is controlled with a VFD driven motor (M-101) which turns a screw, transporting sand from the pyrolysis unit to the combustion unit.

3.2.4 Condenser unit

The condenser unit consists of three glass cylinders for quenching demisting and bio-oil collecting (Q-301, D-301, and BC-301 respectively), a helical PD (positive displacement) pump (P-301), a brazed plate and frame heat exchanger (HE-301), a filter unit (FL-301), one pressure transducer (PT-301), four thermocouples (TT-301, TT-302, TT-303, TT-304, and TT-305), a rotameter (FI-301), a water cooling tower unit (CT-301), and a gas blower (BL-301). A basic schematic of the condenser unit is shown in Figure 9.

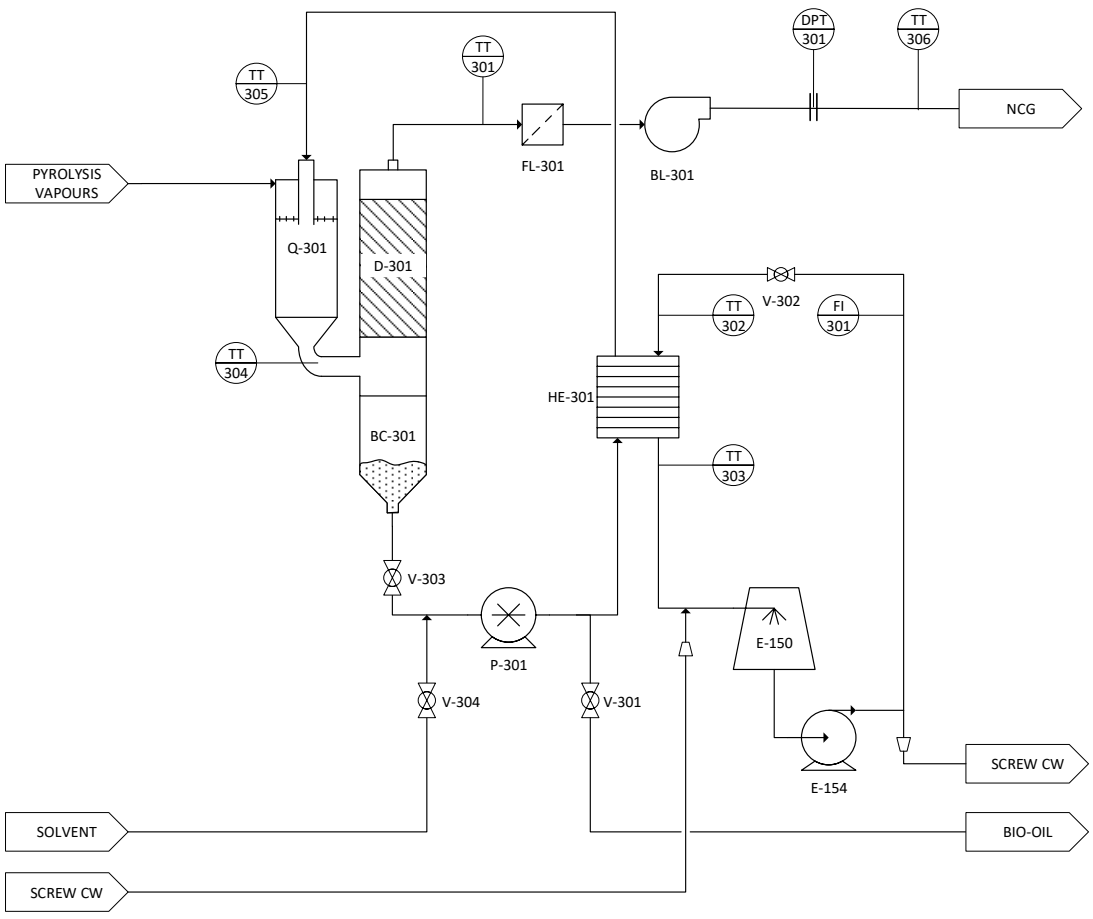

Figure 9: CRIPS 2 condenser unit

Pyrolysis vapours enter the top of the condensing unit through a perpendicular opening

whereby cooled bio-oil is mixed with the vapours via a swirling/centripetal injector setup, i.e. the pyrolysis vapours are forced into a swirling and outward spraying stream of cold bio-oil. The mixture flows down the first glass cylinder, the quencher, into a modified hydrocyclone. The mixture exits the hydrocyclone and, via gravity, the bio-oil (containing the newly condensed liquids) spirals down the edges of the second glass cylinder (bio-oil collection vessel) where it collects in the suction line of the helical PD pump. The pump transports the bio-oil through a plate and frame heat exchanger where it is cooled by cold water from the water cooling tower. Following this, the cold bio-oil travels to the swirling/centripetal injector setup where it is used to quench more bio-oil from the hot vapour stream. The bio-oil accumulates in the bio-oil collection vessel until the run has been halted or it can be tapped off during the pyrolysis phase if the vessel is too full.

Above the bio-oil collection glass cylinder, the gaseous products flow up through a final glass cylinder termed the demister. The suction generated by BL-301 pulls liquid into the demister through a slotted plate which allows more contact time with any uncondensed product, aiding in the recovery of bio-oils. Finally, the gas travels through a 100 µm filter (FL-301) to remove any particulates/condensate before it is returned to the pyrolysis unit blower (BL-301) to continue fluidising the pyrolysis bed (the "dry" gas at this point is called the NCG).

3.2.5 Extraction unit

The extraction unit consists of an inline duct fan, three flexible hoses, one thermocouple (TT-401), a steel manifold box (X-401), an inline duct fan (F-401), and three additional flexible extraction hoses. A basic schematic of the extraction unit is shown in Figure 10.

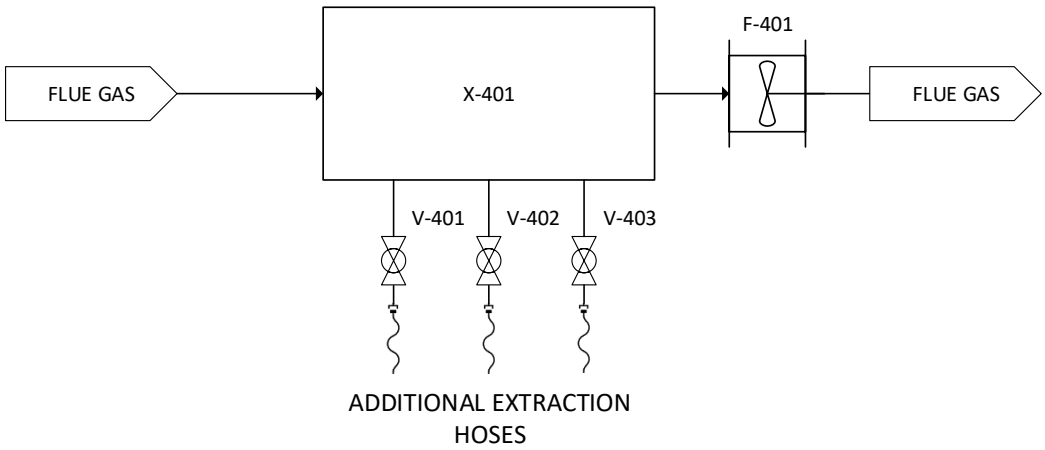

Figure 10: CRIPS 2 extraction unit

The pilot bay is located indoors and thus sufficient extraction will be required for the safety of plant operators and nearby personnel. The steel manifold box connects to an inline duct fan situated at the top of the building via a long set of ducts. The top of the cyclone of the combustion unit is fixed to the base of the manifold where it allows the flue gases to be removed safely from the vicinity of the unit. Three flexible hoses, also attached to the extraction box, are available for additional extraction around the unit. The temperature of the extraction box is monitored via a thermocouple (TT-401).

3.2.6 SCADA

The SCADA (Supervisory Control and Data Acquisition) system for the CRIPS 2 unit allows the plant operator to safely control the process and record data for further processing and analysis. LabVIEW was used for its ability to communicate with data acquisition devices and its simple GUI (Graphical User Interface), which comprises live data from the transmitters and transducers. Furthermore, background calculations are performed to determine extrinsic data such as mass flow rates, heat losses, etc. LabVIEW communicates with a National Instruments cRIO-9022 controller which receives the measurement signals and transmits the control signals, to and from the SCADA system and the CRIPS 2 unit. The layout of the SCADA systenm is illustrated in Figure 11.

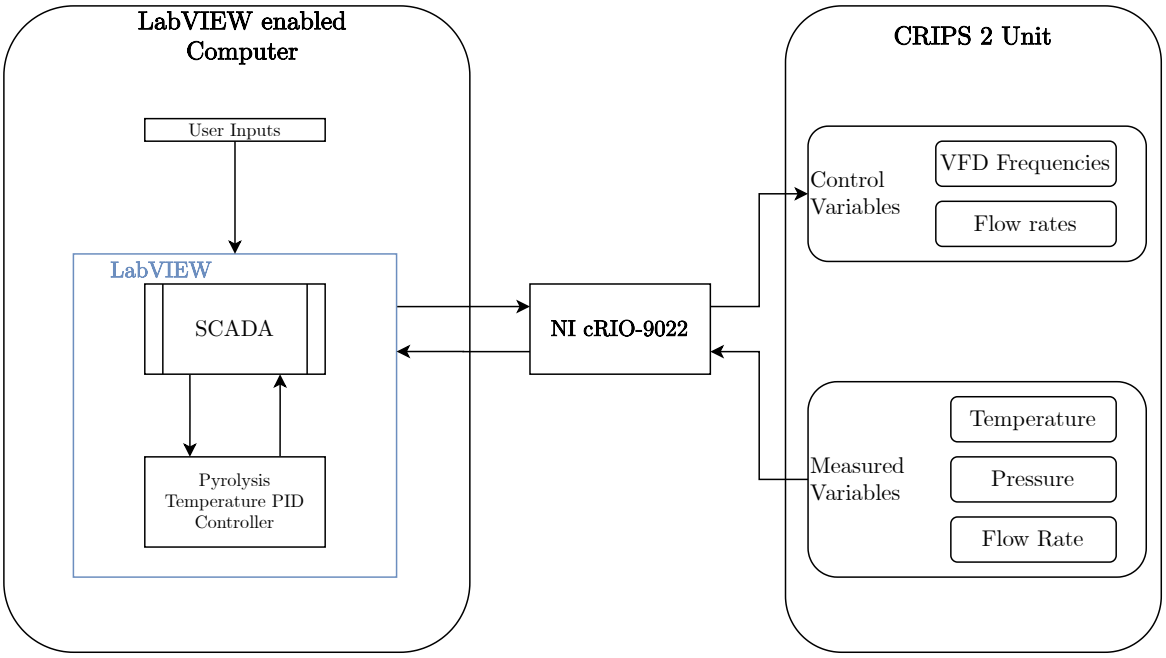

Figure 11: Communications schematic for the operation of the CRIPS 2 unit

The GUI for the SCADA system is shown in Figure 12.

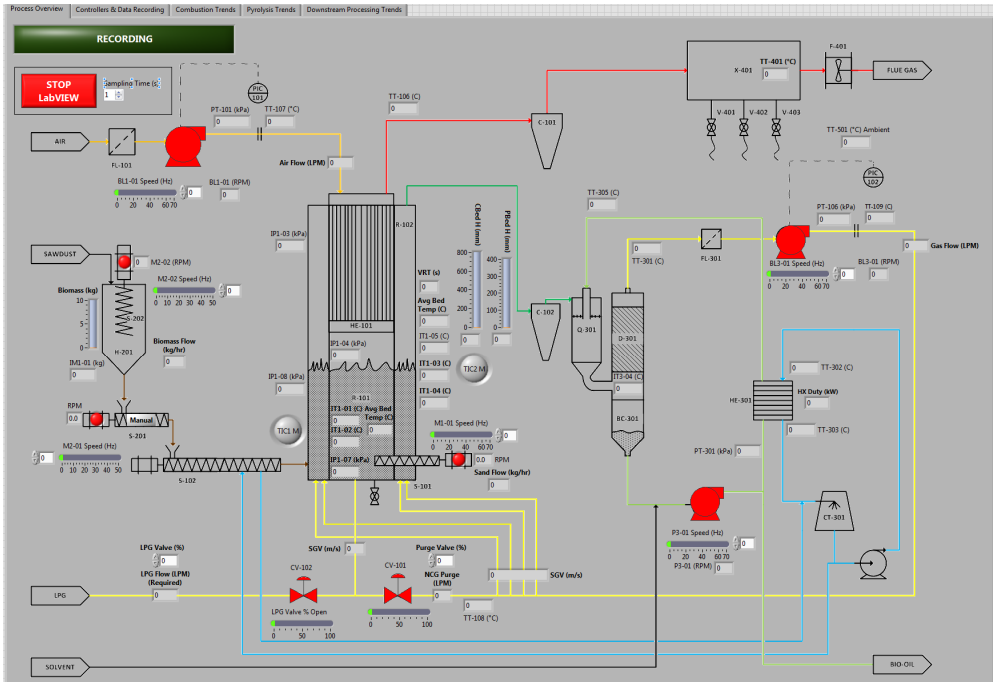

Figure 12: The GUI for the SCADA system

A summary of all the CRIPS 2 equipment is given in Table 17 and a summary of all the measured variables for the CRIPS 2 unit is presented in Table 18.

Table 17: CRIPS 2 process equipment list with corresponding IDs

ID	Description
R-101	Combustion unit
R-102	Pyrolysis unit
HE-101	Air preheater (APH)
HE-301	Bio-oil heat exchanger
H-201	Biomass hopper
M-101	Sand recycle motor
M-201	Biomass screw feeder motor
M-202	Biomass conveyor motor
M-203	Biomass agitator motor
M-202	Biomass hopper eccentric motor
BL-101	Combustion air blower
BL-301	NCG recycle blower
C-101	Biochar cyclone
C-102	Flue gas cyclone
Q-301	Bio-oil quencher
D-301	NCG demister
BC-301	Bio-oil Collector
P-301	Bio-oil pump
P-302	Cooling water pump
CT-301	Cooling water tower
S-101	Sand recycle screw
S-201	Biomass screw feeder
S-202	Biomass screw conveyor
S-203	Biomass agitator helix

Table 18: CRIPS 2 instrument list with corresponding IDs and descriptions

ID	Type	Measured Variable	Description
TT-101	Transmitter	Temperature	Lower combustion bed thermocouple
TT-102	Transmitter	Temperature	Upper combustion bed thermocouple
TT-103	Transmitter	Temperature	Pyrolysis thermocouple 1
TT-104	Transmitter	Temperature	Pyrolysis thermocouple 2 (below vapour exit)
TT-105	Transmitter	Temperature	Pyrolysis thermocouple 3 (biomass feed entrance)
TT-106	Transmitter	Temperature	Flue gas thermocouple
TT-107	Transmitter	Temperature	Incoming combustion air thermocouple
TT-108	Transmitter	Temperature	NCG sample point thermocouple
TT-301	Transmitter	Temperature	NCG leaving demister thermocouple
TT-302	Transmitter	Temperature	Cooling water entrance thermocouple
TT-303	Transmitter	Temperature	Cooling water exit thermocouple
TT-304	Transmitter	Temperature	Quenched bio-oil thermocouple
TT-305	Transmitter	Temperature	Cooled bio-oil thermocouple
TT-306	Transmitter	Temperature	NCG recycle thermocouple
TT-401	Transmitter	Temperature	Extraction manifold thermocouple
TT-501	Transmitter	Temperature	Ambient air thermocouple
PT-103	Transmitter	Pressure	Lower pyrolysis unit pressure transducer
PT-104	Transmitter	Pressure	Lower combustion unit pressure transducer
PT-107	Transmitter	Pressure	Upper combustion unit pressure transducer
PT-108	Transmitter	Pressure	Upper pyrolysis unit pressure transducer
PT-301	Transmitter	Pressure	Bio-oil pressure transducer
DPT-101	Transmitter	Differential pressure	Combustion air DP cell
DPT-301	Transmitter	Differential pressure	NCG recycle DP celll
PI-101	Indicator	Pressure	LPG regulator pressure gauge
PI-102	Indicator	Pressure	LPG line pressure gauge (for start-up)
FI-301	Indicator	Flow rate	Cooling water rotameter

3.3 CRIPS 2 construction

3.3.1 Initial construction

The CRIPS 2 reactor was designed and its parts were constructed to conclude the thesis of de la Rey (2015). As noted in Section 3.2, two key differences between CRIPS 1 and CRIPS 2 are the internal heat exchanger and the combination of the two units into a single cylindrical vessel. The condensation and biomass feeding unit was relatively unchanged from the CRIPS 1 unit.

The construction and assembly of CRIPS 2 started with the placement of the inner refractory separating the combustion and pyrolysis zones (Figure 13). The overflow holes and skirting are visible in the image as well as the dead-zone where the bed material is transferred back to the pyrolysis zone (the vertical cut out in the refractory on the left side of the distribution ring in Figure 13).

Figure 13: The inner refractory of the CRIPS 2 unit that separates the combustion and pyrolysis units. Note the two holes are for bed overflow and the skirting just below them

Following this, the outer shell of the unit was bolted onto the stand. Figure 14 shows the interior of the CRIPS 2 reactor setup with the stainless steel wall (metallic material) and refractory material separating the annular reactor from the combustion zone (beige material). It also shows the outer shell portion of the CRIPS 2 reactor being lowered onto the reactor stand.

Figure 14: Left: Reactor interior Right: Top view of the outer shell

After fitting the outer shell, the heat exchanger was lowered into the CRIPS 2 unit and fastened with bolts. Borosilicate glass windows were subsequently secured above the pyrolysis and combustion viewports. They allow operators to view the reactions taking place as well as visual confirmation of the combustion operation. The APH heat exchanger is shown in Figure 15 with its associated inlet and outlet flexible hoses. Two hoses were used for the flue gases produced from the combustion unit whereby the gas is sent out of the pilot plant area via extraction. The other hose is the inlet hose which transports ambient air to the tube bundle (also shown in the image) where the air is heated by the exiting flue gases before entering the combustion bed.

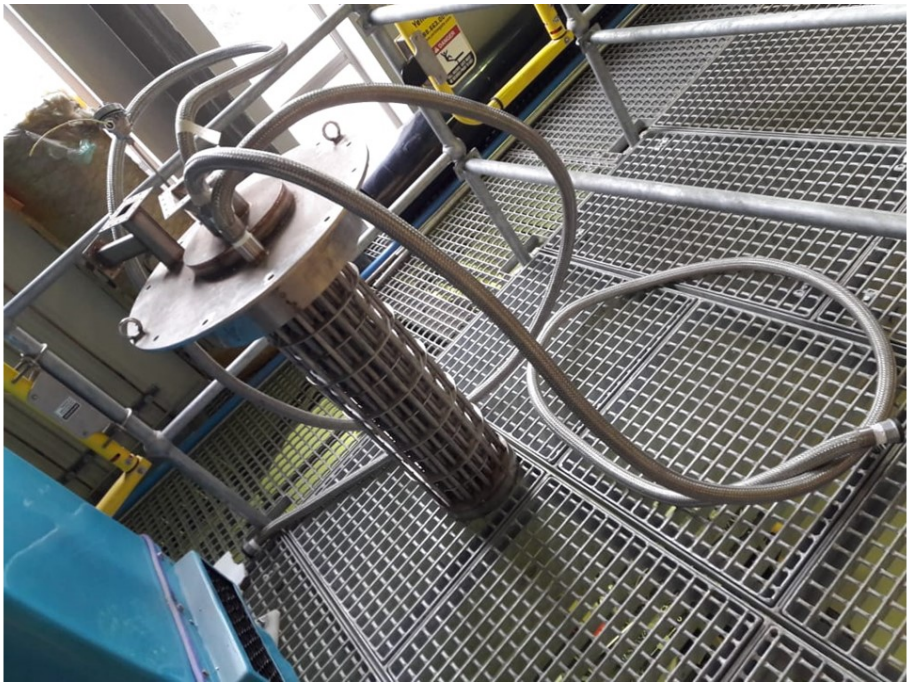

Figure 15: The internal heat exchanger with flexible incoming combustion air and exit flue gas piping

Gaskets were also fitted between all the bolted connections to ensure airtight connections throughout the unit. The partially assembled reactor is shown in Figure 16. The combustion and NCG recirculation blowers can be seen in the bottom right corner of the image. The biomass hopper can also be seen in the top right corner of the image.

Figure 16: Partially assembled CRIPS 2 unit (note that the insulation has not yet been installed)

The reactor's insulation was installed following the completion of the basic assembly. This involved cutting glass fibre sheets to size and wrapping them around the outer shell of the reactor. The characteristics of the insulation used in CRIPS 2 is described in Section 4.3.2. The two layers of insulation are shown in Figure 17.

Figure 17: Insulation for the CRIPS 2 unit. Left: High-temperature inner insulation. Right: Reinforced outer insulation

During the basic assembly, the wiring of the system was also installed. All transmitted signal wiring (4 to 20 mA) consisted of shielded cabling and all the thermocouples were connected via type-K thermocouple extension cabling, which extended from the data acquisition device to the respective sensors (see Section 3.2.6 for instrument lists).

The cooling water tower next to the CRIPS 2 unit provides cold water to the unit's operation by evaporative cooling, where the hot cooling water from the CRIPS 2 unit is sprayed down over baffles while air is blown up through the water, partially evaporating it and thus removing heat. The water collects in a sump and top-up water is provided through a float valve. A hose connecting municipal water to the cooling water was installed to ensure a consistent supply of top-up water. The connections between the cooling tower and the CRIPS 2 unit were fastened with PVC cement and thread seal tape where necessary. The delivery line to the bio-oil cooling heat exchanger was fitted with a water-calibrated rotameter for accurate flow measurement. The cooling tower and respective rotameter are shown in Figure 18.

Figure 18: Left: Water cooling tower with delivery pump Right: Cooling water rotameter

3.3.2 Modifications

Cold and hot runs were performed following the initial construction and assembly of the CRIPS 2 unit. These provided opportunities for troubleshooting and adaptations for a robust operation. Furthermore, these runs meant that the reactor's safety was thoroughly investigated.

The torque from the bed material transfer motor bent and buckled its stand during early commissioning operations. A new stand was constructed with thicker steel, which included diagonal braces to withstand the forces generated by transporting bed material between the units (Figure 19).

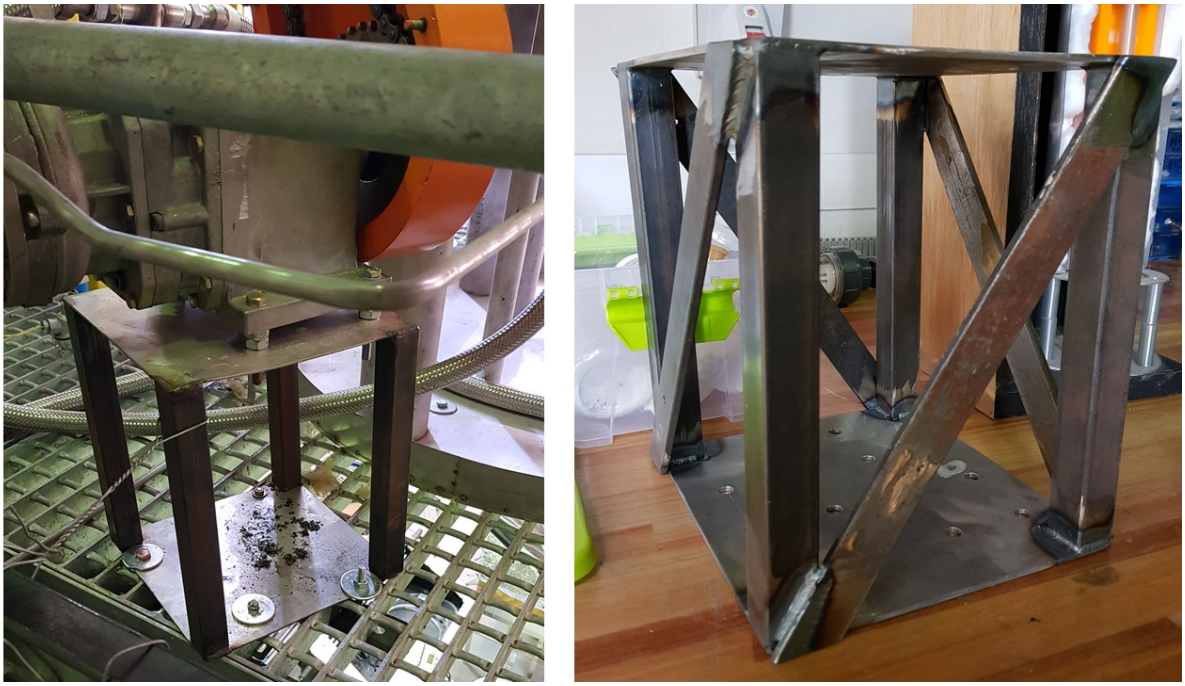

Figure 19: Left: The previous bed transfer motor stand Right: The new stand for the bed transfer motor

Initial testing of the biomass screw feeder found that the previous design of the hopper and delivery system prevented the uninterrupted flow of biomass. Various additions to the screw were implemented, starting with a more robust bearing system consisting of a mounted flanged bearing, key, and corresponding shaft keyway. The tests again proved to be unsuccessful as the pitch of the screw decreased along the length of the screw. This meant that the biomass would compact along the screw and block the transport pipe and prevent flow. A whole new design was required, and changing the hopper positioning was also considered. The initial hopper position meant that a long section of pipe was required to transport the feedstock to the conveyor screw into the pyrolysis bed. Therefore the hopper was moved as close as possible to the reactor to allow the biomass to leave the feed screw and with gravity, drop into the screw conveyor.

The new screw consists of a new stainless steel shaft and spiralled plate. The stock was turned down and the spiralled plate (also known as the flight) was welded onto it. The new screw feeder is shown in Figure 20.

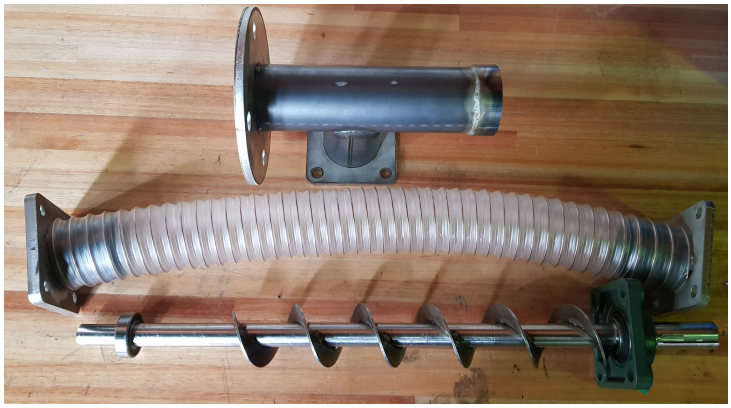

Figure 20: From top to bottom: Screw housing extension, flexible hose attachment, and the new screw feeder

With the new design the biomass will disengage from the feed screw and falls vertically into the path of the screw conveyor. The extended screw feeder requires stability and thus the end of the screw shaft was attached to a bearing mounted to a flanged end-piece. The flanged end allows for easier maintenance of the front end of the screw feeder and also supports the screw feeder from the front. This guarantees that the torque of the motor is transferred into moving the biomass. The extension of the screw housing was welded on the end of the original piping with the disengagement zone situated above the entrance of the screw conveyor. A comparison of the two feeding mechanisms is shown in Figure 21 and Figure 22.

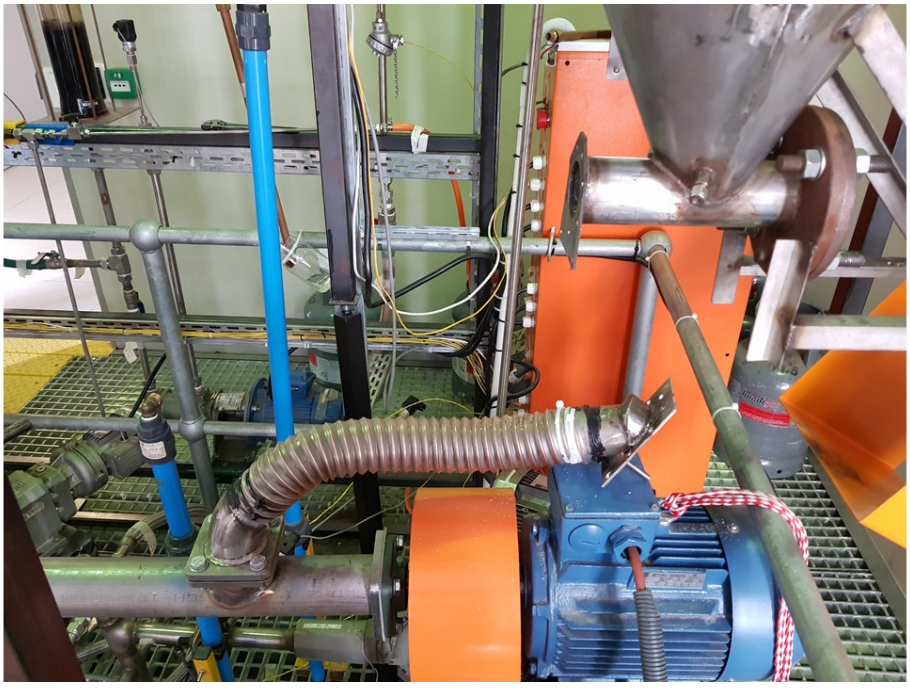

Figure 21: The original screw feeder assembly

Figure 22: The final screw feeder assembly.

With further testing, it was evident that the hopper required more agitation to feed biomass into the screw feeder for consistent flow. An eccentric motor (single-phase) was attached via rubber supports onto the base of the hopper to assist in biomass transport. This solution proved successful and the hopper was ready for consistent biomass transport. The biomass flow rate of the screw feeder was calibrated following the hopper modifications (see Section 4.2.3), and an example of the steady feed rate is shown in Section 5.1.2.

Figure 23: Side and rear view of the biomass hopper with the orange eccentric motor seated above the screw feeder coupling assembly

Machine guards were also installed around the bed return chain-and-gear assembly, and the biomass screw conveyor coupling assembly. These precautions were considered as both motors and mechanisms are a hazard to those working in close proximity to the unit. Photos of the guards are shown in Figure 24.

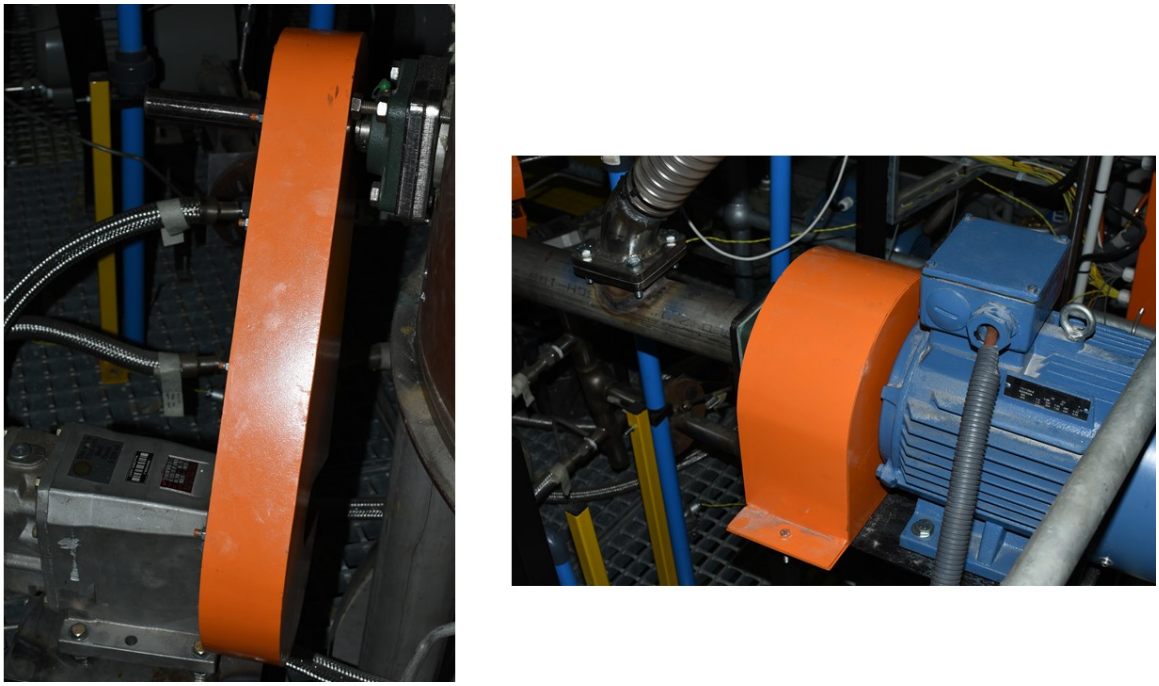

Figure 24: Left: Sand auger machine guard Right: Biomass screw conveyor machine guard

The four pressure transducers at either end of the orifice plates, for NCG recycle and combustion flow rate determination, were replaced with two Fuji Electric FCX AIII differential pressure cell transmitters, commonly known as DP cells. They are much more sensitive to pressure differentials compared to the subtraction of two transducer signals, each operating with much larger pressure ranges thus leading to a lot more noise. Photos of the two transmitters are shown in Figure 25.

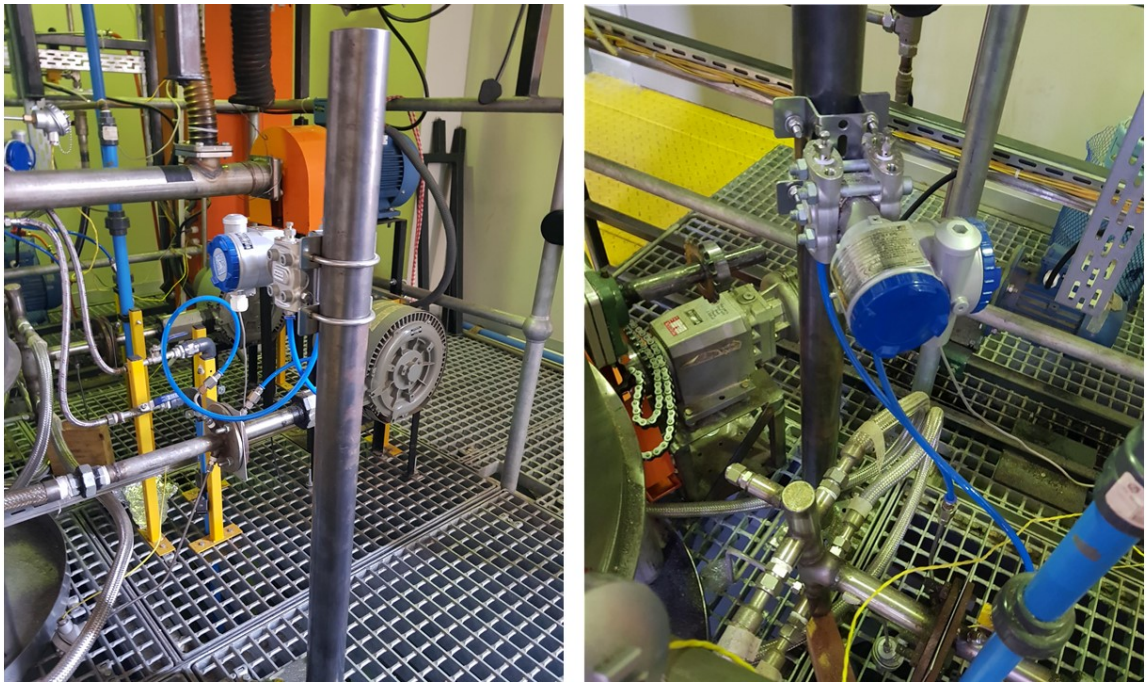

Figure 25: Differential pressure transmitters connected to the high and low pressure ends of the corner taps

4 Process operation and experimental methods

4.1 Biomass feedstock and pretreatment

The biomass chosen for this project, as for the previous iteration of the CRIPS unit, was *E. grandis*. The feedstock was delivered to the University of Pretoria in large bags of wood chips, each weighing approximately 10 to 14 kg. The wood chips were dried on delivery; nevertheless, additional drying was carried out on the first bin of wood chips as shown in Figure 26 to see how effective drying in the winter sun would be.

Figure 26: Drying of wood chips on the roof

The wood chips were rotated every few hours to ensure that all the chips were exposed to the elements. The chips were dried from 5.93 % to 5.45 % over a 6-hour period. The additional drying was considered unnecessary for the subsequent bins of wood chips as the conditions were too cold to sufficiently dry the chips by more than 0.5 % before the winter sun started to set. Bridgwater (2012) also states that typical moisture contents can go up to 10 %, with the only hindrance being the additional energy required to get the water in the wood up to pyrolysis temperatures. Details regarding the physical and chemical characteristics of the feedstock are given on in Section 5.2.1.

4.2 Commissioning

4.2.1 Introduction

Numerous methods were employed throughout the commissioning of the CRIPS 2 unit, they include:

1. Cold-runs
2. Hot-runs
3. Calibrations
4. Experimental runs

Throughout these trials, different measurements were taken and variables monitored to characterise the system. The instruments for the CRIPS 2 unit are summarised in Table 44 (Appendix B).

4.2.2 Cold and hot test runs

Before adding LPG to the combustion zone, the pyrolysis unit must undergo cold-runs to understand the system and its interactions with all the instruments. The most important information gained from the cold-runs is the fluidisation requirements for combustion and pyrolysis zones, bed loading requirements for the unit, general maintenance, and instrumental issues.

Silica sand (SiO_2: 98.7 %) was bought from a local supplier with the particle size distribution given in Figure 27. The mass of sand required for the unit was calculated from the volumes of the combustion and pyrolysis zones. Contingency was added to this calculation by assuming this volume consisted of unfluidised sand, thus a total mass of 25 kg of sand was determined for the bed of the unit.

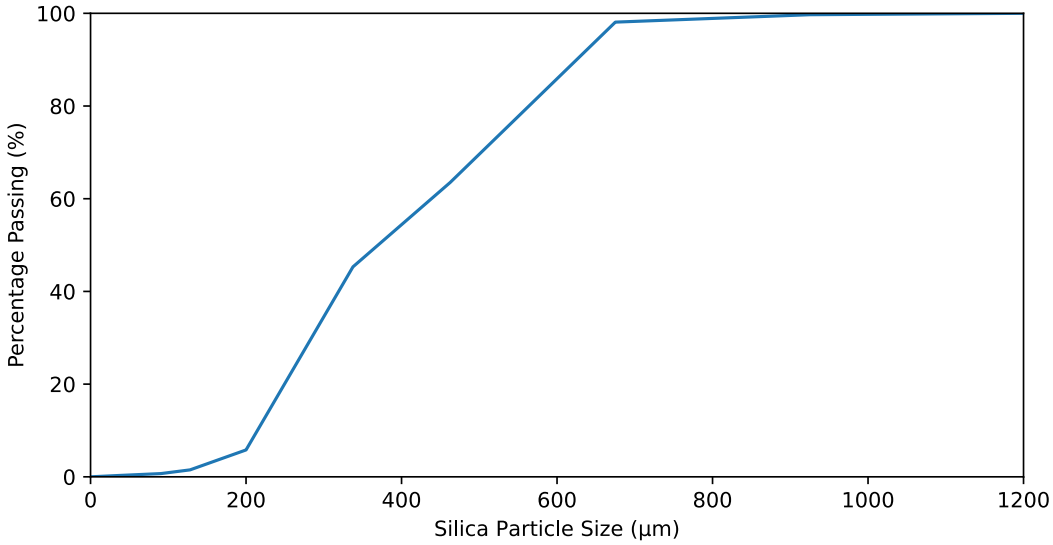

Figure 27: Cumulative particle size distribution of the silica bed

All the particle characterisation, fluidisation theory, and subsequent calculations are based on the work by Rhodes (2008). The minimum fluidisation conditions required for a silica bed with an average particle size from Figure 27 are determined at the point where the force of gravity pulling the particles down is equal to the upward force exerted on the particles via the fluidising medium. The minimum fluidisation velocity (u_{mf}) calculated using the Archimedes number (Ar), the Reynolds number at incipient fluidisation (Re_{mf}), and correlations from Wen and Yu. Equations 3 and 4 describe Ar by rearranging the Ergun equation describing the pressure drop over a packed bed:

$$Ar = 150\frac{1-\epsilon}{\epsilon^3}Re_{mf} + 1.75\frac{1}{\epsilon^2}Re_{mf}^2 \tag{3}$$

$$Ar = \frac{\rho_f(\rho_p - \rho_f)gx_{sv}^3}{\mu^2} \tag{4}$$

where ϵ is the bed voidage, ρ_p is the particle density (note the bulk bed density which is $1300\,\mathrm{kg/m^3}$), ρ_f is the fluid density (this will change with temperature and fluid composition), g is the gravitational acceleration constant of $9.81\,\mathrm{m/s^2}$, x_p is the equivalent spherical diameter of the particles, and μ is the dynamic viscosity of the fluid. Re_{mf} is described in Equation 5 by

$$Re_{mf} = \frac{u_{mf}x_p\rho_f}{\mu} \tag{5}$$

A typical approximation of $\epsilon_{mf} = 0.4$ is used as the bed voidage at incipient fluidisation is unknown. A correlation was also developed by Wen and Yu to account for the unknown voidage at minimum fluidisation conditions. It describes Ar as

$$Ar = 1652Re_{mf} + 24.51Re_{mf}^2 \tag{6}$$

The values calculated for the minimum fluidisation characteristics are summarised in Table 19 with a range of velocities from the simple approximation of $\epsilon_{mf} = 0.4$ to the correlation in Equation 6. Note that Rhodes (2008) points out that the harmonic mean of the mass distribution is equivalent to the arithmetic mean of the surface distribution and thus can be used as the hydrodynamic diameter for fluidisation calculations.

Table 19: Minimum fluidisation velocities for the combustion and pyrolysis unit

Parameter	Value
x_p	400 µm
u_{mf}: Combustion bed (25 °C)	0.13 to 0.15 m/s
u_{mf}: Combustion bed (900 °C)	0.055 to 0.065 m/s
u_{mf}: Pyrolysis bed (500 °C) [a]	0.073 to 0.085 m/s

[a] Grobler NCG composition

For maintenance reasons, the base of the combustion unit is fitted with a ball valve which allows operators to drain the bed from the unit. To remove the bed from the pyrolysis unit, the NCG recycle blower is switched on, fluidising the pyrolysis bed and rotating it to the dead zone and into the sand recycle screw. The sand recycle screw is switched on as well, allowing the sand to exit into the combustion unit and out through the valve of the base. As noted earlier, the bed is reloaded through a chute above the combustion unit. After reloading the unit with 25 kg of sand, all that mass was recovered from the pyrolysis and combustion zones.

Following the cold runs, the next step in commissioning is to perform the hot-runs where LPG is fed into the combustion unit and combusted with air. The most important information collected from the hot-runs is the LPG and combustion air pressure requirements, start-up procedures, unit safety and stability, and general diagnostics. Leaks discovered during the hot runs will be fixed using either new gaskets or a liquid gasket maker where necessary.

The first step is to devise a way to obtain consistent start-up of the combustion unit. This

consisted of adjusting the LPG pressure and combustion air flow rate. Furthermore, an appropriate ignition source had to be decided on. Many ideas were discussed from spark plugs, ignition coils, and even to pilot burners. However, the intense heat and abrasive environment of the combustion unit would eventually mean the termination of any quick fix. The final solution is the easiest, which consisted of lighting a firelighter and dropping it down the fluidised bed chute. The flame of the ignition source could then be identified by an operator looking through the combustion zone viewing port. The combustion air and LPG parameters which guaranteed consistent start-up are summarised in Table 20. These conditions provided minimum fluidisation without large bubbling or slugging which would inevitably extinguish the LPG flame.

Table 20: LPG and combustion air parameters for a successful start-up

Parameter	Value
LPG pressure (open valve)	4 to 8 kPa
Combustion air blower frequency	18 Hz
Combustion air flow rate	140 l/min

An important note for starting the reactor is that the LPG line requires a burst of pressure to remove any sand blocking the nozzle due to the pressure from the combustion air. As the start-up procedure begins with the combustion air bringing the bed to minimum fluidisation before LPG gas is introduced, the LPG nozzles can become blocked up with bed material. The unblocking procedure consists of passing 5 bar of compressed air through the LPG line (without LPG running through the line) while ramping up the combustion air flow rate. Straight after ramping the blower to 60 Hz, the combustion air is brought back down to 18 Hz and the pressure gauge (PI-102) should read close to no pressure indicating that the nozzles are open, while the compressed air is still applied to the LPG line.

4.2.3 Calibrations

Calibrations are done on the biomass feed hopper, feeder screw mechanism and differential pressure gauges prior to the commissioning of the unit. The hopper calibration is used not only to calibrate the feed rate but all subsequent experimental pyrolysis runs. The calibration was performed through the TDC550 load cell indication unit and calibration weight (3.5 kg). The hopper is emptied and zeroed on the indication unit. Next, the calibration weight is placed on the hopper and the weight entered on the indication unit.

A bin of biomass with a known mass is placed on the top of the hopper to confirm the calibration before its contents are emptied into the vessel.

The calibration of the hopper feeder screw was done by varying the frequency of the screw feeder motor while recording the change in mass via the biomass hopper's load cells. The hopper was loaded with ≈ 10 kg at the start of the calibration and was reloaded when the mass was sufficiently low. The calibration curve is shown in Figure 28.

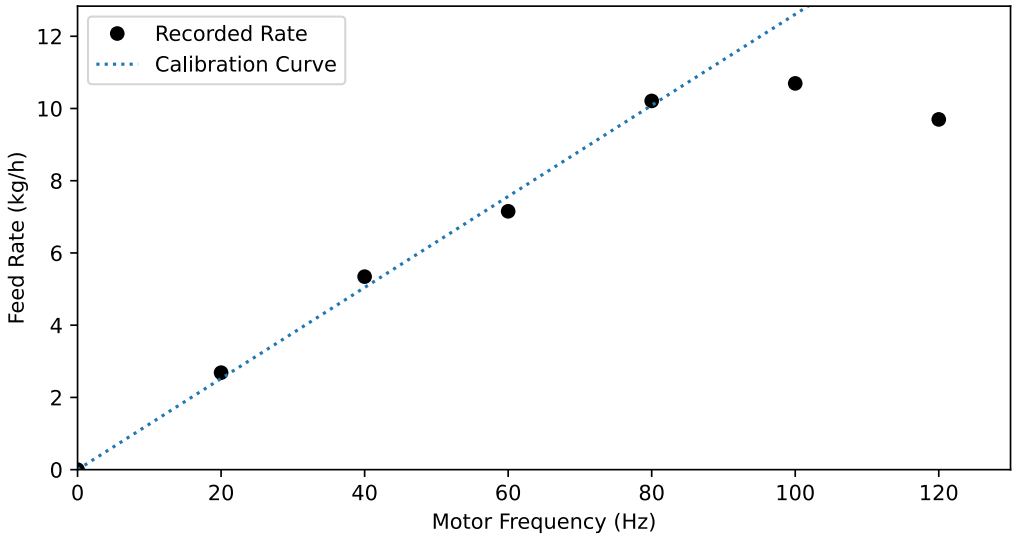

Figure 28: Calibration curve for the dry biomass flow rate and the motor frequency of the screw feeder

The torque from the motor's gearbox limits the frequency from the VFD to around 120 Hz. Below 80 Hz, the motor's rotations are very consistent with an R^2 calibration value of 0.9899. A linear calibration curve can thus be used to operate the feed rate of the biomass from a SCADA. The calibrated flow rate used also takes into account the moisture content of the wood. The moisture content of the wood charged to the hopper for calibrations was determined using ASTM D4442 – 16 (Method 2). This value was used in the development of an accurate representation of the dry biomass flow rate into the reactor compared to the frequency of the VFD operating the screw feeder motor. Equation 7 describes the linear relationship between the frequency (f) and mass flow rate of biomass ($\dot{m}_{dry}$) between 0 and 80 Hz with respect to the moisture content ($x_{moisture}$) of the chips.

$$\dot{m}_{dry} = \frac{0.1261 f}{(1 - x_{moisture})} \tag{7}$$

The last calibration involves the Fuji Electric DP cells and their measurement sensitiv-

ity. The units were delivered pre-calibrated; however, their sensitivity ranged from 0 to 13 kPa. The ranges at which the units operate were altered to take into account the sensitivity of the actual range the which cell will experience and the noise generated by the NI 9203 analogue current input modules. These ranges are tested against a known pressure such as that from a pressure-regulator coupled to a CO_2 gas cylinder. The units are also zeroed before experimental runs to ensure accurate results.

4.2.4 Pyrolysis runs

Once the CRIPS 2 unit has been calibrated and all the leaks are sealed, the experimental pyrolysis runs can begin. Wood chips, namely the *E. grandis* species used in this project, are loaded into the biomass hopper after a representative sample has been removed for analysis (see Section 4.4). One bin of wood chips (approximately 10 to 12 kg) at a time is placed in the hopper and is reloaded between runs when biomass levels are low (around 1 kg). This ensures that the feed is consistent with the representative sample taken before the run. The unit is started with LPG and combustion air at the conditions described in Table 20. Once autoignition temperature is reached (between 450 °C and 550 °C depending on the LPG cylinder used), the combustion air and LPG can be increased to the values given in Table 21. Note that as combustion takes place, the backpressure increases and the blower's frequency needs to be increased to match the flow rates required for consistent fluidisation. Furthermore, an increase in the air is required to combust the additional LPG.

Table 21: Plant parameters used at autoignition conditions

Parameter	Value
LPG pressure (open valve)	8 kPa
Combustion air blower frequency	21 Hz
Combustion air flow rate	180 l/min

After the autoignition temperature in the combustion unit has been reached, the LPG flame should be submerged in the fluidised bed with blue flashes of light being given off, indicating stoichiometric combustion conditions. At this point the flue gases, following the ash cyclone, are analysed with a KANE255 combustion gas analyser to determine the combustion efficiency and flue gas products. The information obtained from the device are compositions of oxygen, carbon dioxide, and carbon monoxide. Additionally, it can calculate the combustion efficiency based on the fuel used (in our case LPG), and the temperature of the sampled gases.

The temperature will rapidly rise to about 900 °C whereby the bed transfer begins. The pyrolysis unit will start cold as the only energy it has received is through conduction via the refractory walls separating the two units. The control is done through labVIEW, which applies proportional control to the sand recycle motor. However, as sand leaves the combustion zone to heat the pyrolysis unit, the temperature of the combustion unit decreases drastically. Therefore the sand recycle will be paused when the combustion zone achieves a minimum of 700 °C, when it can return to around 800 to 900 °C. This back-and-forth heating up of the pyrolysis unit is performed a few more times until the average temperature of the pyrolysis unit is around 500 °C with the coldest zone being above 450 °C.

Once the correct temperatures have been reached, feeding of the biomass can take place. The procedure described below was followed to achieve a consistent flow of biomass to the pyrolysis unit:

1. Check that extraction is working correctly the additional extraction tubes are placed in the appropriate locations without disturbing the hopper.
2. Turn on the spiral mixer of the hopper and set the VFD to 15 Hz.
3. Increase the biomass screw conveyor to 30 Hz (directly entered into the VFD).
4. Weigh the LPG bottles attached to the delivery line.
5. Check that the sand is controlling the pyrolysis temperatures correctly.
6. Turn on the eccentric motor to vibrate the hopper and also enter the appropriate frequency for the biomass screw feeder.

The surface temperature of the pyrolysis vapour exit pipe, biomass entrance tube, flue cyclone exit, and the reactor's outer panelling are determined using a FLIR TG165 infrared thermometer. A layer of black heat-resistant paint is sprayed onto the areas where the surface temperatures will be taken, due to the poor emissivity of stainless steel. The thin black layer will give accurate surface temperature readings without the emissivity setting on the infrared thermometer having to be changed. The measurements are taken at 15-minute intervals throughout the pyrolysis run. The thermal images are recorded on the device and can be analysed after the run. An example of the images produced is shown Figure 49 in Section 5.3.1.

Various parameters were used to determine the operating capacities of the reactor. The primary objective was to dilute the ethylene glycol from the first run to produce a nearly-pure bio-oil at the end of the project. The run parameters are summarised in Table 22 and Table 23.

Table 22: CRIPS 2 parameters used in the first set of experimental runs (note that pyrolysis unit is abbreviated as PU)

Parameter	Run-1	Run-2	Run-3	Run-4
Biomass feed rate[a] (kg/h)	5	2	2	2
NCG blower frequency (Hz)	40	40	40	40
NCG recycle flow rate (l/min)	228	228	228	228
NCG recycle flow rate in PU (l/min)	591	591	591	591
SGV base of skirting (m/s)	0.70	0.70	0.70	0.70
SGV top of skirting (m/s)	0.21	0.21	0.21	0.21
VRT[b] (s)	6.12	6.12	6.12	6.12
PU temperature (°C)	500	500	500	500

[a] Feed rate excluding experimental halts

[b] At PU conditions

Table 23: CRIPS 2 parameters used in the second set of experimental runs

Parameter	Run-5	Run-6	Run-7	Run-8
Biomass feed rate[a] (kg/h)	4	1.4	1.4	5
NCG blower frequency (Hz)	40	30	30	30
NCG recycle flow rate (l/min)	228	135	135	135
NCG recycle flow rate in PU (l/min)	591	350	350	350
SGV base of skirting (m/s)	0.70	0.41	0.41	0.41
SGV top of skirting (m/s)	0.21	0.12	0.12	0.12
VRT[b] (s)	6.12	10.33	10.33	10.33
PU temperature (°C)	500	500	500	500

[a] Feed rate excluding experimental halts

[b] At PU conditions

The biomass feeding system and the LPG feed are shut off once sufficient biomass has been transported into the pyrolysis unit. The NCG is recycled for up to 20 minutes to allow all the residual biomass in the reactor to be consumed, which will be indicated by no visible smoke in the glass cylinders of the condensing unit.

The SCADA's data for the run is saved on .lvm files (proprietary LabVIEW Measurement Files) which can later be exported into Excel spreadsheets with the help of the Python lvm-read module. Manual measurements such as the masses of the LPG cylinders are

also measured at the end of the run for mass and energy balance calculations. The bio-oil is removed from the system from a bio-oil sampling tap-off point and the bio-oil PD pump is also drained of any bio-oil in the casing. Then the combustion air blower is set to a high frequency to force out any residual bio-oil in the bio-oil cooling heat exchanger. The biochar cyclone is also emptied and its contents weighed. The NCG filter and casing are weighed and the casing is subsequently cleaned. Finally, the contents of the flue ash cyclone are emptied into a bucket. As the combustion process produces water, a lot of water condenses in the cyclone. The ash-water slurry is dried before being weighed.

4.3 Plant performance analysis

4.3.1 Mass and energy balance

The first step in performing a mass and energy balance is to define the boundaries of where the mass and energy transfers take place. Figure 29 illustrates how the mass and energy balance is performed, where CU and PU stand for the combustion unit and pyrolysis unit respectively. The incoming and outgoing mass streams are indicated by straight arrows, heat loss by a curved arrow, and the system boundary by a dotted red border. It was decided that the boundary of the outgoing stream of pyrolysis products would be just before the biochar cyclone, which means that the calculations will not be affected by the condensing unit. Mass flow data are collected from measured variables during an experimental run or calculated from the measured variables to achieve minimal error in the mass balance. The energy flows are determined by the temperatures measured, the heat capacities of the streams and their components, the higher heating values of the streams and their components, and finally the heat losses. Another solution would be to overfill the combustion unit with sand to ensure that the overflow holes are consistently filled with sand during operation, consequently limiting the possibility air leakage.

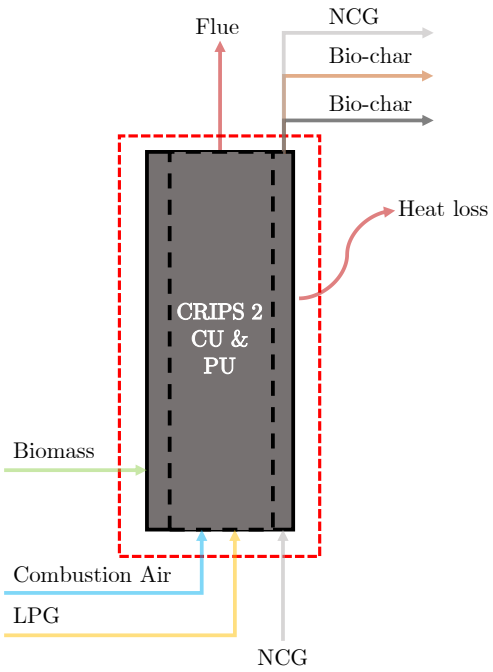

Figure 29: Illustration of the mass and energy balance for the CRIPS 2 unit with the boundary shown by a dotted red line

The following assumptions are used in the mass and energy balance:

- The moisture content in the air is negligible and thus moisture in the flue gas is determined from the free moisture and combustion alone.
- Negligible accumulation occurs in the reactor unit.
- All the water from the pyrolysis unit is condensed and thus the NCG returning to the pyrolysis unit has a negligible water content.

The overall mass balance for the system is determined by Equation 8:

$$\frac{dm}{dt} = \dot{m}_{\text{in}} - \dot{m}_{\text{out}} \tag{8}$$

where $\frac{dm}{dt}$ is the accumulation of mass in the control volume, $\dot{m}_{\text{in}}$, is the incoming mass stream, and $\dot{m}_{\text{out}}$ is the outgoing mass stream. As the unit will be operating at steady state in terms of the masses, the accumulation term is zero: $\frac{dm}{dt} = 0$. Considering the complexities of the components in the system, the mass balance worked on the elemental compositions of incoming and outgoing streams, thus there is no need to consider the effects of reaction rates. The elemental mass balance is given by Equation 9:

$$\sum \dot{m}_{i_{\text{in}}} = \sum \dot{m}_{i_{\text{out}}} \tag{9}$$

where $\dot{m}_{i_{\text{in}}}$ is the incoming mass flow of element i and $\dot{m}_{i_{\text{out}}}$ is the outgoing mass flow of element i.

Following the mass balance calculations, the energy calculations can be done. The overall energy balance for the CRIPS 2 unit is given in Equation 10:

$$\frac{dE_{\text{system}}}{dt} = -Q_{\text{loss}} - Q_{\text{rxn}} - W + \dot{E}_{i_{\text{in}}} - \dot{E}_{i_{\text{out}}} \tag{10}$$

where $\frac{dE_{\text{system}}}{dt}$ is the accumulation of energy within the system boundaries, Q_{loss} is the heat loss, Q_{rxn} is the heat generated by chemical reactions, W is work done by the system, $\dot{E}_{i_{\text{in}}}$ is the energy entering the system in the incoming mass flow, and $\dot{E}_{i_{\text{in}}}$ is the energy leaving the system in the outgoing mass flow. No work is done by the system on the environment, so $W = 0$ and the water leaving the system will be in the gas phase ($T > 100\,^{\circ}\text{C}$) and the latent heat of evaporation must be accounted for, therefore Equation 10 is simplified to:

$$\dot{E}_{i_{\text{in}}} = Q_{\text{loss}} + \dot{E}_{i_{\text{out}}} + Q_{\text{rxn}} + \lambda_{\text{H}_2\text{O}} \tag{11}$$

The incoming and outgoing energy flows by the components are computed using component enthalpies and the HHV of the component. By doing this, the combustion energy or lack thereof is already computed by the balance of the energy flows (Equation 12).

$$\dot{E}_{i_x} = \dot{m}_{i_x} c_{p_{i_x}} (T_{i_x} - T_{ref}) + \text{HHV}_i \tag{12}$$

where $\dot{E}_{i_x}$ is the energy flow of component i with x as a placeholder for in/out, $\dot{m}_{i_x}$ is the flow rate, $c_{p_{i_x}}$ is the averaged heat capacity of component i between the reference temperature and the stream temperature, T_{i_x} is the stream temperature in which the component exists, T_{ref} is the reference temperature ($25\,^{\circ}\text{C}$), and HHV_i is the higher heating value of the component.

4.3.2 Heat loss determination

Calculating the heat lost to the environment involves several heat transfer equations and the data captured throughout the runs. The first scenario that will be discussed is the

conduction through the walls inside and surrounding the CRIPS 2 unit. A radial slice of the CRIPS 2 unit is visualised in Figure 30, which aids in understanding the heat transfer calculations. Note that the stainless steel shell and panelling are indicated in the diagram by thick black lines on either side of the the insulation layers as their thicknesses are a mere 1.5 mm. The layer properties are detailed in Table 24.

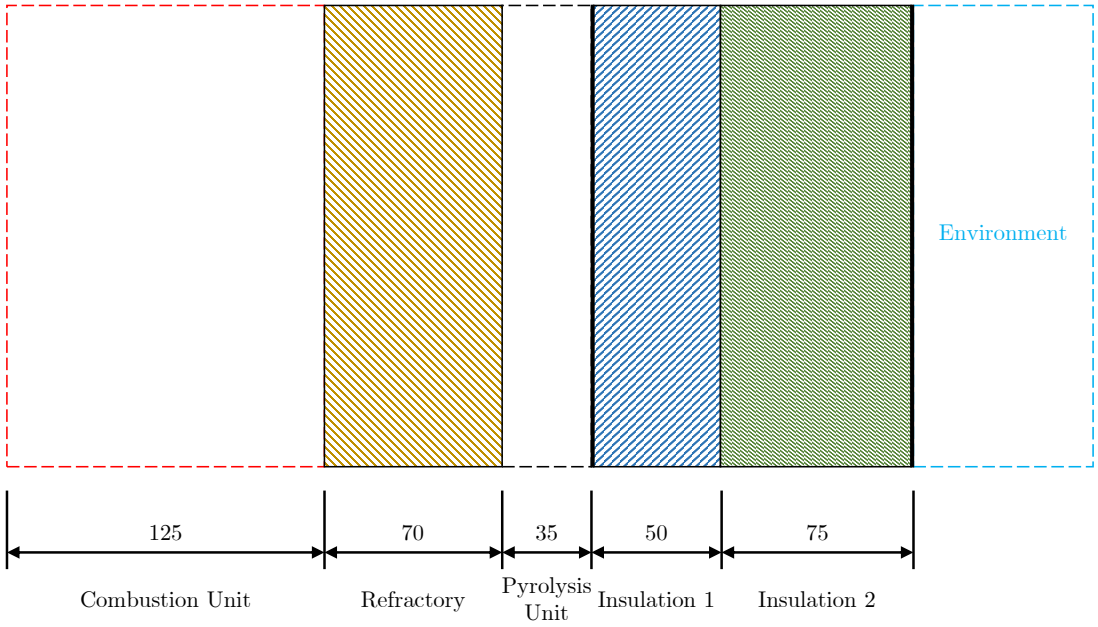

Figure 30: A cross-section of the CRIPS 2 unit illustrating the resistance network (units are in mm) Left to right: Centre of combustion unit (centre of CRIPS 2 unit) to the edge of the CRIPS 2 unit

Table 24: Thermal properties of the layers in Figure 30

Layer	Thermal Conductivity (W/(m K))	Thickness (mm)
Base refractory: ACTlite HC TC	0.50	70
Upper refractory: ACTlite 40c TC	0.29	70
Stainless steel	15.60	1.5
Inner insulation	0.12	50
Outer insulation: ISOVER U Thermo Matt	0.10	75

All the equations and theory of conductive and convective heat transfer are based on the work by Çengel & Ghajar (2015). One-dimensional and steady-state heat transfer is assumed for the radial heat transfer in the reactor units. It is also assumed that

the bed is sufficiently well mixed such that the reactor wall temperatures are equal to the fluidised bed temperatures. With these assumptions, Equation 13 can be used to determine the heat transfer through the walls between the cylindrical reaction zones and the environment.

$$\dot{Q}_{Refr.} = \frac{T_{CU(outer)} - T_{PU(inner)}}{R_{Refr.}} \tag{13}$$

The heat transfer ($\dot{Q}_{Refr.}$) is calculated between the combustion unit and the pyrolysis unit with corresponding temperatures, $T_{CU(outer)}$ and $T_{PU(inner)}$ respectively. The refractory's resistance ($R_{Refr.}$) is calculated in Equation 14:

$$R_{Refr.} = \frac{\ln(r_1/r_2)}{2\pi L k_{Ref.}} \tag{14}$$

where r_1 is the outer edge of the combustion unit, r_2 is the inner edge of the pyrolysis unit, L is the length of the cylinder, and k is the thermal conductivity of the refractory material.

A similar set of equations, Equation 15 and Equation 16, are used to determine the heat leaving the pyrolysis unit towards the environment:

$$\dot{Q}_{Ins.} = \frac{T_3 - T_7}{R_{Ins.}} \tag{15}$$

Similarly, the heat transfer ($\dot{Q}_{Ins.}$) is calculated between two temperatures. In this case, the pyrolysis unit and the reactor's external temperatures (T_3 and T_7 respectively) are used to solve for the temperatures in between the reactor's shell and layered insulation using the known thermal conductivities of every component in the heat transfer pathway. The refractory's resistance ($R_{Ins.}$) is calculated by Equation 16:

$$R_{Ins.} = \frac{\ln(r_3/r_4)}{2\pi L k_{SS}} + \frac{\ln(r_4/r_5)}{2\pi L k_{Ins.-1}} + \frac{\ln(r_5/r_6)}{2\pi L k_{Ins.-2}} + \frac{\ln(r_6/r_7)}{2\pi L k_{SS}} \tag{16}$$

where r_3 is the outer edge of the pyrolysis unit, r_4 is the inner edge of the first layer of insulation (the outer edge of the stainless steel shell), r_5 is the inner edge of the second layer of insulation, r_6 is the outer edge of the second insulation (the inner edge of the reactor's stainless steel panelling), r_7 is the outer edge of the reactor's stainless steel panelling, and L is the length of the cylinder. The thermal conductivities of the stainless

steel shell/panelling and insulation (layers 1 and 2) are given by k_{SS}, $k_{Ins.-1}$, and $k_{Ins.-2}$ respectively.

The two other areas on the CRIPS 2 unit where heat losses to the environment will occur are the biomass conveyor tube and the top surface of the unit. The heat lost from these two locations can be calculated via natural convection and radiation heat transfer, whereas the convection and radiation components of the vertical panelling are not required as there are sufficient internal and surface temperature data. The radiation emitted by the surfaces of the CRIPS 2 unit can be described by Equation 17.

$$\dot{Q}_{rad} = \epsilon_{rad}\sigma A_s(T_s^4 - T_{surr}^4) \tag{17}$$

where $\dot{Q}_{rad}$ is the rate of radiative heat loss, ϵ_{rad} is the emissivity of the surface, σ is the Stefan-Boltzmann constant ($\sigma = 5.670 \times 10^{-8}\,\mathrm{W/m^2K^4}$), A_s is the external surface area, T_s and T_{surr} are the surface and surrounding temperatures respectively. The convective heat transfer is calculated with the convective heat transfer coefficient (h) through the use of the Nusselt number (Nu). The relationship between the two is described as

$$Nu = \frac{hL_c}{k} \tag{18}$$

where L_C is the characteristic length of the surface being analysed, and k is the thermal conductivity of the fluid (in this case air). As natural convection occurs due to the change in the buoyancy of the surrounding fluid due to the heat transfer from the surface, the Rayleigh number (Ra_L) is used to describe the relationship with the buoyancy of the fluid and the dynamic viscosity (ν) as shown in Equation 19:

$$Ra_L = \frac{g\beta(T_s - T_\infty)L_c^3}{\nu^2}Pr \tag{19}$$

where g is the gravitational acceleration, β is the coefficient of volume expansion which is the inverse of the average fluid temperature (T_f) in Kelvin ($\beta = 1/T_f$), and Pr is the Prandtl number. Empirical correlations are used for the Nusselt number in specific scenarios and will be applied to the sections of the unit experiencing natural convective heat loss. The first scenario is described in Equation 20 (for $10^4 < Ra < 10^7$) and Equation 21 (for $10^7 < Ra < 10^{11}$) for a horizontal plate where the upper surface is hot, i.e. the top surface of the CRIPS 2 unit.

$$Nu = 0.59Ra_L^{1/4} \tag{20}$$

$$Nu = 0.1Ra_L^{1/3} \tag{21}$$

The second scenario is described in Equation 22 for a horizontal cylinder where the entire surface is hot, i.e. the biomass feed conveyor tube.

$$Nu = \left\{ 0.6 + \frac{0.387Ra_D^{1/6}}{[1 + (0.559/Pr)^{9/16})]^{4/9}} \right\}^2 \tag{22}$$

Finally, the heat transfer due to natural convection can be determined using Equation 23.

$$\dot{Q}_{\text{conv}} = hA_s(T_s - T_\infty) \tag{23}$$

The locations where the temperatures on the reactor unit are measured to determine accurate surface temperatures are illustrated in Figure 31. Note that the X in the side view of Figure 31 corresponds to the temperature transmitter number as the temperature reading areas are at the same height at 120° angles relative to each other, i.e. x is in place of 3, 4, and 5. Other areas coated with a layer of black paint for thermal analysis is the biomass screw conveyor, the pyrolysis vapour piping (before and after the biochar cyclone), and the flue gas cyclone.

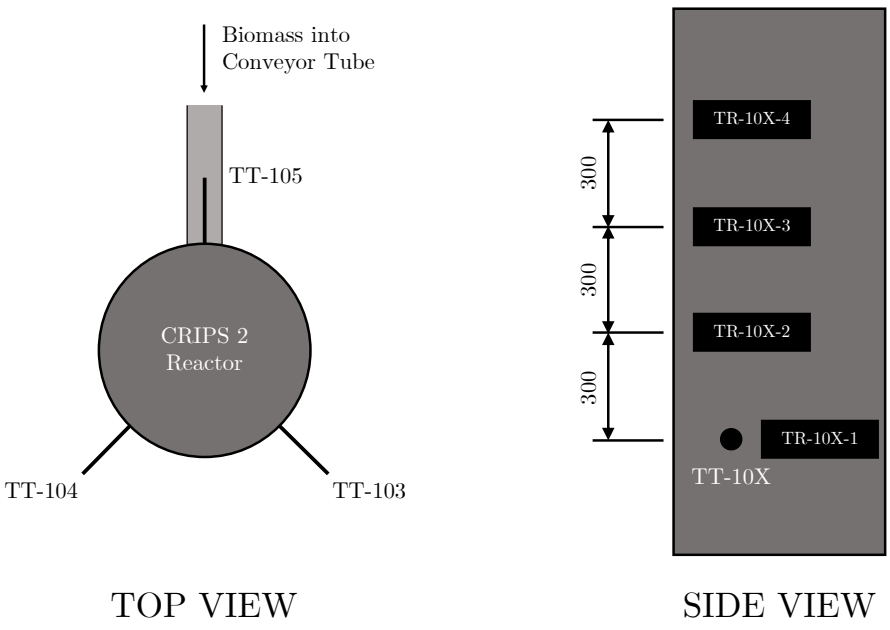

Figure 31: Illustration of the CRIPS 2 reactor unit indicating temperature transmitter location (top view) and corresponding temperature reading locations (side view), units are in mm

.

Figure 32: Photos of the temperature reading locations (black rectangles) Left to right: TR-103, TR-104, and TR-105

4.3.3 Air preheater efficiency

The air preheater efficiency is calculated using heat exchanger calculations provided by Çengel & Ghajar (2015). One can calculate the total energy transferred ($\dot{Q}$) by the heat exchanger by using the flue gas flow rate ($\dot{m}_{\text{flue}}$), the incoming and outgoing flue gas temperatures ($T_{\text{flue}_{\text{in}}}$ and $T_{\text{flue}_{\text{out}}}$) and its respective averaged heat capacity ($c_{p_{flue}}$) with Equation 24.

$$\dot{Q} = \dot{m}_{\text{flue}} c_{p_{\text{flue}}} (T_{\text{flue}_{\text{in}}} - T_{\text{flue}_{\text{out}}}) \tag{24}$$

Once the energy transferred is known, the same equation can be used to determine the outgoing combustion air temperature, assuming all the energy is transferred to the air. This is done by exchanging T_{fluein}, T_{flueout}, $c_{p\text{flue}}$, and $\dot{m}_{\text{flue}}$ with $T_{\text{air}_{\text{out}}}$, $T_{\text{air}_{\text{in}}}$, $c_{p\text{air}}$, and $\dot{m_{\text{air}}}$ respectively. Now that all the temperatures are known, the log mean temperature difference can be calculated using Equations 25, 26 and 27.

$$\Delta T_{LM} = \frac{\Delta T_1 - \Delta T_2}{\ln(\Delta T_1 / \Delta T_2)} \tag{25}$$

where,

$$\Delta T_1 = T_{\text{flue}_{\text{in}}} - T_{\text{air}_{\text{out}}} \tag{26}$$

$$\Delta T_2 = T_{\text{flue}_{\text{out}}} - T_{\text{air}_{\text{in}}} \tag{27}$$

Finally, the overall heat transfer coefficient (U) can be determined using the log mean temperature difference, the surface area of the heat exchanger (A_s), and the heat transfer in Equation 28.

$$\dot{Q} = U A_s \Delta T_{LM} \tag{28}$$

4.4 Feedstock and product characterisation

4.4.1 Introduction

Various methods were employed to characterise the biomass feedstock and the products from the commissioning of the CRIPS 2 unit. These methods are outlined in Sections 4.4.2 to 4.4.9. However, the same methods of analysis were utilised for several samples, and

some only for one. The results from the CRIPS 2 unit will be compared to the aforementioned literature values, the CRIPS 1 unit, a mobile demonstration CRIPS unit by AA Boateng *et al* (2019), and the data obtained from the spouted bed reactor (SBR) unit which was also developed by the Department of Bioprocessing (University of Pretoria). The SBR unit is a smaller laboratory scale pyrolysis rig which allows for easier testing of various feedstocks and catalysts. Table 25 summarises the methods used for analysis and subsequent characterisation.

Table 25: Samples and their corresponding methods used for analysis marked with an X

Analytical Method	Biomass	Bio-oil	Bio-char	NCG	Ash
Particle size	X		X		
Moisture content	X	X	X		X
Ash content	X		X		X
ICP-OES	X		X		X
TGA	X		X		X
Bomb calorimetry	X	X	X		
BET	X		X		
GC				X	
Proximate Analysis		X			
Ultimate Analysis		X			

4.4.2 Particle size analysis

The particle size distribution was determined via a set of sieve trays and a Filtra Vibración IRIS FTL-0300 sieve shaker. The following sieves were utilised for both the biochar and the wood chips: 2.36 mm, 1.7 mm, 1 mm, 500 µm, 300 µm, 250 µm, 150 µm, 125 µm, 90 µm, and 75 µm (ASTM E11-95). A sieve base was used to collect the fines from the smallest sieve tray following the final tray.

The quartering method was employed to obtain a representative sample of each of the wood chip bins. For every bin of wood chips, its entire contents were placed on a plastic sheet in a mound. The mound is subsequently separated along its vertical and horizontal axes starting from the centre of the pile which produces four individual quarters. Two of the quarters are removed and the two remaining piles are mixed into one another and the process is repeated itself until a manageable sample remains (see Figure 33 for reference). This procedure also allows a representative sample for the moisture and ash content analysis to be collected.

Figure 33: Example of the quartering method employed to obtain a representative biomass sample

4.4.3 Moisture content analysis

For the solid samples, the moisture content was determined with the ASTM D4442-16 method (specifically Method B). For the wood chips, three samples were removed from the quartered bin to ensure a representative sample, and placed in glass bottles. The bottles were weighed both with and without the biomass before being placed in a LABOTEC EcoTherm convection oven at 103 °C.

For the bio-oils, the moisture content was determined using Karl-Fischer titration. The instrument that was utlised for the analsysis was a Metrohm 701 KF Titrino. Bruce Sithole and his team from the CSIR kindly performed the analysis for the bio-oil moisture content.

4.4.4 Ash content and analysis

The ash content was determined with the ASTM D1102-84 method. This method was applied to all the solid samples fed to and produced from the CRIPS 2 unit, i.e. the starting biomass, the cyclone, ash, and the wood-based biochar samples. Around 2 g of sample is placed in a pre-weighed crucible, following a drying session at 600 °C. The sample and crucible are then placed in a CARBOLITE AAF 1100 ashing furnace set to

600 °C. It was determined that around four hours wouldbe needed to successfully combust all the carbonaceous material in the sample. This was confirmed by removing the sample from the oven and letting it dry in a desiccator. Following the cooling, the sample was weighed. If no significant mass change was noted at half-hourly intervals of ashing, then the sample was deemed to be completely ashed.

ICP-OES was used to determine the inorganic components in the ash. Firstly, the ashed samples were digested in a 1:1 solution of 32 % hydrochloric acid and de-ionised water (total volume of 20 mL). This solution was then mixed and kept at 80 °C via a hot water bath.

Figure 34: Left: Ash samples post-drying Right: Digestion of ash in hot concentrated HCl

Next, the solution is vacuum filtered and the collected solution is diluted to 500 mL for analysis. The samples were analysed using a SPECTRO ARCOS ICP-OES with the following elements included in the calibration standards: K, Ca, Al, Fe, Mg, O, Co, Cr, Ca, Mn, Ni, S. By determining the most prevalent inorganic element in the ash of the woody biomass and quantifying this quality, one can determine the biomass-related ash content in the biochar, with the balance being the silica content.

4.4.5 Proximate analysis

The proximate analysis comprises of the moisture, volatile, fixed carbon and ash content of a sample. All of these can be determined with the use of a thermogravimetric analyser

(TGA). TA compared the use of a TGA with traditional ASTM methods in determining the proximate analysis. It was found to be a much quicker method of analysis without losing accuracy (TA Instruments, 2020). The TA TGA5500 was used for the proximate analysis. The instrument was set to Hi-Res mode with a heating rate of 50 °C/min which allowed incredibly accurate thermogravimetric analysis. Nitrogen was used initially until 900 °C, at which point the inert gas was switched to air, allowing combustion to occur. The procedure starts with approximately 20 mg of the sample being weighed out and placed in an alumina crucible on a platinum pan. The sample is then placed on an auto-sampler and undergoes the aforementioned heating procedure.

4.4.6 Ultimate analysis

The ultimate analysis comprises of the carbon, hydrogen, oxygen, nitrogen and sulphur content of a sample. This information was determined through the use of a Perkin Elmer CHNSO Series II 2400 instrument. Bruce Sithole and his team from the CSIR kindly performed the ultimate analysis determination for various samples.

4.4.7 Higher heating value analysis

The higher heating value (HHV) was determined using a Parr 6200 Isoperibol Calorimeter coupled to a Parr Water Handling System for bomb water replacement. Samples were carefully weighed and inserted into a bomb and pure oxygen was introduced at a pressure 30 bar. Next, the bomb was submerged in a predetermined amount of water dispensed via the water handling system. If the sample was known to have either a low heating value or was difficult to ignite, a spike of benzoic acid was added to the sample to create successful ignitions and thus successful and accurate results.

As noted in Section 4.2.4, the liquid in the cooling loop was not be replaced with ethylene glycol after every run but with a portion of the previous run's bio-oil product. This ensures a more accurate analysis of the bio-oil product after a few runs as the solvent becomes more dilute. Therefore the composition and thus higher heating values of the fresh oil will have to be adjusted to take into account the dilution not only of the ethylene glycol solvent from the first run, but also the bio-oil from the previous runs. Equations 29 and 30 were used to determine the adjusted HHV of the bio-oil, the water composition, and the ideal bio-oil composition (based on a 'typical' bio-oil containing 12 % reaction water with an HHV of 17.5 MJ/kg (Bridgwater, 2013)):

$$\mathrm{HHV}_{\mathrm{Mixture}} = (\mathrm{HHV}_{EG})(x_{EG}) + (\mathrm{HHV}_{BO})(x_{BO}) \tag{29}$$

where $\mathrm{HHV}_{\mathrm{Mixture}}$ is the HHV of the as-produced mixture, HHV_{EG} is the HHV of the ethylene glycol (19.15 MJ/kg), HHV_{BO} is the HHV of the produced bio-oil, x_{EG} is the mass fraction of ethylene glycol in the mixture, and x_{BO} is the mass fraction of the bio-oil in the mixture. Assuming the bio-oil (including the moisture) and ethylene glycol are the only compounds in solution, the following relationship is true: $x_{EG} + x_{BO} = 1$. The non-pyrolytic water is determined by

$$\mathrm{HHV}_{BO} = (\mathrm{HHV}_{\mathrm{ideal}})(x_{\mathrm{typical}}) + (\mathrm{HHV}_{\mathrm{H_2O}})(x_{\mathrm{H_2O}}) \tag{30}$$

where $\mathrm{HHV}_{\mathrm{typical}}$ is the typical HHV for bio-oils noted above, $\mathrm{HHV}_{\mathrm{H_2O}}$ is the higher heating value of water (0 MJ/kg), x_{typical} is the calculated mass fraction of the typical bio-oil, and $x_{\mathrm{H_2O}}$ is the calculated mass fraction of non-pyrolytic water in the bio-oil produced. The typical bio-oil and non-pyrolytic water form a binary system in the BO fraction where $x_{typical} + x_{\mathrm{H_2O}} = 1$ is assumed.

A similar procedure using combustible energy is employed for the non-biomass ash (bed material) content in the biochar samples as shown in Equation 31, where $\mathrm{HHV}_{\mathrm{ash-freeBC}}$ is the HHV for dry and ash-free biochar, HHV_{BC} is the dry biochar without silica, (x_{BC}) is the mass fraction of the biochar without silica, $(\mathrm{HHV}_{\mathrm{ash}})$ is the higher heating value of silica ash (0 MJ/kg), and (x_{ash}) is the corresponding mass fraction.

$$\mathrm{HHV}_{\mathrm{ash-freeBC}} = (\mathrm{HHV}_{BC})(x_{BC}) + (\mathrm{HHV}_{\mathrm{ash}})(x_{\mathrm{ash}}) \tag{31}$$

4.4.8 Surface area analysis

The surface area was determined using a Micromeritics TriStar II BET analyser. Samples for analysis were loaded into the BET tubes, filling at least half of the bulb, and dried extensively using the Micromeritics VacPrep 061 at 103 °C. After a day of drying, the sample tubes were attached to the TriStar II, and liquid nitrogen loaded was into the machine's dewer. After the sample preparations have been done, the analysis is a hands-free operation.

4.4.9 Gas analysis

The non-condensable gases were analysed via a sampling point after the recycle blower. SKC sample bags were initially purged with pure nitrogen before being used to purge

the sampling line. Following this, the sample bag was filled with recycled NCG and its sample was subsequently analysed using a Varian STAR 3400 CX gas chromatograph (GC). To quantify the concentrations of the compounds in the NCG, mixtures with known concentrations of known pyrolysis NCG compounds were also analysed. These results are summarised in Table 26.

Table 26: Calibrations used for GC analysis

Component	Determination
O_2	Based off >99.9 % purity sample.
N_2	Based off >99.9 % purity sample.
CO_2	Based off >99.9 % purity sample.
CO	Based off 95 % purity sample (CO_2 as balance).
CH_4	Based off heat capacity ratio.

5 Results and discussion

The CRIPS 2 pilot unit was successfully operated on eight occasions with the products of the first two runs combined. Note that throughout the results section, a samples identity is linked to the corresponding run, for example Bio-oil-4 signifies the bio-oil collected after the fourth run, i.e. Run-4.

5.1 Plant operation

5.1.1 Start-up

The start-up of the CRIPS 2 unit is relatively easy if the correct procedures and parameters are used. The LPG required for start-up was around 1 kg/h with start-up times averaging 4 to 5 h. Experimental runs were also planned to be done close to each other to take advantage of the retained thermal energy from the previous run. Typical temperatures of the pyrolysis and combustion units are shown in Figure 35, where the bed transfer affects the combustion bed temperatures. Initially, there is no bed transfer (for the first $\approx$ 110 minutes) so that the combustion bed can sufficiently warm up and therefore the increase in temperature in the pyrolysis bed is only caused by conduction through the combustion refractory walls. Figure 35 illustrates this with a gradual increase in the temperature of the pyrolysis bed compared to a much sharper increase in the temperature of the combustion bed. Once the bed transfer is initiated, the hot sand leaving the combustion unit is replaced with cold sand from the pyrolysis unit. The energy transferred is significantly higher when the pyrolysis bed is cold. It is interesting to note that the sharp peaks on the graph indicate the bed transfer between the combustion and pyrolysis units. As the pyrolysis temperature bed temperature increases, we see a sharp decrease in the combustion bed.

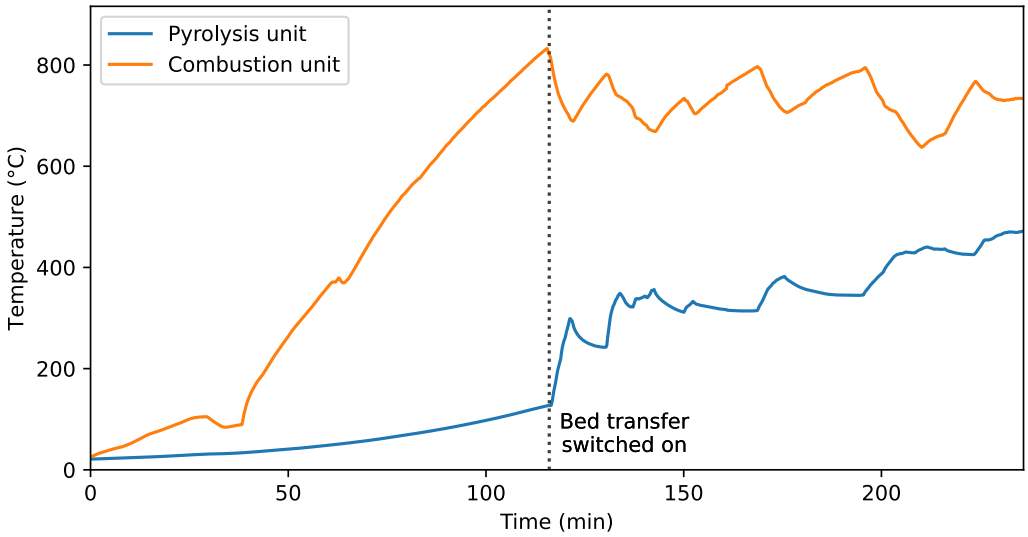

Figure 35: Comparing the typical temperatures of the combustion and pyrolysis beds during start-up

The combustion air flow rate for the same run is shown in Figure 36. It is interesting to note that just before the 50-minute mark in Figure 35 the temperature of the bed suddenly increases, which correlates with the increase in blower frequency in Figure 36. The frequency of the combustion air blower was manually increased to reach incipient fluidisation velocities which would help the bed mix better, and thus we see the temperature increasing rapidly. The correlation between the blower speed is directly proportional to the flow rate of air entering the system The noise in the data is due to the sensitivity of the instruments. The changes in the blower speed setpoints are performed manually and are reduced during biomass feeding to reduce the oxygen in the system while retaining the fluidisation of the combustion bed.

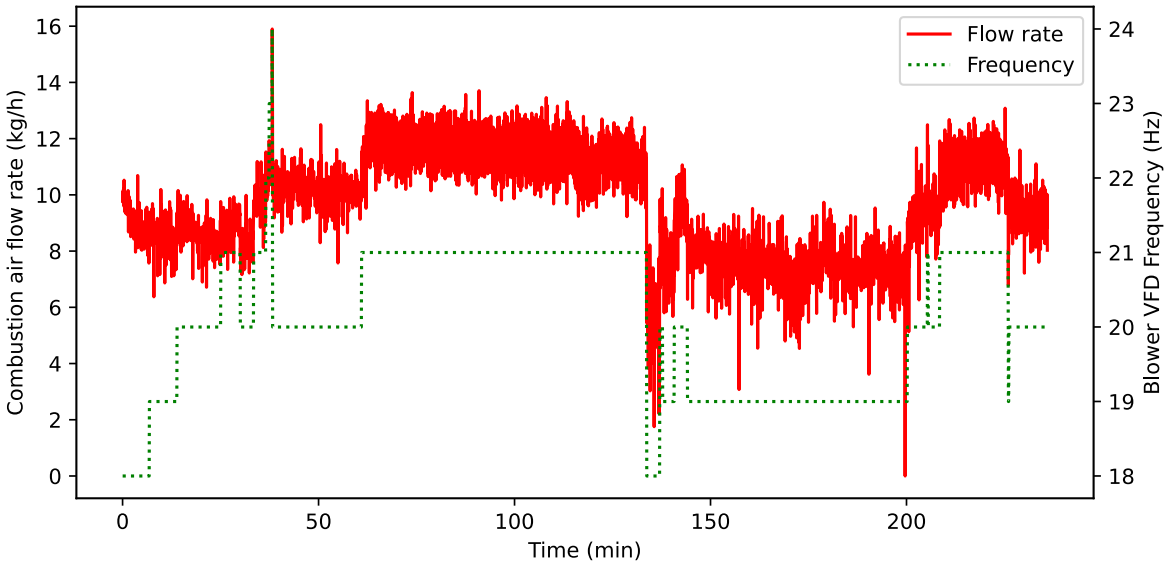

Figure 36: Typical combustion blower flow rate and VFD frequency set-point

The flue gas analysis and LPG usage for the start-up procedures are summarised in Tables 27 and 28. Higher LPG flow rates were used in the later experimental runs as the unit was controlled better and therefore the start-up times could be reduced.

Table 27: Flue gas analysis

Parameter	Run-1	Run-2	Run-3	Run-4	Run-5	Run-6	Run-7	Run-8
O_2 v/v%	9.2	5.6	8.9	5.5	4.2	5.2	4.6	5.6
CO_2 v/v%	7.9	10.3	8.1	10.6	10.9	10.4	10.9	10.1
CO (ppm)	>3970	>3923	>3912	2360	>3957	>3854	>3866	>3860
Temperature (°C)	45.7	47.8	49.7	49.3	59.9	49.3	49.1	52.2

Table 28: Average LPG flow rates during the start-ups for the experimental runs

Parameter	Run-1	Run-2	Run-3	Run-4	Run-5	Run-6	Run-7	Run-8
LPG flow rate (kg/h)	0.44	0.66	0.74	1.13	1.34	0.90	0.90	1.27

Images taken through the combustion viewing port are shown in Figure 37. The combustion bed temperature also rises rapidly after the bed reaches the autoignition temperatures of LPG (450 to 550 °C). The ignition of the LPG and combustion air sinks

into the fluidised bed, which both stabilises the combustion flame and guarantees a high combustion efficiency.

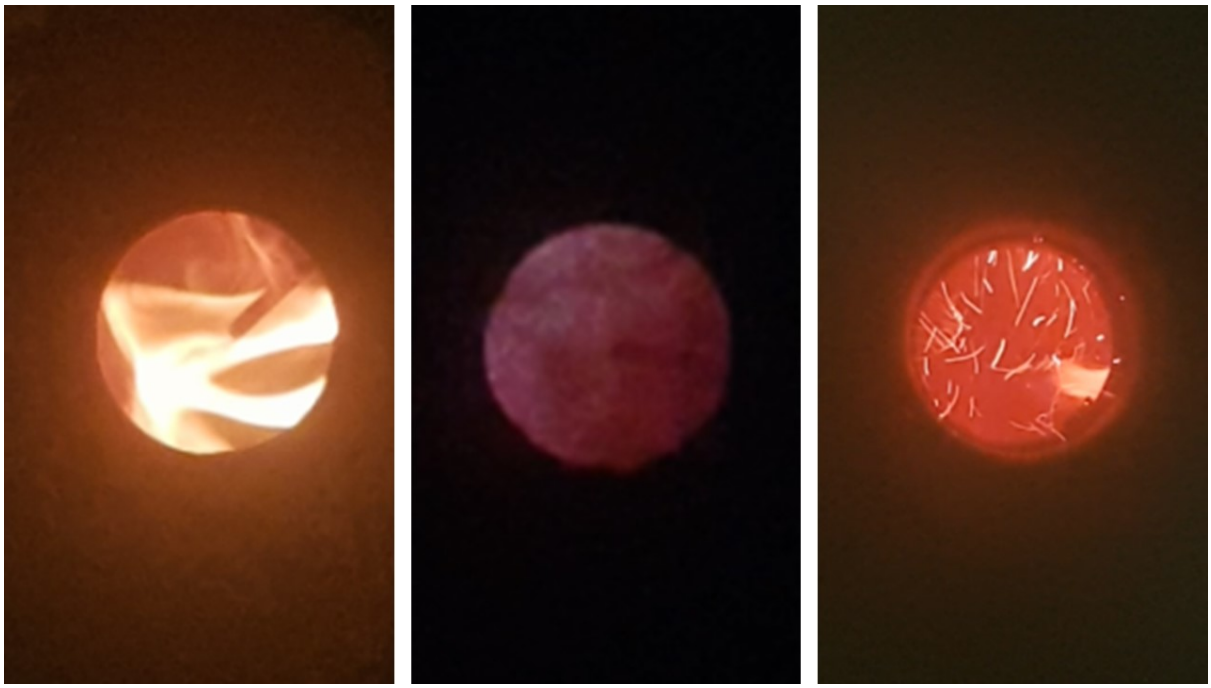

Figure 37: Left: Combustion of LPG below autoignition temperatures Centre: Combustion of LPG above autoignition temperatures Right: Combustion of the biochar during bed transfer

5.1.2 Pyrolysis

Once the average temperature of the pyrolysis bed was above 450 °C **and** the entrance to the pyrolysis unit was above 500 °C, the procedure for wood chip feeding began. The control of the pyrolysis bed temperature was based on the rate of bed transfer governed by the screw revolutions per minute. The temperature of the combustion bed, pyrolysis bed, and the associated bed transfer frequency for controlling the temperatures is illustrated in Figure 38. The increase in the pyrolysis bed temperature is directly correlated with the sand transfer rate and therefore the unit can be sufficiently controlled. During the lower through-put runs (Run-6 and 7), the sand transfer is noticeably lower. This is because of the lower energy requirements for biomass pyrolysis, i.e. less energy is taken up by a lower biomass flow rate and therefore less sand is required. The combustion air and LPG feed rates are decreased so a sufficient level whereby the temperature of the combustion bed is constant and the bed remains fluidised. The fluidisation halts when insufficient air is fed to the unit.

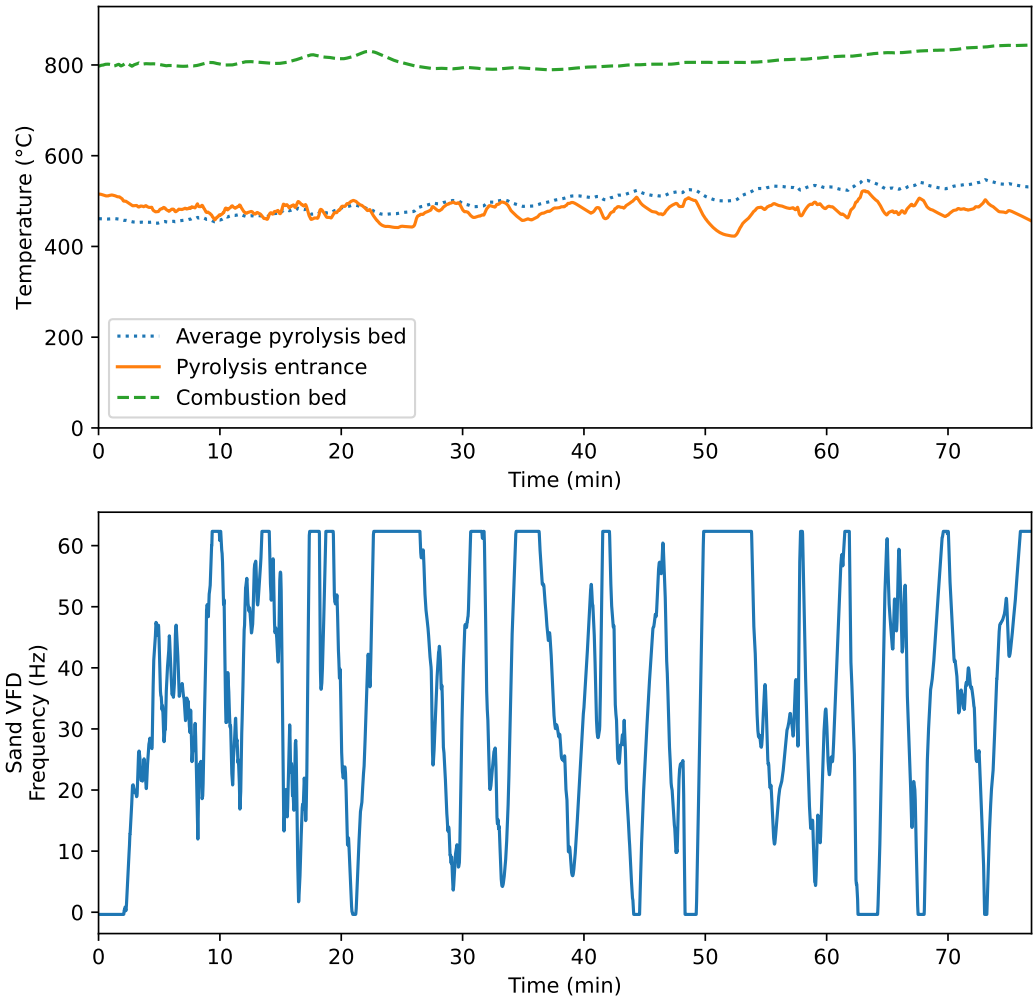

Figure 38: Typical temperatures of the combustion and pyrolysis unit, and bed transfer VFD control during the pyrolysis stage of the run

The flow of the pyrolysis product is immediately noticeable when the biomass feeding mechanism is switched on. Figure 39 shows the condensation unit in operation, with the opaque vapours entering the quenching unit at the top left. A very viscous product is also formed (image on the right) which did not seem to dissolve in the bulk flow of the recirculation fluid.

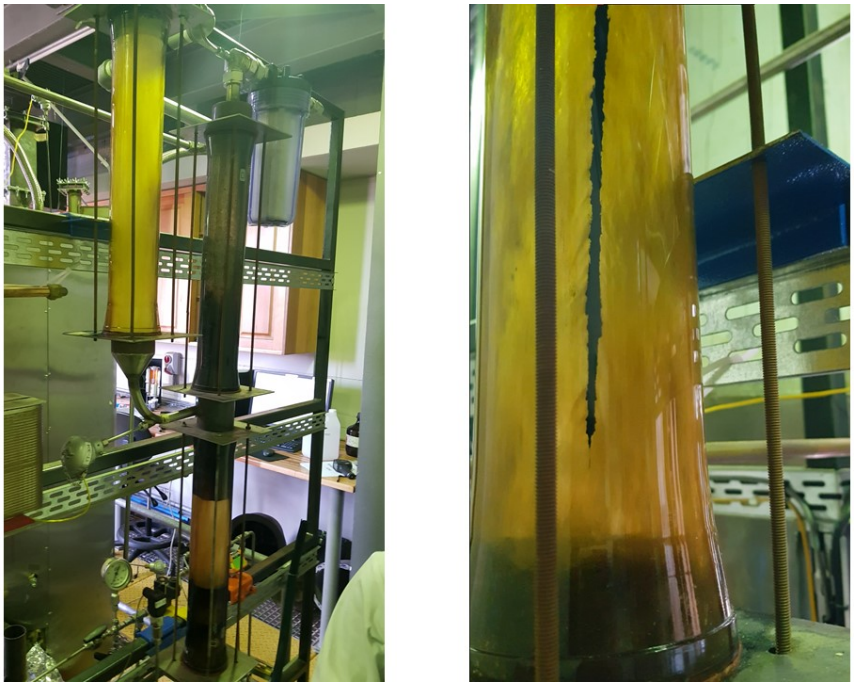

Figure 39: Left: The bio-oil condensation unit Right: A close-up image of the thicker pyrolysis oil streaking down the quencher

Figure 40 illustrates the consistency of biomass feeding from the upgraded hopper and delivery system. This was all thanks to the improved vertical drop zone, redesigned screw, and eccentric motor attachment. The flanged bearing mount at the rear of the screw feeder was also significantly more airtight than the previous friction mounting, which brings about a safer working environment.

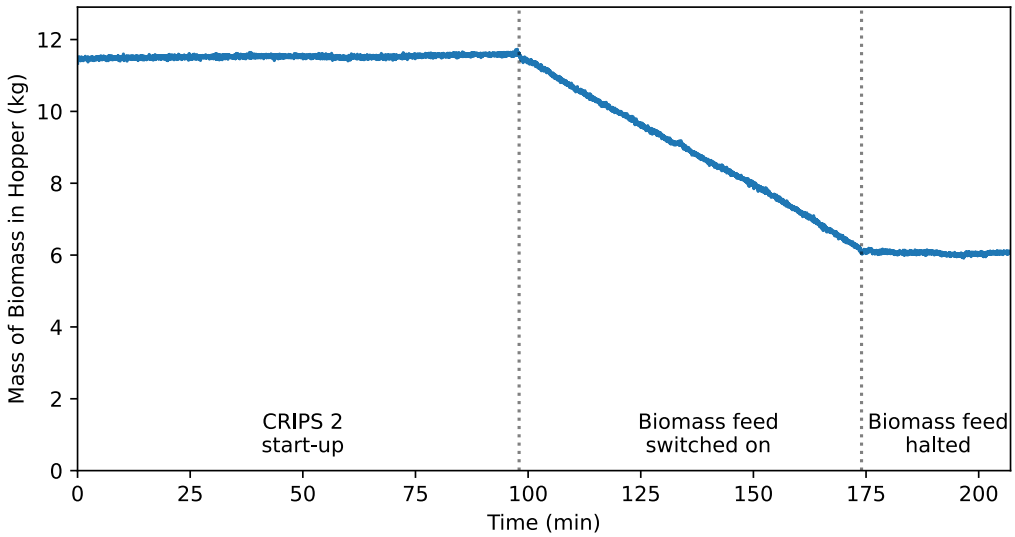

Figure 40: Typical biomass hopper mass drop during pyrolysis

Cooling water was used to cool the recycled bio-oil, which was used to rapidly cool the incoming pyrolysis vapour stream. The temperatures of the incoming and outgoing cooling water streams are shown in Figure 41 with the corresponding calculated heat transfer rates. The cooling water was operated at the maximum flow rate of 12501/h to ensure that all the vapours were sufficiently condensed and not lost to the NCG stream returning to the blower. The initial peak correlates to the initial heat load when the cooling water system starts up. Then one can observe the temperature difference increase and subsequent increase in heat transfer at 100 minutes where the biomass feeding begins. This illustrates the cooling required for condensation as the temperature of the pyrolysis vapours increases.

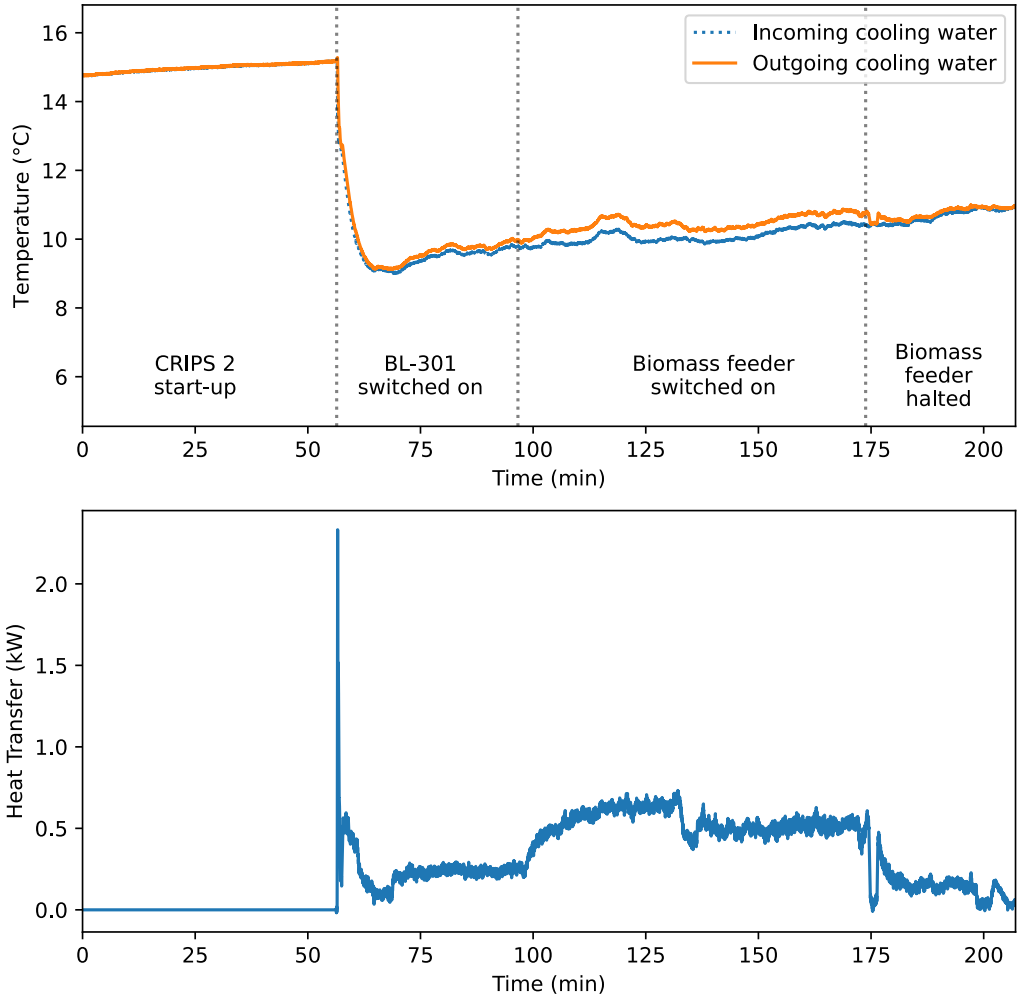

Figure 41: Typical cooling water operation for the condensation unit

The plant data collected over all the successful pyrolysis runs is summarised in Tables 29 and 30. The theoretical yields of biochar and NCG have not been included in the summaries due to the high oxygen content in the pyrolysis unit, which would cause extensive partial oxidation. All the values displayed in the tables are averaged over the entire run which includes the time spent removing biochar and sorting out any process issues.

Table 29: Summarised results for the first set of CRIPS 2 experimental pyrolysis runs

Parameter	Run-1	Run-2	Run-3	Run-4
Biomass feed rate[a] (kg/h)	4.23	1.81	2.21	0.99
LPG feed rate (kg/h)	5.05	0.61	0.25	0.46
Bio-oil yield (%)	-	33.98	33.99	35.91
NCG recycle flow rate (l/min)	26.00	163.43	136.07	220.35
NCG recycle flow rate in PU (l/min)	67.42	423.80	352.85	571.40
SGV base of skirting (m/s)	0.08	0.50	0.42	0.67
SGV top of skirting (m/s)	0.02	0.15	0.13	0.20
VRT (s)	53.65	8.53	10.25	6.33
PU temperature (°C)	468.84	471.84	514.15	505.72
PU entrance temperature (°C)	494.86	507.08	493.35	510.82
PU vapour temperature (°C)	189.60	183.75	212.81	243.40
CU temperature (°C)	900.05	791.76	796.40	779.67
Flue gas temperature (°C)	167.73	164.87	176.50	166.29

[a] The average feed rate of biomass including stoppage time.

Table 30: Summarised results for the second set of CRIPS 2 experimental pyrolysis runs

Parameter	Run-5	Run-6	Run-7	Run-8
Biomass feed rate[a] (kg/h)	4.26	1.78	1.44	3.17
LPG feed rate (kg/h)	0.25	0.38	0.37	0.39
Bio-oil yield (%)	24.43	27.65	33.02	29.96
NCG recycle flow rate (l/min)	166.61	144.93	99.77	138.21
NCG recycle flow rate in PU (l/min)	432.05	375.83	258.72	358.40
SGV base of skirting (m/s)	0.51	0.44	0.31	0.42
SGV top of skirting (m/s)	0.15	0.13	0.09	0.13
VRT (s)	8.37	9.62	13.98	10.09
PU temperature (°C)	500.83	488.86	491.56	492.53
PU entrance temperature (°C)	479.51	496.41	498.44	469.57
PU vapour temperature (°C)	217.25	175.35	142.10	200.68
CU temperature (°C)	809.38	728.06	760.18	715.78
Flue gas temperature (°C)	195.95	149.00	161.57	160.50

[a] The average feed rate of biomass including stoppage time.

de la Rey (2015) designed the pyrolysis unit to operate with an SGV of 0.91 m/s which is significantly higher than the velocities used during the CRIPS 2 experimental runs. The lower SGV means higher vapour residence times which, discussed in Section 2.4.2, leads to secondary reactions generating more NCG. The pyrolysis vapours left the unit at a relatively low temperature (≈200 °C) which is significantly lower than the bed temperature. A significant amount of heat is lost through the top of the reactor, and the cooler flue exit (≈160 °C) will act as a heat sink for the pyrolysis vapours and NCG leaving the system, i.e. the pyrolysis vapours are losing energy to the central combustion unit.

5.2 Feed and product characteristics

5.2.1 Biomass feedstock

The biomass chosen for the commissioning of the CRIPS 2 unit was *Eucalyptus grandis*. The woody biomass was delivered to at the University of Pretoria in the form of wood chips which had already undergone size reduction and drying. The size distribution of the wood chips is important as the conduction of heat through a larger particle would lead to inefficient pyrolysis, and too small a particle would allow fines to bypass the pyrolysis

cyclone. Three bins of wood chips (each approximately 10 kg in mass) were used during the commissioning of the CRIPS 2 unit. The size distributions of the wood chips from the three bins are shown in Figure 42.

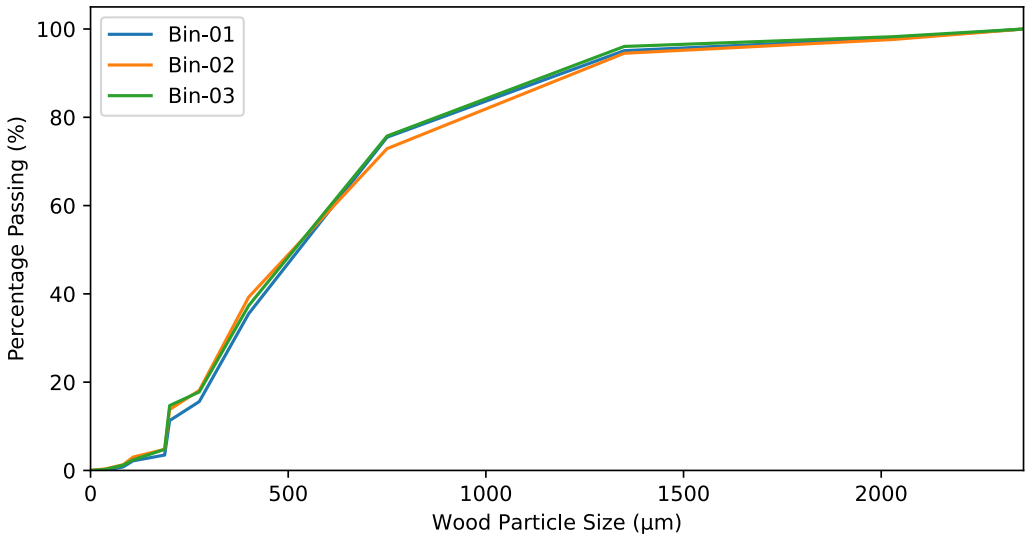

Figure 42: Particle size analysis of the wood chips used in the CRIPS 2 commissioning

The proximate analysis of the wood chips was performed with the use of thermogravimetric analysis (TGA). The analysis provided the moisture, volatiles, fixed carbon, and ash content of the wood chips. The TGA curve for the wood chip sample is shown in Figure 43 with the balance of the mass at the end of the run reported as the ash content. The moisture and ash content of the wood were also determined via the ASTM D4442-16 and D1102-84 methods respectively. The differences between the two analyses yielded 1.2 % relative to the total mass. This variability is probably due to the small sample size required for the TGA (lower representability); however, the analysis is sufficient for these purposes. A compilation of the analytical results for the wood chips is given in Table 31.

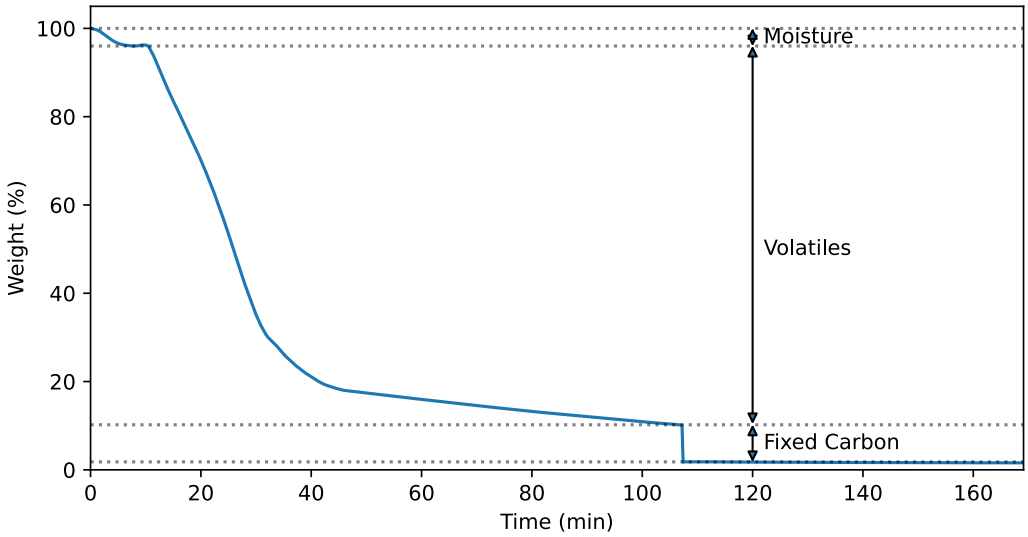

Figure 43: TGA results from a sample of the *E. Grandis* wood chips

Table 31: Summary of the biomass characterisation using various analytical techniques

Parameter	Value
ASTM analysis:	
Moisture content (%)	5.45 - 7.60
Ash content (% d.b.)	0.68
TGA Proximate analysis:	
Moisture (%)	4.04
Volatiles (%)	85.36
Fixed Carbon (%)	8.80
Ash (%)	1.80
TGA Ash content (% d.b.)	1.88
Energy content	
HHV (MJ/kg)	18.96 ± 0.62

5.2.2 Bio-oil

The CRIPS 2 unit produced pyrolysis oil with two phases that were not miscible with one another. The first phase was a watery liquid, deep red to brown in colour (depending on the amount of exposure to air) with a very strong pyrolysis odour. The second phase of the pyrolysis oil was a thick dark brown to black liquid reminiscent of honey which was completely opaque. The smell of this tar-like substance was very similar to that of

the first phase. For the remainder of the thesis the two phases, phases 1 and 2, will be referred to as the aqueous phase and the oil phase respectively (see Figure 44).

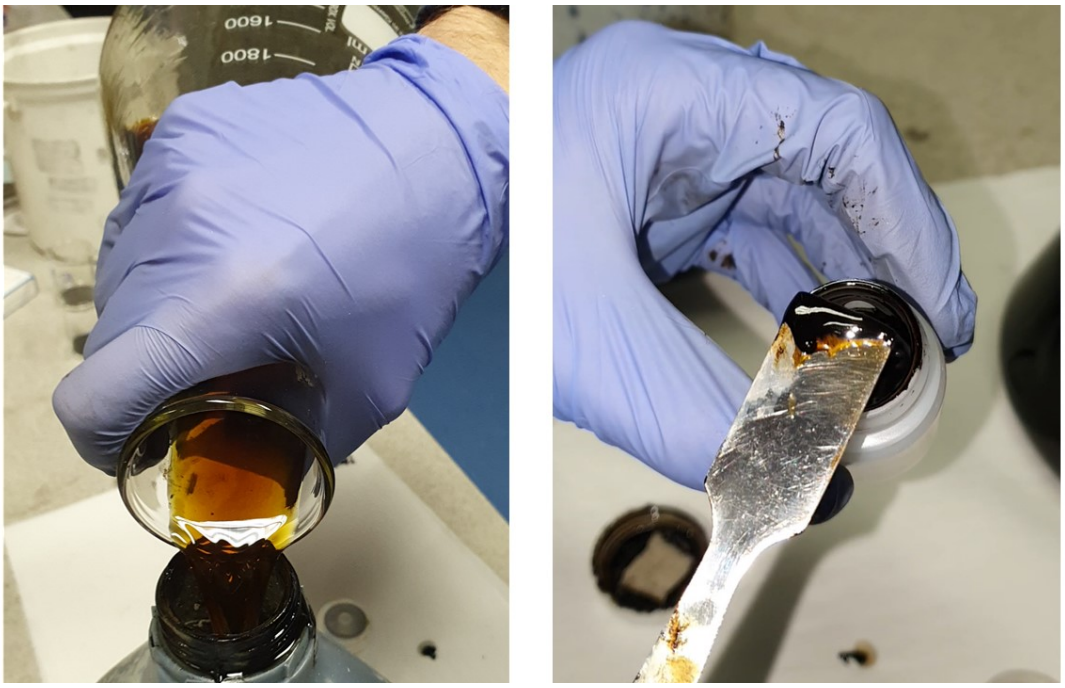

Figure 44: Left: Aqueous phase Right: Oil phase

The energy content of the pyrolysis oils was determined with a bomb calorimeter (see Section 4.4). As ethylene glycol was used as the initial solvent in the bio-oil condensing unit, the mass fraction of the bio-oil containing the solvent must be taken into account as it changes the heating value. As shown in Table 32, the unadjusted HHV of the bio-oils decreases after every run as the ethylene glycol is diluted with the product.

Table 32: Ethylene glycol content in the bio-oil products and the adjusted HHV values after dilutions

Sample	Overall yield (%)	Ethylene glycol content (%)	Total bio-oil content (%)	$HHV_{as\ produced}$ (MJ/kg)	HHV_{actual} (MJ/kg)
Bio-oil-1/2	33.99	64.65	35.35	13.87	4.22
Bio-oil-3	33.99	37.43	62.57	10.48	5.81
Bio-oil-4	35.92	23.19	76.81	8.63	5.62
Bio-oil-5	24.43	12.71	87.29	8.38	8.07
Bio-oil-6	27.65	8.78	91.22	7.34	5.02
Bio-oil-7	33.02	6.47	93.53	6.21	3.06
Bio-oil-8	29.96	3.35	96.65	6.68	7.19

The bio-oils produced from runs with higher biomass feed rates (Run-5 and Run-8) had the highest HHV compared to the bio-oils produced from the lower feed rates. The reason behind this is probably due to the oxygen content in the NCG, which both pyrolyses and partially oxidises the product. This is further explained in Section 5.2.4. The bio-oils produced from the high NCG recycle flow rates tended to have higher solids contents due to biochar bypassing the cyclone. This issue was resolved in Run-6 to 8 with reduced NCG flow rates, resulting in little to no biochar being transported to the final liquid product.

The final run, Run-8, used both the lower NCG flow rate and the higher biomass feed rate to achieve a relatively high HHV compared to the lower biomass flow rates and a better yield than Run-5. Furthermore, following Run-8, a subsequent run had to be scrubbed as thick bio-oil had started collecting in the condensation unit. Run-8 produced a significant amount of the thicker oil phase that was not miscible with the aqueous phase, and due to the low temperatures in the condensation unit, the oil phase started collecting in the base of the quenching unit. The high viscosity of this phase (at the low temperatures) and the immiscibility with the aqueous phase demonstrated some of the shortfalls of the condensation unit. The bio-oil vapours would also condense before the quencher, which would eventually start restricting flow. The CRIPS unit utilised by AA Boateng *et al* (2019) was able to achieve a bio-oil yield of $49.4 \pm 6.5\%$ which falls in between the design value of 62.07 % proposed by de la Rey (2015) and the values obtained from the CRIPS 2 unit. However, we do see very similar values to that of the CRIPS 1 unit which does fall at the bottom end of the yields from AA Boateng *et al* (2019). The reason for this is elaborated in Section 5.2.4.

Considering the higher oxygen content in the pyrolysis zone, the lower-than-expected HHV would go hand in hand with higher water content as the products of pyrolysis are eventually oxidised to water and carbon dioxide. The water content analysis of two bio-oil samples confirm the aforementioned prediction and this data is summarised in Table 33 with the addition of the spouted bed reactor (SBR) and typical wood pyrolysis bio-oil results for comparison.

Table 33: Comparison of CRIPS 2, SBR, AA Boateng *et al* (2019) CRIPS unit, and typical bio-oils

Sample	Water content (%)	HHV(MJ/kg)
Bio-oil-5	52.80	8.07
Bio-oil-7	59.18	3.06
SBR light[1]	42.39	11.33 – 18.01[3]
SBR heavy[2]	17.26	17.66 – 20.11[3]
Boateng CRIPS	36.84	18.16
Typical bio-oil	25.00	17 – 18

[1]The fraction of oil from the condenser unit

[2]The fraction of oil from the electrostatic precipitator unit

[3] Wu (2020)

The laboratory scale SBR unit makes use of heating elements as opposed to the combustion zone used in the CRIPS 2 unit. It is reasonable to assume that the oxygen in the SBR unit is very low as the NCG is constantly recycled therefore, any residual oxygen is consumed until extinction. This is confirmed with the water content in the bio-oils from the unit being significantly lower and an increase in the HHV than those from the CRIPS 2 unit. This point is further justified by the results from AA Boateng *et al* (2019) where a lower water content and a higher HHV value was measured. The elemental analysis for the pyrolysis oil produced and comparative values are summarised in Table 34.

Table 34: Elemental analysis of the CRIPS 2, SBR, AA Boateng *et al* (2019) CRIPS unit, and typical bio-oils

Property	CRIPS 2	SBR light	SBR heavy	Boateng CRIPS[1]	Typical bio-oil
Carbon (%)	60.69	60.69	58.15	60.55	56
Hydrogen (%)	6.90	6.90	9.29	6.13	6
Oxygen (%)	32.29	32.29	32.25	29.52	38
Nitrogen (%)	0.09	0.09	0.11	0.45	0 – 0.1
Sulphur (%)	0.02	0.02	0.20	n.d.	Negligible

[1] Elemental analysis done on the ESP oil i.e. higher quality pyrolysis oil

The light fraction of bio-oil produced by the SBR unit has an almost identical elemental composition to that of the CRIPS 2 unit (excluding the moisture). Furthermore, the

heavy fraction of bio-oil produced by the SBR unit has significantly more hydrogen than all the other oils which is indicative of its greater HHV. To summarise, the bio-oil produced from the CRIPS 2 unit is very similar to that of typical bio-oils however with the high moisture content, adaptions and optimisation must take place to make the unit feasible for increased pyrolysis oil production. Furthermore, the composition of the bio-oil produced by the CRIPS 2 unit is comparable to that of the unit described by AA Boateng *et al* (2019) which meets ASTM D7544 (specification for pyrolysis liquid biofuel).

5.2.3 Biochar

Biochar is the solid product of the biomass pyrolysis process. It is a black material reminiscent of the starting biomass; however it is much lighter and more compressible than the wood chips fed to the system. The biochar produced from the CRIPS 2 unit is shown in Figure 45.

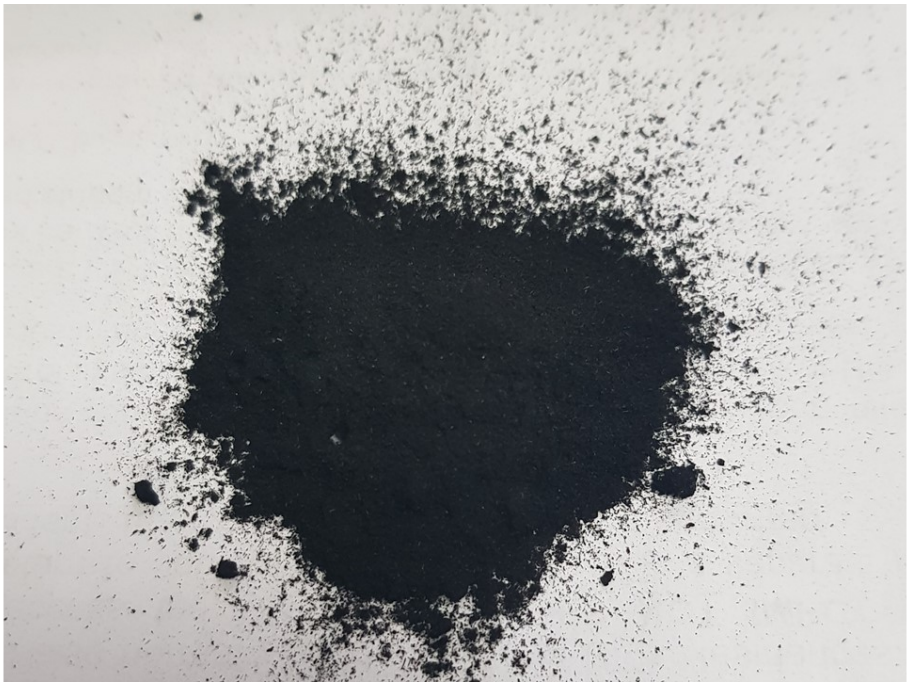

Figure 45: A sample of biochar produced from the CRIPS 2 unit

At lower NCG flow rates, 140 l/ min compared to $>$ 200 l/ min, there was significantly less overflow of solids (silica and biochar) from the cyclone. The final biochar sample produced, Biochar-08, was subjected to particle size analysis to characterise the cyclone's efficiency at the specified flow rate (Figure 46). Note that the larger particle sizes measured (above 1500 µm) are due to the clumping of the particles probably caused by condensed bio-oil and moisture. The harmonic mean diameter of the biochar is 122 µm, which is significantly lower than that of the feedstock. This is due both to the size reduction of the biomass during pyrolysis and the fact that only a small amount of biochar is leaving the pyrolysis unit.

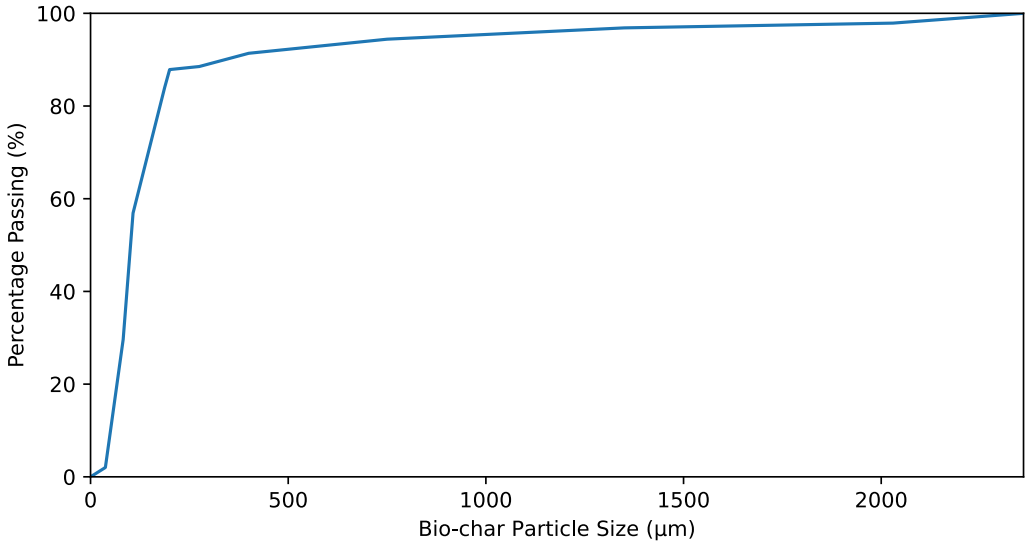

Figure 46: The cumulative particle size distribution of the biochar collected from the pyrolysis cyclone

TGA was performed on the biochar to determine the proximate analysis. The TGA curves are given in Figure 47.

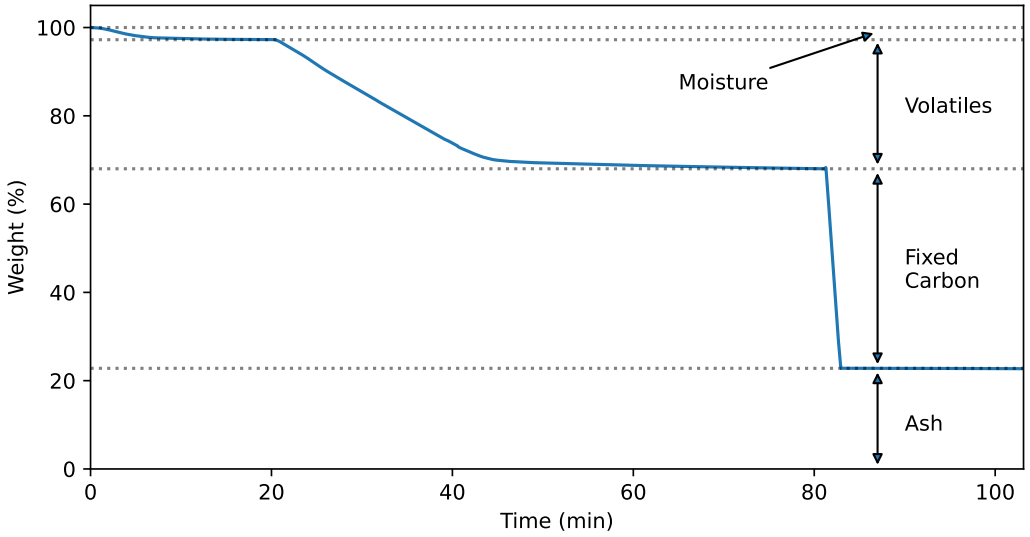

Figure 47: TGA results from a sample taken from the Biochar-08 (biochar produced in the final commissioning run)

The final biochar produced, Biochar-08, was analysed and the results were compared with the TGA runs with the biochar produced in the spouted bed reactor (SBR). The TGA proximate analysis is tabulated with the ASTM moisture and ash content in Table 35. As noted in Section 2.5.2, the biochar from pyrolysis can be used in various applications due

to the pore size and large surface area. BET analysis was performed on various biochars from the CRIPS 2 runs and their results are summarised in Table 35.

Table 35: Analytical results for the biochar produced by CRIPS 2 and the SBR (spouted bed reactor)

Parameter	CRIPS 2 Value	SBR Value
ASTM analysis:		
Moisture content (%)	2.12	-
Ash content (% d.b.)	23.85	-
TGA Proximate analysis:		
Moisture (%)	2.74	3.18
Volatiles (%)	29.27	35.42
Fixed carbon (%)	45.18	25.21
Ash (%)	22.81	31.18
Volatiles (% d.b.)	30.09	38.58
Fixed carbon (% d.b.)	46.45	27.46
Ash (% d.b.)	23.45	33.96
Energy content		
HHV (d.b.) (MJ/kg)	22.51±0.25	18.75
Surface characteristics		
BET surface area (m^2/g)	0.8	70.57
Micropore area (m^2/g)	-	41.93
External surface area (m^2/g)	0.99	28.63

The ash content and subsequent metal analysis were performed on the final biochar because of its higher quality (HHV) and quantity. The results of the biochar ash analysis are shown in Table 36. Biochar-6 and Biochar-7 were not included as Run-6 and Run-7 did not produce enough biochar for accurate analysis. From the results, the lower feed rate runs with higher NCG produce char with higher silica content (non-biomass ash) due to pneumatic transport of the bed material. The silica content decreases as the feed rate is increased (Run-5) and an additional decrease in NCG recycle flow rate produced biochar with the lowest silica content (Run-8).

Table 36: The distribution of biomass ash and non-biomass ash (silica) for the biochar samples produced by the CRIPS 2 unit

Sample	Biomass ash (% d.b.)	Non-biomass ash (% d.b.)
Biochar-1/2	9.24	90.76
Biochar-3	16.50	83.50
Biochar-4	3.99	96.01
Biochar-5	23.68	76.32
Biochar-8	36.26	63.74

The low surface areas of the biochars produced in the CRIPS 2 reactor could be due to insufficient pyrolysis as the higher surface area biochars produced by the SBR are fully reacted with the cyclone seated in the reaction unit. However, the biochar captured by the pyrolysis cyclone only accounted for 4.55 to 11.37 % of the possible biochar yield and thus cannot be representative of all the biochar produced. In other words, the biochar remaining in the pyrolysis bed, which subsequently feeds the combustion zone, could be fully pyrolysed without our knowledge.

5.2.4 Non-condensable gases

The NCG (non-condensable gases) formed via the pyrolysis reactions and partial oxidation were sampled after the NCG blower via a tap-off point. As noted in Section 4.4.9, sample bags were purged with pure nitrogen gas followed by purging with the NCG before samples were taken (Figure 48).

Figure 48: SKC sample bag used for NCG gas collection

The gases in the sample bags were then analysed using a GC, and these results are summarised in Table 37.

Table 37: GC results for the NCG recycled in the CRIPS 2 unit based on the lower and higher biomass throughput (units are in mass percentage) as well as the NCG produced by the CRIPS unit by AA Boateng *et al* (2019)

Component	Low throughput	High throughput	AA Boateng *et al* (2019)
O_2 (%)	10.51	7.38	n.d.
N_2 (%)	69.96	56.97	n.d.
CO (%)	5.72	12.92	42.40
CH_4 (%)	0.58	1.64	8.50
CO_2 (%)	13.23	21.09	41.30

From these results, it is evident the low bio-oil and biochar yields from pyrolysis could be caused by the high oxygen concentrations in the pyrolysis unit. The higher throughput run, Run-8, had much higher CO and CO_2 concentrations with better bio-oil yields than the lower throughput run, Run-7. Furthermore, the N_2 concentration in the higher throughput run also indicates that pyrolysis gases have diluted the nitrogen in the system and therefore less air is present in the pyrolysis unit. The major difference between these runs is the rate at which the wood chips were fed into the pyrolysis unit (5 kg/h versus

1.5 kg/h). It can be speculated that the higher wood chip feed rate consumes residual oxygen in the pyrolysis unit, allowing less combustion and more pyrolysis to take place. However, this does not solve the root problem that oxygen was leaking into the pyrolysis unit.

The NCG recycle is a closed loop and therefore oxygen was not expected to be present, especially throughout the pyrolysis runs. The pyrolysis unit is separated from the combustion unit via a layer of refractory material which should be air-tight. Therefore oxygen can only enter the pyrolysis unit via the two transfer interfaces: the silica return screw and the silica overflow holes. The outlet of the silica return screw is located close to the combustion air outlets and the higher pressure at the base of the fluidised bed could push air back through the silica return screw into the pyrolysis unit due to the compressibility of gases. Or the flow of sand into the pyrolysis unit through the overflow holes could transport un-reacted combustion air via the bulk flow, i.e. air inbetween sand particles. To solve either of these concerns, the flow rate of air into the unit should be reduced. However, the sand return screw mechanism will require strengthening as it cannot turn without the combustion bed fluidising. It is also recommended that an oxygen meter should be installed on the exit flue gas line and/or the return NCG line to indicate the oxygen concentrations in the unit during a run.

5.3 Mass and energy balance

The mass and energy balance of the CRIPS 2 unit is summarised in Table 38 with the use of literature values for the bio-oil composition. Table 39 uses the laboratory based ultimate analysis for the bio-oil composition and both yield very similar results verifying the CRIPS 2 process. The mass balance is very accurate, with under half a percent error with the incoming and outgoing streams, yet there appears to be a 35 % discrepancy with the incoming and outgoing energy. This is caused by the unit not operating at its thermal steady state which is explained in detail in Section 5.3.2. Therefore, by changing the temperatures of the outgoing streams, the energy balance will show significantly reduced errors. To prove this point, the same energy balance was performed, but instead the exit flue and pyrolysis vapour temperatures from the work of de la Rey (2015) were used and the error in the energy balance was reduced to around 6 %.

Table 38: The mass and energy balance for the CRIPS 2 unit with measured and calculated heat flow data (literature based bio-oil composition)

Component	Mass flow (kg/h)	Energy (kW)
In		
Air	17.61	0.01
LPG	0.39	5.50
Biomass	3.17	15.43
NCG	9.27	5.72
Out		
Flue	19.99	5.44
Latent Heat water	-	0.92
NCG	9.27	6.16
Biochar	0.03	0.20
Bio-oil	0.98	2.13
Latent Heat water	-	0.42
Pyrolysis	-	0.33
Ash	0.04	0.00
Overall Heat loss	-	2.04
Net value	**−0.12**	**9.02**
Absolute Error	**0.41 %**	**33.82 %**

Table 39: The mass and energy balance for the CRIPS 2 unit using laboratory data

Component	Mass flow (kg/h)	Energy (kW)
In		
Air	17.61	0.01
LPG	0.39	5.50
Biomass	3.17	15.43
NCG	9.27	5.72
Out		
Flue	20.00	5.27
Latent Heat water		0.94
NCG	9.27	6.16
Bio-char	0.03	0.20
Bio-oil	0.98	2.13
Latent Heat water		0.36
Pyrolysis		0.37
Ash	0.03	0.00
Heat loss	-	2.04
Net value	**–0.12**	**9.20**
Error	**−0.40 %**	**34.50 %**

The mass flow of air into the system caused issues in the mass balance calculations as too much carbon was left over after optimising the elemental balances. As all products were weighed using accurate scales, the culprit would have to be the incoming air flow rate determined by the flow meter. However, the DP cells were calibrated correctly and orifice plates were correctly mounted. Greef & Skinner (2000) clarify the situation with the use of the Reynolds number (Re), noting that additional calibration of the orifice plate should take place when $Re < 30000$. The current orifice calculations yield $Re \approx 5400$, which is well below the suggested flow characteristic for not using the additional flow calibrations. To satisfy the mass balance, a correctional factor of 2.2 was calculated, by which the combustion air flow rate was multiplied, see Appendix C.1 and C.2 for reference to the calculations. The combustion flue gas was analysed and combined with mass balance data from start-up conditions to accurately determine the only unknown being the air flow rate entering the CRIPS 2 unit i.e., pyrolysis not having an effect on the calculations. Also see Appendix C.3 and C.4 for the full breakdown of the component balance for the

CRIPS 2 unit (Run-8).

5.3.1 Heat loss determination

The heat loss from the CRIPS 2 unit is crucial in determining an accurate energy balance and evaluating the efficiency of the reactor's novel design. The energy provided to the unit through the combustion of LPG and residual biomass can be lost through various means. The key areas of thermal heat loss in the unit are the following: the heat transferred to the pyrolysis unit from the combustion unit through the refractory wall, the heat lost to the environment through the walls and tubing, the heat lost to the flue gas, and the heat lost in heating the reactor (thermal non-steady state).

The energy transferred between the combustion unit and the pyrolysis unit through the refractory is calculated using the thermal conductivities of the refractory and the temperature data gathered through the SCADA. The heat loss to the environment is determined by the thermal conductivities of the insulation and steel shell, and the pyrolysis temperatures (SCADA) and outer surface temperatures. The surface temperatures were measured using an infrared thermometer, the FLIR TG165, as noted in Section 4.2.4. A few of the images recorded by the FLIR TG165 are shown in Figure 49.

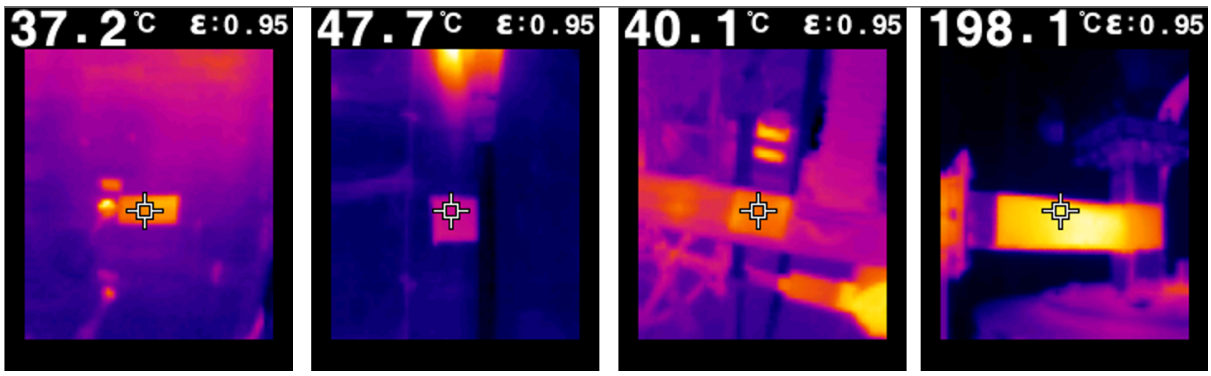

Figure 49: Examples of the thermal images and corresponding temperatures taken with the FLIR TG165 Left to right: TT-103-1, TT-104-4, biomass conveyor tube, and pyrolysis vapour exit

The averaged temperature profiles of the upper and lower regions of the reactor are shown in Figure 50.

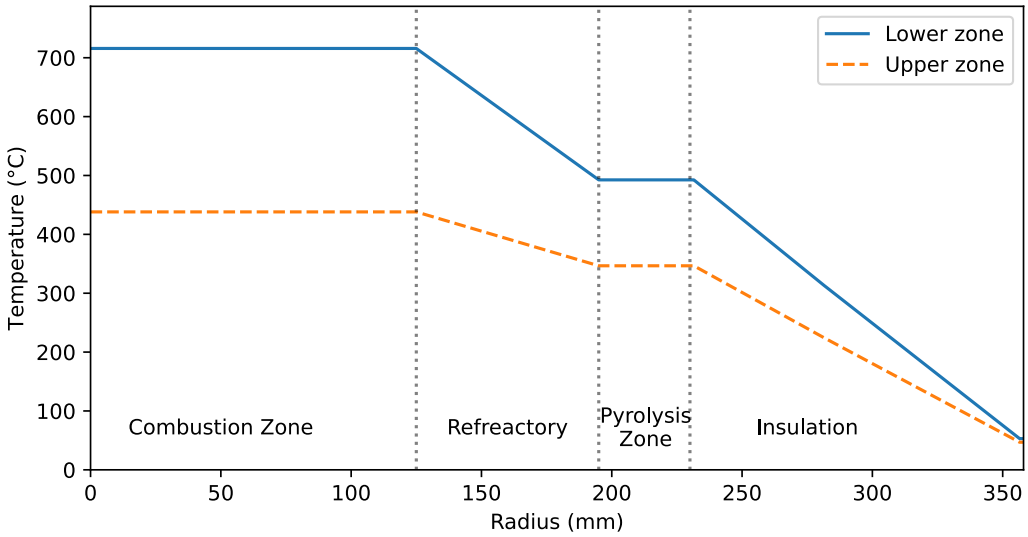

Figure 50: Temperature profile of the CRIPS 2 reactor unit

A summary of the heat lost to the environment is shown in Table 40.

Table 40: Heat losses through various means in and around the CRIPS 2 unit

Parameter	Average Value (kW)
Heat from CU to PU (conduction only)	1.16
Heat loss through panelling	0.82
Heat loss from biomass conveyor	0.32
Heat loss from pyrolysis products before condenser	1.14

The heat transfer will need to be standardised to compare the heat losses between the previous iteration of the unit, CRIPS 1, and the CRIPS 2 unit. This can be done by dividing by the heat transferred by the total surface area, also known as the heat flux. The heat fluxes to the environment for the CRIPS 1, CRIPS 2, and the theoretical CRIPS 2 (using modelled temperatures) are summarised in Table 41.

Table 41: Heat losses from the CRIPS 1 and 2 outer surfaces

Parameter	Heat flux (W/m^2)
CRIPS 1[a]	2.71
Actual CRIPS 2	0.48
Theoretical CRIPS 2[b]	1.63

[a](Grobler, 2014)
[b](de la Rey, 2015)

The design of the CRIPS 2 unit emphasised the importance of heat recovery, and conservation and the experimental runs confirm this. The CRIPS 2 design reduces the heat losses by 82 % when only taking into account the heat losses from conduction to the environment. Furthermore, at the design temperatures and operating conditions, the unit theoretically reduces the heat fluxes to the environment by 40 %.

5.3.2 Thermal soaking

The CRIPS 2 unit can consume up to 5 kg of LPG to achieve pyrolysis conditions when the unit is started from room temperature. The incredible mass of steel and refractory means that the unit has a very large thermal mass. Therefore performing an energy balance over the unit is very tricky as a large portion of the energy entering the reactor initially goes into heating it up. This phenomenon is termed thermal soaking, which eloquently describes how the heat of combustion is "soaking" into the refractory walls, steel sections, bed material, etc. This is clearly demonstrated in Figure 51, where the flue gas temperature is continually increasing before and throughout the pyrolysis run even when the combustion zone temperature is decreasing.

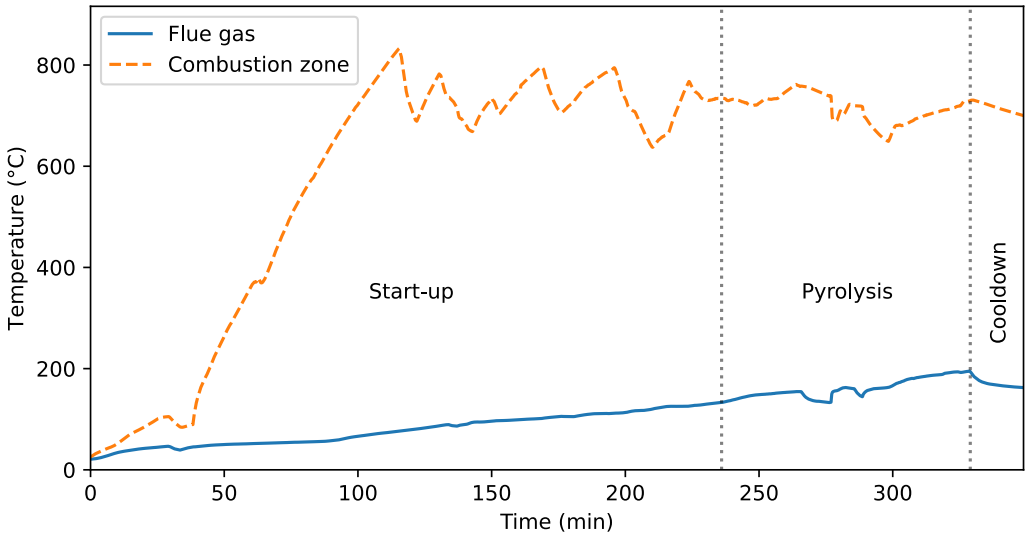

Figure 51: Comparison of combustion temperatures to flue gas temperatures to demonstrate thermal soaking

The increasing flue gas temperature indicates that the thermal steady state has not been achieved within the unit. This is also evident from a steady increase in the surface temperatures around the unit during pyrolysis. To prove this mathematically, a mass and energy balance was performed at the end of the start-up with flue gas analysis performed at the start of the LPG auto-combustion phase. The results are summarised in Table 42.

Table 42: Mass and energy balance during the start-up of the CRIPS 2 unit

Component	Mass flow (kg/h)	Energy (kW)
In		
Air	21.41	0.00
LPG	1.27	17.68
Out		
Flue gas	22.46	2.15
Heat flow		
Heat loss CRIPS 2	-	2.04
Latent heat of water	-	1.38
Net value	**0.22**	**12.11**

Thus with 12.11 kW unaccounted for (approximately 68 % of the incoming energy cannot be detected), it can be concluded that the unit was not operating at its thermal steady

state and therefore the energy balance over the pyrolysis operation will include thermal soaking. Factors such as reaching a thermal steady state are outside the scope of this work as the goal of the project was based on commissioning and not optimisation. Furthermore, the amount of LPG used for a short commissioning run is unfeasible for long-term work and additional operators would be required to get the unit safely to steady state.

5.3.3 APH effectiveness

The APH unit was designed to make the CRIPS 2 unit more efficient by transferring heat from the hot flue gas to the incoming cold combustion air. As described above, the thermal soaking would skew energy balance calculations as a portion of the incoming energy is removed in heating the unit. However, data were captured at the conclusion of Run-5 which would allow one to perform energy balance calculations without being concerned about thermal soaking. The pyrolysis was stopped and the additions of LPG halted, which means that the only incoming and outgoing mass and energy are the combustion air and thermal losses from the surfaces of the unit. The temperatures of the incoming combustion air, the combustion unit (flue starting temperature), and exit flue (hot combustion air) are shown in Figure 52. The average temperatures of the combustion unit differ by 5 % compared to the starting value, thus the heat exchanger is considered to be operating in a quasistatic state as the measured temperatures do not change significantly.

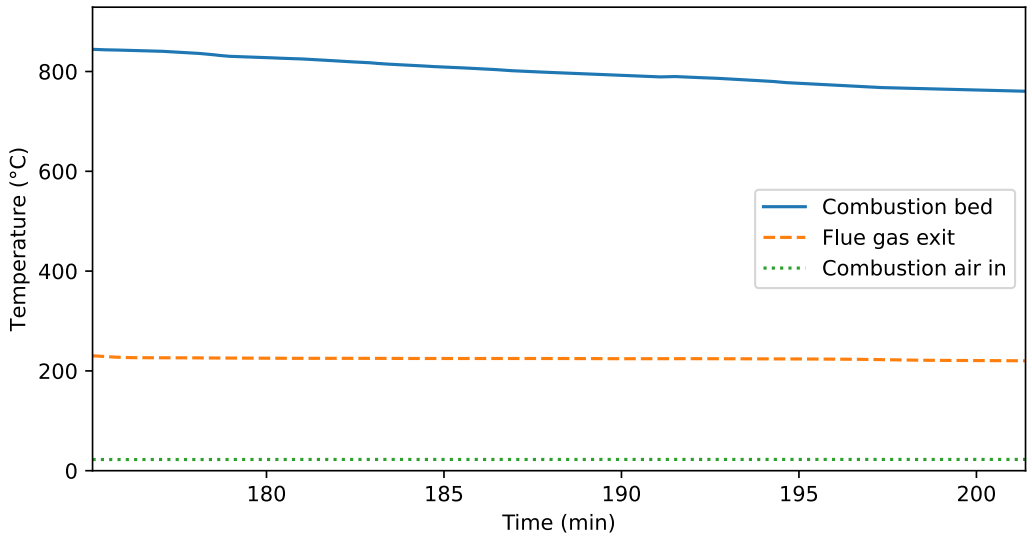

Figure 52: Temperatures illustrating the thermal-steady state of the CRIPS 2 unit

Including the heat loss from the upper combustion zone to the pyrolysis unit ($\approx 375\,\mathrm{W}$), the heat transferred by the heat exchanger is approximately 4 kW. The summarised

results from the heat transfer calculations are given in Table 43.

Table 43: Values measured and calculated to determine the APH effectiveness

Parameter	Value
Air flow rate (kg/h)	27.47
T_{airin} (°C)	22.51
T_{fluein} (°C)	799.83
T_{flueout} (°C)	224.38
Calculated T_{airout} (°C)	570.53
Heat transferred (kW)	4.42
ΔT_{LM} (°C)	215.3
U_{measured} (W/(m^{2}K))	17.40
U_{ideal} (W/(m^{2}K))	21.00

The measured overall heat transfer coefficient is 34 % out compared to the design value of 26.4 W/(m^{2}k). However, the measured value takes into account the large temperature differences between the combustion and pyrolysis freeboard zones. During continuous operation of the unit, where thermal steady state is realised, more heat from the flue will be exchanged with the incoming combustion air. In this scenario, the overall heat transfer coefficient is only 14.6 % out from the design value, which is probably due to fouling caused by the ash and undetermined inefficiencies (flow bypassing the baffles, differing thermal conductivities, etc.).

6 Conclusions and recommendations

6.1 Conclusions

6.1.1 Feedstock

E. grandis was the biomass chosen as the feed for the CRIPS 2 unit. It is sustainably grown in large plantations and is used in the timber and pulping industry. It was also used as feedstock in the previous iteration of the CRIPS design, which allows more consistent comparisons. Furthermore, woody biomass is consistent in its composition and characteristics compared to other types of biomass.

The biomass was delivered in the form of wood chips with drying and size reduction pretreatments already completed. The average particle size was 448 to 489 µm. All the bags of wood chips showed very similar characteristics, which means that there was adequate consistency of the feedstock. The moisture content of the wood chips varied from 5.93 to 7.60 % with an energy content (HHV) of approximately 18.96 MJ/kg. No additional drying was performed due to the weather conditions and the moisture content of the wood chips was below the maximum required value.

6.1.2 Construction and commissioning

The CRIPS 2 unit was successfully and safely commissioned, and provided valuable results from eight experimental pyrolysis runs. The commissioning was performed over four phases: cold runs, hot runs, calibrations, and finally the experimental runs.

The cold runs were started by choosing an appropriate fluid bed material which brought light to the requirements for fluidisation in the combustion and pyrolysis units. Silica sand with a harmonic mean diameter of 400 µm was chosen as the bed material and according to its characteristics, the minimum fluidisation velocities were determined. The cold runs also allowed all the VFD-driven motors to be tested. The sand transfer between the two units was tested and the design of the unit was successfully implemented as all of the charged material reported out of the base of the combustion unit after trialling the bed transfer mechanism. The biomass feeding mechanism was also tested and various modifications were made to ensure consistent flow from the hopper to the pyrolysis unit via a screw feeder and conveyor. The modifications consisted of redesigning the screw feeder mechanism and attaching an eccentric motor to the base of the biomass hopper, which produced very favourable results. The blowers were also tested to determine their

abilities and flow rates. The sensitivities of the transducers over the orifice plates were inadequate and thus they were swapped out for more accurate DP cells.

Following the cold runs, LPG was introduced into the combustion zone and manually ignited. These runs were conducted with safety as the main priority leak tests were performed around the CRIPS 2 unit and all auxiliary equipment. Furthermore, the parameters and procedures used for consistent start-ups were determined during this phase of the commissioning.

Calibrations were subsequently carried out on the DP cells and the biomass hopper. The DP cells were pre-calibrated at the factory; however, during signal setups and zeroing they were double-checked against a known pressure from a CO_2 cylinder fitted with an accurate regulator. The hopper calibrations were done with a known weight after every experimental run. The biomass feeding mechanism was calibrated following the modifications. The results show a very accurate calibration curve (Hz versus kg/h) with consistent flow and a maximum flow rate just under 12 kg/h.

The final step in the commissioning phase was the experimental work where the operation of the CRIPS 2 unit could be performed with confidence, especially where safety was concerned. Eight experimental runs were carried out with varying biomass feed rates and NCG recycle flow rates. It was discovered that feeding wood chips too slowly would produce lower quality oil due to the presence of oxygen in the pyrolysis unit, and recycling the NCG at too high a flow rate would transport biochar past the cyclone into the condensation unit. At the upper limit of the wood chip feed rate, 5 kg, the feed blocked up at the pyrolysis entrance. The unit was operated at a slightly lower NCG flow rate (140 l/min) and a higher feed rate (5 kg) to produce the highest quality oil without biochar in the condensation unit. The larger throughput of biomass also consumed more oxygen in the NCG as was evident from the better quality product. The air leaking into the pyrolysis zone requires the utmost attention as all other operations are invalid if more oxidation occurs than pyrolysis. The leaks are suspected to come from the two mechanisms of sand transfer, i.e. overflow holes and/or the transfer screw. For the overflow holes, more sand can be added to the unit to ensure that they are always filled or the bottom refractory requires redesign. For the transfer screw, redesign of the combustion air distribution would be required, but with the current design, the combustion air fed to the combustion zone should be decreased to incipient fluidisation to allow good mixing and the ability to transfer bed material between the two units. Thus additional trials are required to definitively decide whether large modifications to the unit are needed.

In terms of operational issues, the problems were typically solved within 15 minutes and the operation was able to continue, which goes to show the robust design of the CRIPS 2

unit. The extraction unit was also vital to the safe operation of the unit as the high concentrations of carbon monoxide were removed from the surrounding area.

6.1.3 Product characterisation

The bio-oil produced by the CRIPS 2 unit consisted of two separate phases, namely the aqueous phase and oil phase. The majority of the bio-oil produced throughout the experimental runs consisted of the aqueous phase, and this was due to the oxidation reactions in the pyrolysis, which lent itself to the high oxygen content in the NCG recycle stream. The bio-oil HHV ranged from 3.06 to 8.07 MJ/kg – these values were very dependant on the biomass feed rate. The non-reaction water (oxidation water) was determined to make up around 54 to 59 % of the bio-oil product from the runs with higher feed rates. The thicker oil phase that lined the base of the collection bottles and the inside of the condensation unit had an HHV of 22.11 MJ/kg with a majority of the substance collected during Run-8. Karl-Fisher titration confirmed the calculated bio-oil water content of approximately 50 to 60 % which reaffirms the hypothesis that oxygen is entering the pyrolysis unit and thus partially oxidising the products of pyrolysis. Finally, the ultimate analysis of the bio-oils displayed very similar elemental concentrations as that of a typical bio-oil minus the water content. Again, this validates that the pyrolysis is successfully taking place however, the hurdle of oxygen in the pyrolysis zone will need to be attended to so that the CRIPS 2 unit can feasibly produce bio-oil.

The choice of using larger wood chips, meant that more biochar would remain in the system and produce additional energy through combustion. The biochar that was collected from the pyrolysis vapour cyclone tended to have more silica when the NCG flow rates were increased, which makes sense as the fines would be transported from the bed to the cyclone. The highest quality biochar was produced in the final experimental run with a harmonic mean particle diameter of 122 µm. The HHV of the biochar on a silica-free basis was determined as 26.54 MJ/kg, which is in line with the data from literature. Thus the biochar from the process can find uses in various heating applications. The BET surface area result for the biochar was significantly lower than that of the biochar produced in the laboratory-scale SBR: 0.80 m^2/g compared to 70.57 m^2/g. Post-treatment of the chips with steam activation can significantly increase the adsorption and surface area properties. However, as the chips were oversized for the experimental runs, the surface areas are not representative of all the biochar produced. As noted in Section2.5.2, the biochar can be used for its high adsorption properties and soil remediation capabilities. As shown with this unit, the biochar can also be combusted to provide additional energy to the system.

The recycled NCG used to fluidise the pyrolysis unit was analysed using gas chromatography. The composition of the NCG produced in the low-throughput runs (Run-6 and Run-7) showed much higher concentrations of oxygen and nitrogen compared to the high-throughput runs (Run-8). Methane, carbon monoxide, and carbon dioxide were significantly higher in the high-throughput runs compared to the low-throughput runs. These observations prove that the higher throughput of wood chips into the CRIPS 2 unit dilutes the extent of oxidation; however, the fact that there was significant oxygen (7.38 %) present during the more successful runs means that oxygen was leaking into the pyrolysis unit from the combustion unit.

6.1.4 Plant performance

Notwithstanding the oxygen present in the pyrolysis unit, the CRIPS 2 unit as a whole was able to process a total of 25 kg of wood chips without any major complications. The insulation of the unit was surprisingly good, with the surface temperatures of the panelling never exceeding 80 °C, with a maximum heat loss of 1.1 kW from the reactor panelling and 1.14 kW from the top of the unit. The thermal heat loss of the CRIPS 2 unit was calculated as 0.48 kW/m^2, which significantly better than the 2.71 kW/m^2 of the CRIPS 1 unit, which is an 82 % reduction in heat loss. Even after assuming the heat losses with the modelled temperature values from de la Rey (2015), the CRIPS 2 unit would have a theoretical heat loss of 1.63 kW/m^2, which translates into a heat loss reduction of 40 %. This improvement is due to the integrated combustion and pyrolysis units with the addition of an air preheater. The designed and measured overall heat transfer coefficients of the APH differ only by 14.6 %, which reduces the LPG requirements by up to 49 %. Furthermore, the CRIPS 2 unit was able to easily operate at a biomass feed rate of 5 kg/h compared to the 2 kg/h maximum capacity of the CRIPS 1 unit.

The energy balance of the CRIPS 2 unit could not be fully realised as there was a large discrepancy between the incoming and outgoing energy flow, therefore thermal accumulation had to be occurring. Thermal soaking was determined to be the reason for this, where the large thermal mass of the unit requires a substantial amount of energy to reach a thermal steady state. Furthermore, the APH consistently exchanges heat with the incoming air, so that reaching a thermal steady state would take even longer than expected.

6.1.5 The bigger picture

Once the concerns regarding the CRIPS 2 unit have been ironed out, it is an ideal process to use for reducing biomass waste and producing valuable products. The unit has a very small footprint and therefore will not take up a lot of space. It can easily be transported around locations such as farms and tree plantations. The possibility of using it with other carbonaceous feedstocks will also require testing, which could open doors to municipal and industrial waste valorisation. The opportunities for such a piece of equipment are limitless: it not only solves waste issues, but also adds momentum to the commercialisation of biorefinery concepts which are crucial in an age in which sustainable processes are becoming more urgent.

Valuable research has been done at the University of Pretoria into the commissioning and design of fluidised beds and pyrolysis units. The work carried out in this project will hopefully be continued and create further opportunities for pyrolysis and fluidised bed research as the foundations for a safe and reliable unit have been laid. There are countless opportunities for additional postgraduate research projects with the CRIPS 2 unit, such as the optimisation of the bed transfer mechanism, modifying the biomass entrance location, testing various biomass feedstocks, implementing a safe NCG purge mechanism, etc. This work will also serve as an additional foundation in the research for the sustainable energy sector as the world heads into the uncharted territory of climate change and limited resources. For it is work such as this that can inspire our future engineers to think outside the box for solutions that will benefit society as a whole.

6.2 Recommendations for CRIPS 2

- **Reduce the oxygen transfer through operation and unit modifications:** The main issue with the pyrolysis unit is its high oxygen content leading to extensive oxidation reactions. The mass of bed material should be increased to such an extent that the sand overflow holes are consistently filled, which equates to approximately 30 kg of total silica. This might be able to mitigate the extent of oxygen transfer from the combustion unit to the pyrolysis unit. The operating parameters should also be optimised, such as the combustion air flow rate to reduce the oxygen entering the unit, for example by reducing the combustion air flow rate when the pyrolysis phase begins without losing fluidisation. Finally, if all else fails, the design of the distributors and CU/PU interfaces should be altered to reduced the oxygen transfer between the units.
- **Change the biomass screw conveyor delivery arrangement:** During the

startup of the process, any sand that overflows into the pyrolysis region has a high chance of blocking the biomass screw conveyor. The screw will struggle to push the sand back into the pyrolysis zone as it will only compact it as opposed to transporting it. This could be alleviated by increasing the feed pitch of the screw or feeding tangentially to the sand rotation. The current procedure to resolve the stuck screw issue is to have the screw rotating before the plant startup procedure is begun (see also Section 5.1.1). The sand can not only cause difficulties with the screw conveyor but also with the feed rate of the biomass. At too high a feed flow rate (>5 kg), the biomass compacts at the entrance to the pyrolysis unit as the rotating bed does not adequately remove pyrolysing material.

- **Redesign the bio-oil condenser unit:** The recovery of vapours was more than adequate as the NCG recycle showed no more moisture than normal air. However, difficulties arose with the two immiscible liquid phases and the possibility of blockages in the recirculation loop. As noted by Bridgwater (2012), vapour recovery should be performed as quickly as possible to reduce secondary reactions. As demonstrated with this unit, the exposed 2 m of piping between the cyclone and the condensing unit creates an additional opportunity for fouling and blockages as the temperature across the piping can drop by around 100 °C. The best options would be to have the condensing unit as close as possible to the biochar cyclone or to insulate the piping.

- **Add cyclones in series for better biochar recovery:** As the unit was operated with oversized wood chips, the cyclone was efficient at lower NCG velocities. However, if the particle sizes were to be decreased, additional cyclones would be able to deal with varying biomass sizes and allow for contingencies. The fluffy nature of the biochar would also restrict recovery as it would clump up and restrict the underflow. Furthermore, the unit should be operated at a much higher SGV to reduce vapour residence times – the additional cyclones would reduce the biochar/bed material in the overflow.

- **Increase cyclone capacity:** Increasing the cyclone capacity will allow easier recovery and would decrease the risk of solids build-up in the piping following the cyclone unit.

- **Add pilot burner and flame detection unit:** The combustion taking place in the combustion unit is sustained through careful management of the combustion air and LPG flow rates. However, additional safety outside of small-scale conditions will require a better solution than relying only on these mechanisms and visual confirmation through the combustion viewing port. Adding a flame detection unit will allow safer operation as the flame can be invisible to the naked eye and adding a

pilot burner unit would ensure safe start-up and operation to sustain the LPG/NCG combustion.

- **Add a separate distribution manifold for recycled NCG:** The NCG recycle purge line currently shares the line for the LPG. This can cause difficulties with efficient burning and can be dangerous if there is residual oxygen in the purge line, i.e. to carry oxidiser and fuel in the same line is very dangerous.
- **Provide additional insulation:** As noted in Section 5.3.1, a lot of heat is potentially lost from the top surface of the unit when operating at thermal steady state. By retaining this energy, less combustion energy will be required to heat the unit.
- **Add a viewing port directly above the pyrolysis entrance:** Fluidisation cannot be visually confirmed for the entire pyrolysis section. Adding a sight glass above the feed entrance would allow easier troubleshooting without the need to remove the screw, or in a worst-case scenario, disassembling the entire reactor.

7 References

Adjaye, JD and Bakhshi, NN (1995) "Production of hydrocarbons by catalytic upgrading of a fast pyrolysis bio-oil. Part I: Conversion over various catalysts" *Fuel Processing Technology*, *45*, (3): 161–183 DOI: 10.1016/0378-3820(95)00034-5.

Agblevor, FA and Besler, S (1996) "Inorganic compounds in biomass feedstocks. 1. Effect on the quality of fast pyrolysis oils" *Energy & Fuels*, *10*, (2): 293–298 DOI: 10.1021/ef950202u URL: https://doi.org/10.1021/ef950202u.

Agblevor, F, Besler, S and Wiselogel, A (Apr. 1996) "Production of oxygenated fuels from biomass: impact of feedstock storage" *Fuel Science and Technology International*, *14*, (4): 589–612 DOI: 10.1080/08843759608947599 URL: http://www.tandfonline.com/doi/abs/10.1080/08843759608947599.

Alonso, DM, Wettstein, SG and Dumesic, JA (Nov. 2012) "Bimetallic catalysts for upgrading of biomass to fuels and chemicals" *Chemical Society Reviews*, *41*, (24): 8075 DOI: 10.1039/c2cs35188a.

Beckinghausen, A, Reynders, J, Merckel, R, Wu, YW, Marais, H and Schwede, S (Aug. 2020) "Post-pyrolysis treatments of biochars from sewage sludge and *A. mearnsii* for ammonia (NH4-N) recovery" *Applied Energy*, *271*, 115212 ISSN: 03062619 DOI: 10.1016/j.apenergy.2020.115212 URL: https://linkinghub.elsevier.com/retrieve/pii/S0306261920307248.

Beringer, T, Lucht, W and Schaphoff, S (Aug. 2011) "Bioenergy production potential of global biomass plantations under environmental and agricultural constraints" *GCB Bioenergy*, *3*, (4): 299–312 ISSN: 17571693 DOI: 10.1111/j.1757-1707.2010.01088.x.

Boateng, A and Mullen, C (Mar. 2013) "Fast pyrolysis of biomass thermally pretreated by torrefaction" *Journal of Analytical and Applied Pyrolysis*, *100*, 95–102 DOI: 10.1016/J.JAAP.2012.12.002.

Boateng, AA, Schaffer, MA, Mullen, CA and Goldberg, NM (2019) "Mobile demonstration unit for fast- and catalytic pyrolysis: The combustion reduction integrated pyrolysis system (CRIPS)" *Journal of Analytical and Applied Pyrolysis*, *137*, 185–194 ISSN: 0165-2370 DOI: https://doi.org/10.1016/j.jaap.2018.11.024.

Bridgwater, AV (2012) "Review of fast pyrolysis of biomass and product upgrading" *Biomass and Bioenergy*, *38*, 68–94 DOI: 10.1016/j.biombioe.2011.01.048 URL: http://dx.doi.org/10.1016/j.biombioe.2011.01.048.

Bridgwater, AV (2013) *Fast pyrolysis of biomass for the production of liquids*, Woodhead Publishing: pp. 130–171 ISBN: 9780857091314 DOI: 10.1533/9780857097439.2.130.

Carpenter, D, Westover, TL, Czernik, S and Jablonski, W (2014) "Biomass feedstocks for renewable fuel production: A review of the impacts of feedstock and pretreatment on the yield and product distribution of fast pyrolysis bio-oils and vapors" *Green Chemistry*, *16*, (2): 384–406 DOI: 10.1039/c3gc41631c.

Cayuela, M, Zwieten, L van, Singh, B, Jeffery, S, Roig, A and Sánchez-Monedero, M (2014) "Biochar's role in mitigating soil nitrous oxide emissions: A review and meta-analysis" *Agriculture, Ecosystems & Environment*, *191*, 5–16 DOI: 10.1016/J.AGEE.2013.10.009.

Çengel, Y and Ghajar, AJ (2015) *Heat and Mass Transfer: Fundementals and Applications*, 5th ed. McGraw-Hill Education, New York: pp. 27–30, 161–167, 533–547 ISBN: 978-0-07-339818-1.

Chai, L and Saffron, CM (Feb. 2016) "Comparing pelletization and torrefaction depots: Optimization of depot capacity and biomass moisture to determine the minimum production cost" *Applied Energy*, *163*, 387–395 DOI: 10.1016/J.APENERGY.2015.11.018.

Chen, T, Wu, C, Liu, R, Fei, W and Liu, S (2011) "Effect of hot vapor filtration on the characterization of bio-oil from rice husks with fast pyrolysis in a fluidized-bed reactor" *Bioresource Technology*, *102*, (10): 6178–6185 DOI: 10.1016/J.BIORTECH.2011.02.023.

Cherubini, F (July 2010) "The biorefinery concept: Using biomass instead of oil for producing energy and chemicals" *Energy Conversion and Management*, *51*, (7): 1412–1421 ISSN: 01968904 DOI: 10.1016/j.enconman.2010.01.015.

Culp, AW (1991) *Principles of Energy Conversion*, 2nd ed. McGraw-Hill.

de la Rey, J (2015) "Energy Efficiency in Dual Fluidised Bed Fast Pyrolysis" Master's Thesis, University of Pretoria.

Dhyani, V and Bhaskar, T (2018) "A comprehensive review on the pyrolysis of lignocellulosic biomass" *Renewable Energy*, *129*, 695–716.

Duong, LT, Prasertcharoensuk, P and Phan, AN (2019) "Biofuel production from lignocellulosic feedstock via thermochemical routes", in: *Liquid Biofuel Production*, Singh, LK and Chaudhary, G (Eds.), 1st ed. John Wiley & Sons chap. 3: pp. 92–148.

EIA (2018) *Oil and petroleum products explained* URL: https://www.eia.gov/energyexplained/oil-and-petroleum-products/ (visited on 04/03/2020).

Ek, M, Gellerstedt, G and Henriksson, G (2009) *Pulp and Paper Chemistry and Technology - Wood Chemistry and Biotechnology*, 1st ed. De Gruyter: pp. 4–6 ISBN: 9783110213393.

Gandia, LM, Arzamedi, G and Dieguez, PM (2013) *Renewable Hydrogen Technologies - Production, Purification, Storage, Applications and Safety*, Elsevier: pp. 87–108 ISBN: 978-0-444-56352-1.

Gollakota, ARK, Kishore, N and Gu, S (2018) "A review on hydrothermal liquefaction of biomass" *Renewable and Sustainable Energy Reviews*, *81*, 1378–1392 DOI: http://dx.doi.org/10.1016/j.rser.2017.05.178.

Greef, IL and Skinner, W (2000) *Piping System Design*, University of Pretoria, Pretoria: pp. 84–88.

Grobler, A (2014) "Scalable Dual Fluidised Bed System for Fast Pyrolysis of Woody Biomass" Master's Thesis, University of Pretoria.

Guedes, RE, Luna, AS and Torres, AR (Jan. 2018) "Operating parameters for bio-oil production in biomass pyrolysis: A review" *Journal of Analytical and Applied Pyrolysis*, *129*, 134–149 ISSN: 01652370 DOI: 10.1016/j.jaap.2017.11.019.

Gupta, RB and Demirbas, A (2010) *Gasoline, Diesel and Ethanol Biofuels from Grasses and Plants*, 1st ed. Cambridge University Press: pp. 56–58.

Hood, EE, Nelson, P and Powell, R, eds. (Feb. 2011) *Plant Biomass Conversion*, John Wiley & Sons, Inc., Hoboken, NJ, USA ISBN: 9780470959138 DOI: 10.1002/9780470959138 URL: http://doi.wiley.com/10.1002/9780470959138.

Isaksson, J, Åsblad, A and Berntsson, T (Dec. 2013) "Influence of dryer type on the performance of a biomass gasification combined cycle co-located with an integrated pulp and paper mill" *Biomass and Bioenergy*, *59*, 336–347 DOI: 10.1016/J.BIOMBIOE.2013.10.002.

Kan, T, Strezov, V and Evans, TJ (May 2016) "Lignocellulosic biomass pyrolysis: A review of product properties and effects of pyrolysis parameters" *Renewable and Sustainable Energy Reviews*, *57*, 1126–1140 ISSN: 13640321 DOI: 10.1016/j.rser.2015.12.185.

Lehmann, J, Czimczik, C, Laird, D and Sohi, S (2009) "Stability of biochar in soil." In: *Biochar for Environmental Management*, Lehmann, J and Joseph, S (Eds.), Earthscan, London: pp. 183–206.

Lehmann, J, Rillig, MC, Thies, J, Masiello, CA, Hockaday, WC and Crowley, D (2011) "Biochar effects on soil biota – A review" *Soil Biology and Biochemistry*, *43*, (9): 1812–1836 DOI: 10.1016/J.SOILBIO.2011.04.022.

Lødeng, R, Hannevold, L, Bergem, H and Stöcke, M (2013) "11.5.1 Biomass Pretreatment", in: *Role of Catalysis for the Sustainable Production of Bio-Fuels and Bio-Chemicals*, Triantafyllidis, KS, Lappas, AA and Stöcker, M (Eds.), Elsevier: p. 377 ISBN: 978-0-444-56330-9.

Luque, R, Ki Lin, CS, Wilson, K and Clark, J (2016) *Handbook of Biofuels Production - Processes and Technologies (2nd Edition)*, Elsevier: pp. 393–394 ISBN: 978-0-08-100455-5.

Mante, OD, Agblevor, F, Oyama, S and McClung, R (2012) "The influence of recycling non-condensable gases in the fractional catalytic pyrolysis of biomass" *Bioresource Technology*, *111*, 482–490 DOI: 10.1016/J.BIORTECH.2012.02.015.

Meier, D, Oasmaa, A and Peacocke, GVC (1997) "Properties of Fast Pyrolysis Liquids: Status of Test Methods", in: *Developments in Thermochemical Biomass Conversion*, Bridgwater, AV and Boocock, DGB (Eds.), Springer, Dordrecht: pp. 391–408 DOI: https://doi.org/10.1007/978-94-009-1559-6_31.

Oliveira, FR, Patel, AK, Jaisi, DP, Adhikari, S, Lu, H and Khanal, SK (2017) "Environmental application of biochar: Current status and perspectives" *Bioresource Technology*, *246*, 110–122 ISSN: 18732976 DOI: 10.1016/j.biortech.2017.08.122.

Pandey, A, Höfer, R, Larroche, C, Taherzadeh, M and Nampoothiri, KM (2015) *Industrial Biorefineries and White Biotechnology*, Elsevier: p. 5 ISBN: 978-0-444-63453-5.

Pandey, MP and Kim, CS (2011) "Lignin depolymerization and conversion: A review of thermochemical methods" *Chemical Engineering & Technology*, *34*, (1): 29–41 ISSN: 09307516 DOI: 10.1002/ceat.201000270 URL: http://doi.wiley.com/10.1002/ceat.201000270.

Park, YK, Yoo, ML, Heo, HS, Lee, HW, Park, SH, Jung, SC, Park, SS and Seo, SG (2012) "Wild reed of Suncheon Bay: Potential bio-energy source" *Renewable Energy*, *42*, 168–172 DOI: 10.1016/J.RENENE.2011.08.025.

Parrish, DJ and Fike, JH (2005) "The Biology and Agronomy of Switchgrass for Biofuels" *Critical Reviews in Plant Sciences*, *24*, (5-6): 423–459 DOI: 10.1080/07352680500316433.

Perlack, R, Wright, L, Turhollow, A, Graham, R, Stokes, B and Erbach, D (2005) *Biomass as feedstock for a bioenergy and bioproducts industry: the technical feasibility of a billion-ton annual supply*, Oak Ridge National Laboratory.

Pinho, AdR, Almeida, MB de, Mendes, FL, Casavechia, LC, Talmadge, MS, Kinchin, CM and Chum, HL (2017) "Fast pyrolysis oil from pinewood chips co-processing with vacuum gas oil in an FCC unit for second generation fuel production" *Fuel*, *188*, 462–473 DOI:

10.1016/j.fuel.2016.10.032 URL: http://dx.doi.org/10.1016/j.fuel.2016.10.032.

Prasad, S, Singh, A and Joshi, H (2007) "Ethanol as an alternative fuel from agricultural, industrial and urban residues" *Resources, Conservation and Recycling*, *50*, (1): 1–39 DOI: 10.1016/J.RESCONREC.2006.05.007.

Rezaei, PS, Shafaghat, H and Daud, WMAW (Jan. 2014) "Production of green aromatics and olefins by catalytic cracking of oxygenate compounds derived from biomass pyrolysis: A review" *Applied Catalysis A: General*, *469*, 490–511 DOI: 10.1016/J.APCATA.2013.09.036.

Rhodes, M (2008) *Introduction to Particle Technology*, 2nd ed. John Wiley & Sons, Chichester: pp. 1–27, 169–210 ISBN: 978-0-470-01428-8.

Roy, P and Dias, G (2017) "Prospects for pyrolysis technologies in the bioenergy sector: A review" *Renewable and Sustainable Energy Reviews*, *77*, (May 2016): 59–69 ISSN: 18790690 DOI: 10.1016/j.rser.2017.03.136.

Schaschke, C (2014) *Dictionary of Chemical Engineering*, Oxford University Press: pp. 351, 358, 368 ISBN: 978-0-19-965145-0.

Shen, J, Wang, XS, Garcia-Perez, M, Mourant, D, Rhodes, MJ and Li, CZ (Oct. 2009) "Effects of particle size on the fast pyrolysis of oil mallee woody biomass" *Fuel*, *88*, (10): 1810–1817 DOI: 10.1016/j.fuel.2009.05.001.

Singh, J and Trivedi, J (2018) "Raw materials for biofuel production", in: *Biofuels Production and Processing Technology*, Riazi M.R. and Chiaramonti David (Eds.), CRC Press, Boca Raton chap. 5: pp. 127–129.

Singh, LK and Chaudhary, G (2017) *Advances in Biofeedstocks and Biofuels, Volume 2 - Production Technologies for Biofuels*, John Wiley & Sons: p. 45 ISBN: 978-1-119-11752-0.

Swart, S (2012) "Design, Modelling and Construction of a Scalable Dual Fluidised Bed Reactor for the Pyrolysis of Biomass" Master's Thesis, University of Pretoria.

TA Instruments (2020) *Thermal Analysis Application Brief - Proximate Analysis of Coal and Coke* tech. rep.: pp. 1–2.

United Nations (2020) *Climate Change - United Nations Sustainable Development* URL: https://www.un.org/sustainabledevelopment/climate-change/ (visited on 03/30/2020).

Uslu, A, Faaij, AP and Bergman, P (Aug. 2008) "Pre-treatment technologies, and their effect on international bioenergy supply chain logistics. Techno-economic evaluation of torrefaction, fast pyrolysis and pelletisation" *Energy*, *33*, (8): 1206–1223 DOI: 10.1016/J.ENERGY.2008.03.007.

Wang, Z, Zheng, H, Luo, Y, Deng, X, Herbert, S and Xing, B (2013) "Characterization and influence of biochars on nitrous oxide emission from agricultural soil" *Environmental Pollution*, *174*, 289–296 DOI: 10.1016/J.ENVPOL.2012.12.003.

Westover, TL, Phanphanich, M, Clark, ML, Rowe, SR, Egan, SE, Zacher, AH and Santosa, D (Jan. 2013) "Impact of thermal pretreatment on the fast pyrolysis conversion of southern pine" *Biofuels*, *4*, (1): 45–61 DOI: 10.4155/bfs.12.75.

Williams, PT and Besler, S (Mar. 1996) "The influence of temperature and heating rate on the slow pyrolysis of biomass" *Renewable Energy*, *7*, (3): 233–250 ISSN: 0960-1481 DOI: 10.1016/0960-1481(96)00006-7.

Windeatt, JH, Ross, AB, Williams, PT, Forster, PM, Nahil, MA and Singh, S (2014) "Characteristics of biochars from crop residues: Potential for carbon sequestration and soil amendment" *Journal of Environmental Management*, *146*, 189–197 DOI: 10.1016/J.JENVMAN.2014.08.003.

Wornat, MJ, Porter, BG and Yang, NYC (1994) "Single droplet combustion of biomass pyrolysis oils" *Energy & Fuels*, *8*, (5): 1131–1142 DOI: 10.1021/ef00047a018.

Wu, YW (2020) "Catalytic fast pyrolysis of E. Grandis with modi ed layered double hydroxide" phdthesis, University of Pretoria.

Zanzi, R, Sjöström, K and Björnbom, E (Apr. 1996) "Rapid high-temperature pyrolysis of biomass in a free-fall reactor" *Fuel*, *75*, (5): 545–550 DOI: 10.1016/0016-2361(95)00304-5.

Zhang, X, Xia, YS, Shang, YJ, Zhao, QQ and Shi, J (2017) "Effects of biochar (BC) on microbial diversity of cadmium (Cd) contaminated soil" *Zhongguo Huanjing Kexue/China Environmental Science*, *37*, 252–262.

Zhao, YL, Dolat, A, Steinberger, Y, Wang, X, Osman, A and Xie, GH (2009) "Biomass yield and changes in chemical composition of sweet sorghum cultivars grown for biofuel" *Field Crops Research*, *111*, (1-2): 55–64 DOI: 10.1016/J.FCR.2008.10.006.

Zou, S, Wu, Y, Yang, M, Li, C and Tong, J (Jan. 2010) "Pyrolysis characteristics and kinetics of the marine microalgae Dunaliella tertiolecta using thermogravimetric analyzer" *Bioresource technology*, *101*, (1): 359–65 ISSN: 1873-2976 DOI: 10.1016/j.biortech.2009.08.020.

Appendix A Plant diagrams

A.1 CRIPS 1 P&ID

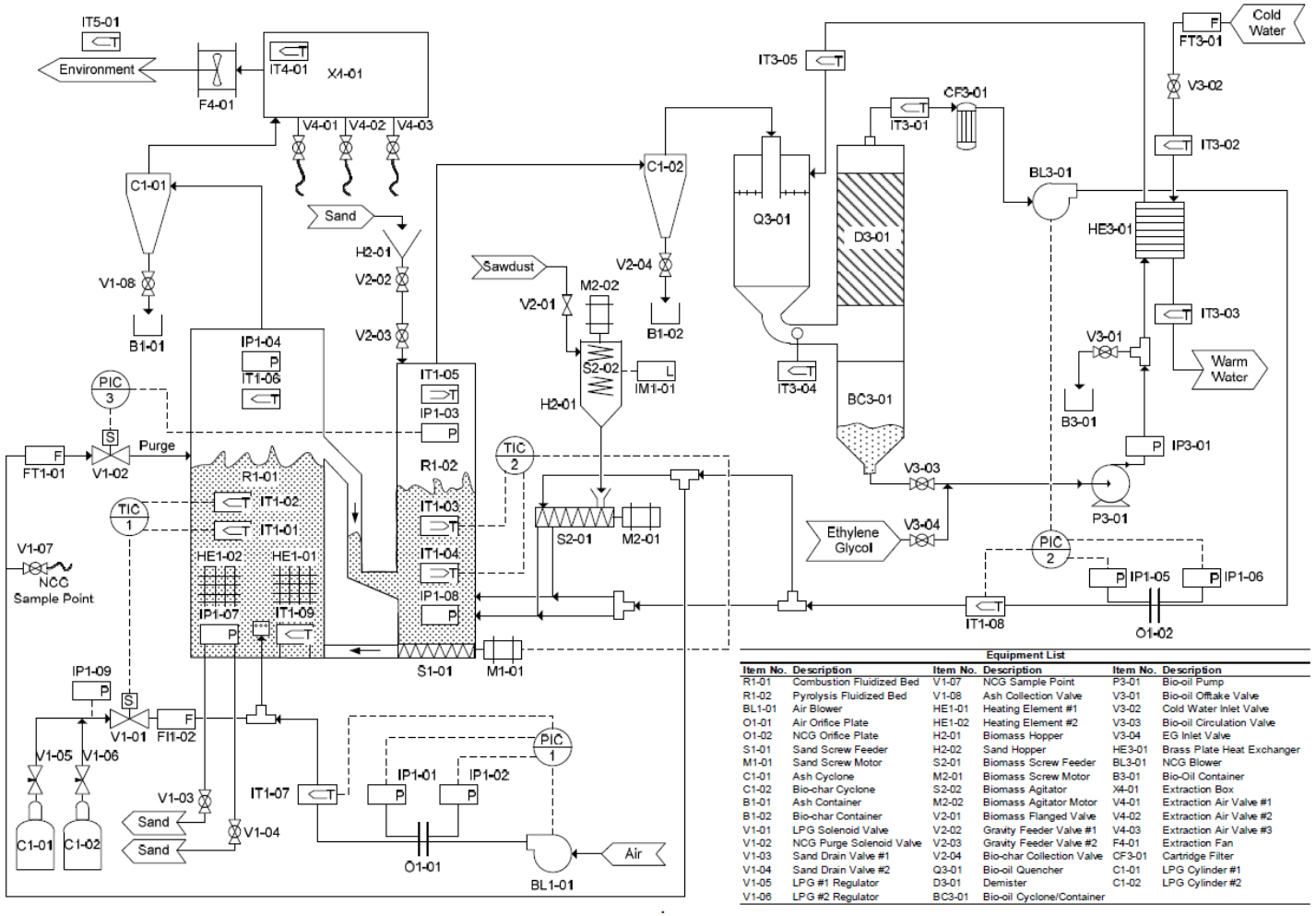

Equipment List

Item No.	Description	Item No.	Description	Item No.	Description
R1-01	Combustion Fluidized Bed	V1-07	NCG Sample Point	P3-01	Bio-oil Pump
R1-02	Pyrolysis Fluidized Bed	V1-08	Ash Collection Valve	V3-01	Bio-oil Offtake Valve
BL1-01	Air Blower	HE1-01	Heating Element #1	V3-02	Cold Water Inlet Valve
O1-01	Air Orifice Plate	HE1-02	Heating Element #2	V3-03	Bio-oil Circulation Valve
O1-02	NCG Orifice Plate	H2-01	Biomass Hopper	V3-04	EG Inlet Valve
S1-01	Sand Screw Feeder	H2-02	Sand Hopper	HE3-01	Brass Plate Heat Exchanger
M1-01	Sand Screw Motor	S2-01	Biomass Screw Feeder	BL3-01	NCG Blower
C1-01	Ash Cyclone	M2-01	Biomass Screw Motor	B3-01	Bio-Oil Container
C1-02	Bio-char Cyclone	S2-02	Biomass Agitator	X4-01	Extraction Box
B1-01	Ash Container	M2-02	Biomass Agitator Motor	V4-01	Extraction Air Valve #1
B1-02	Bio-char Container	V2-01	Biomass Flanged Valve	V4-02	Extraction Air Valve #2
V1-01	LPG Solenoid Valve	V2-02	Gravity Feeder Valve #1	V4-03	Extraction Air Valve #3
V1-02	NCG Purge Solenoid Valve	V2-03	Gravity Feeder Valve #2	F4-01	Extraction Fan
V1-03	Sand Drain Valve #1	V2-04	Bio-char Collection Valve	CF3-01	Cartridge Filter
V1-04	Sand Drain Valve #2	Q3-01	Bio-oil Quencher	C1-01	LPG Cylinder #1
V1-05	LPG #1 Regulator	D3-01	Demister	C1-02	LPG Cylinder #2
V1-06	LPG #2 Regulator	BC3-01	Bio-oil Cyclone/Container		

(Grobler, 2014)

A.2 CRIPS 2 P&ID

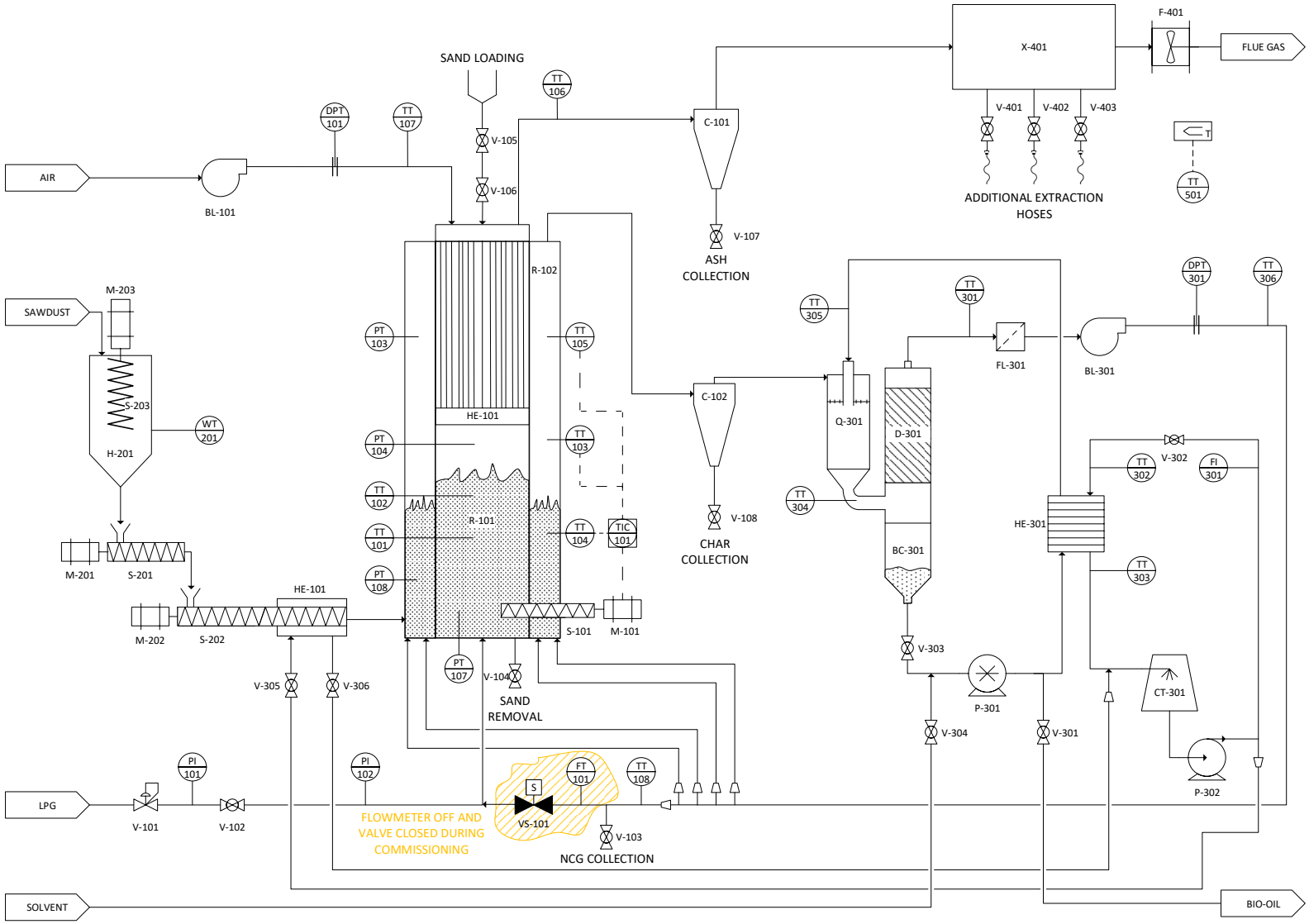

Appendix B Instrumentation Summary

Table 44: Instruments used during the CRIPS 2 unit commissioning for measurement, control, and monitoring.

Type of Measurement	Instrument type	Instrument Details	Purpose
Differential pressure	Differential pressure transmitter	FUJI FCX 'AII' Series	Determine air and NCG flow rate
Pressure	Pressure transducer	WIKA A-10 pressure transducer	Measure CRIPS 2 unit pressures
	Pressure indicator	Standard LPG pressure gauge	Monitor LPG inlet pressure
Temperature	Temperature transmitter	Various K-type thermocouples	Measure CRIPS 2 internal temperatures
	Infrared thermometer	FLIR TG165	Measure CRIPS 2 surface temperatures
Mass	Loadcells	TDC SUB loadcells	Measure biomass hopper weight
	Electronic Scale	Various laboratory scales	Sample and product measuring
Flow rate	Rotameter	Tecfluid water rotameter	Measure cooling water flow rate
Flue gas analysis	Handheld gas analyser	KANE255 combustion gas analyser	Test the flue gas composition
Ambient air analysis	Gas monitor	Crowcon T3	Monitor CO concentration in reactor vicinity

Appendix C Calculations

C.1 Mass balance before combustion air blower adjustments

		MASS BASIS (kg)						MOLAR BASIS (kmol)				
Component	**Property**	**Total Mass (kg)**	**C**	**H**	**O**	**N**	**S**	**C**	**H**	**O**	**N**	**S**
In												
Air		37.9995	0.0000	0.0000	8.8506	29.1489	0.0000	0.0000	0.0000	0.5532	2.0821	0.0000
N2		29.1489	0.0000	0.0000	0.0000	29.1489	0.0000	0.0000	0.0000	0.0000	2.0821	0.0000
O2		8.8506	0.0000	0.0000	8.8506	0.0000	0.0000	0.0000	0.0000	0.5532	0.0000	0.0000
LPG		4.9700	7.9009	0.8883	0.0000	0.0000	0.0000	0.3392	0.8883	0.0000	0.0000	0.0000
Propane		4.4288	4.0710	0.8035	0.0000	0.0000	0.0000	0.3013	0.8035			
Butane		0.2594	3.6157	0.0446	0.0000	0.0000	0.0000	0.0179	0.0446			
Propylene		0.2818	0.2143	0.0402	0.0000	0.0000	0.0000	0.0201	0.0402			
Out												
Flue Gas		39.98929787	1.10152	0.8883	8.85057	29.1489	0	0.09179	0.8883	0.55316	2.08206	0
CO2	10.10%	4.038914052	1.10152	0	2.93739	0	0	0.09179		0.18359		
CO	0.00%	0	0	0	0	0	0	0		0		
H2O	19.99%	7.994659611	0	0.8883	7.10636	0	0		0.8883	0.44415		
N2	72.89%	29.14890568	0	0	0	29.1489	0				2.0821	
O2	-2.98%	-1.193181477	0	0	-1.19318	0	0			-0.0746		

Total In	42.969		
Total Out	39.989		
Total	2.980	Error	6.93558 %

C.2 Mass balance after combustion air blower blower adjustments

		MASS BASIS (kg)							MOLAR BASIS (kmol)				
Component	**Property**	**Total Mass (kg)**	**C**	**H**	**O**	**N**	**S**		**C**	**H**	**O**	**N**	**S**
In													
Air		83.8693	0.0000	0.0000	19.5342	64.3350	0.0000		0.0000	0.0000	1.2209	4.5954	0.0000
N2		64.3350	0.0000	0.0000	0.0000	64.3350	0.0000		0.0000	0.0000	0.0000	4.5954	0.0000
O2		19.5342	0.0000	0.0000	19.5342	0.0000	0.0000		0.0000	0.0000	1.2209	0.0000	0.0000
LPG		4.9700	7.9009	0.8883	0.0000	0.0000	0.0000		0.3392	0.8883	0.0000	0.0000	0.0000
Propane		4.4288	4.0710	0.8035	0.0000	0.0000	0.0000		0.3013	0.8035			
Butane		0.2594	3.6157	0.0446	0.0000	0.0000	0.0000		0.0179	0.0446			
Propylene		0.2818	0.2143	0.0402	0.0000	0.0000	0.0000		0.0201	0.0402			
Out													
Flue Gas		87.96117999	3.20361	0.8883	19.5342	64.335	0		0.26697	0.8883	1.22089	4.59536	0
CO2	10.10%	8.884070716	2.42293	0	6.46114	0	0		0.20191		0.40382		
CO	2.07%	1.821596174	0.78068	0	1.04091	0	0		0.06506		0.06506		
H2O	9.09%	7.994659611	0	0.8883	7.10636	0	0			0.8883	0.44415		
N2	73.14%	64.33502453	0	0	0	64.335	0					4.5954	
O2	5.60%	4.925828958	0	0	4.92583	0	0				0.3079		

Total In	88.839		
Total Out	87.961		
Total	0.878	Error	0.98841 %

C.3 Mass balance using literature bio-oil compositions

		MASS BASIS (kg)						MOLAR BASIS (kmol)				
Component\Parameter	**Property**	**Total Mass (kg)**	**C**	**H**	**O**	**N**	**S**	**C**	**H**	**O**	**N**	**S**
In												
Air		27.2083	0.0000	0.0000	6.3372	20.8711	0.0000	0.0000	0.0000	0.3961	1.4908	0.0000
N2		20.8711	0.0000	0.0000	0.0000	20.8711	0.0000	0.0000	0.0000	0.0000	1.4908	0.0000
O2		6.3372	0.0000	0.0000	6.3372	0.0000	0.0000	0.0000	0.0000	0.3961	0.0000	0.0000
LPG		0.6100	0.9697	0.1090	0.0000	0.0000	0.0000	0.0416	0.1090	0.0000	0.0000	0.0000
Propane		0.5436	0.4997	0.0986	0.0000	0.0000	0.0000	0.0370	0.0986			
Butane		0.0318	0.4438	0.0055	0.0000	0.0000	0.0000	0.0022	0.0055			
Propylene		0.0346	0.0263	0.0049	0.0000	0.0000	0.0000	0.0025	0.0049			
Biomass		4.8970	2.0119	0.2565	2.2099	0.0225	0.0000	0.1677	0.2565	0.1381	0.0016	0.0000
Dry Biomass (Without Ash)		4.5008	2.0119	0.2565	2.2099	0.0225	0.0000	0.1677	0.2565	0.1381	0.0016	0.0000
H2O (moisture)	7.50%	0.3671										
Ash (dry basis)	0.64%	0.028909953										
Out												
Flue Gas		30.88538185	2.250788	0.233514	7.529984	20.8711	0	0.187566	0.233514	0.470624	1.490793	0
CO2	13.75%	4.247811417	1.158494	0	3.089317	0	0	0.096541		0.193082		
CO	8.25%	2.548686971	1.092294	0	1.456393	0	0	0.091025		0.091025		
H2O	6.80%	2.101623371	0	0.233514	1.86811	0	0		0.2335	0.116757		
N2	67.58%	20.87109581	0	0	0	20.8711	0				1.4908	
O2	3.61%	1.116164282	0	0	1.116164	0	0			0.0698		
Flue Ash		0.0428497										
Bio-oil		1.52	0.234666	0.025143	0.159238	0	0	0.0196	0.1309	0.0628	0.0000	0.0000
Pyrolysis oil (17.5 MJ/kg) (D.B.)		0.558728896	0.234666	0.025143	0.159238	0	0	0.0196	0.0251	0.0100	0.0000	0.0000
Reaction water	12.00%	0.067047468		0.00745	0.059598				0.0074	0.0037		
Non-reaction water	58.23%	0.8850808		0.098342	0.786738				0.0983	0.0492		
Biochar		0.0512	0.026056	0.001123	0.011486	0.000585		0.0022	0.0011	0.0007	0.0000	0.0000
Dry Biochar (Without Ash)		0.038164928	0.026056	0.001002	0.010522	0.000585	0	0.0022	0.0010	0.0007	0.0000	0.0000
H2O (moisture)	0.0211774	0.001084283		0.00012	0.000964				0.0001	0.0001		
Ash (dry basis)	0.2384639	0.012209352										

C.4 Mass balance using laboratory determined bio-oil compositions

		MASS BASIS (kg)						MOLAR BASIS (kmol)				
Component\Parameter	**Property**	**Total Mass (kg)**	**C**	**H**	**O**	**N**	**S**	**C**	**H**	**O**	**N**	**S**
In												
Air		27.2083	0.0000	0.0000	6.3372	20.8711	0.0000	0.0000	0.0000	0.3961	1.4908	0.0000
N2		20.8711	0.0000	0.0000	0.0000	20.8711	0.0000	0.0000	0.0000	0.0000	1.4908	0.0000
O2		6.3372	0.0000	0.0000	6.3372	0.0000	0.0000	0.0000	0.0000	0.3961	0.0000	0.0000
LPG		0.6100	0.9697	0.1090	0.0000	0.0000	0.0000	0.0416	0.1090	0.0000	0.0000	0.0000
Propane		0.5436	0.4997	0.0986	0.0000	0.0000	0.0000	0.0370	0.0986			
Butane		0.0318	0.4438	0.0055	0.0000	0.0000	0.0000	0.0022	0.0055			
Propylene		0.0346	0.0263	0.0049	0.0000	0.0000	0.0000	0.0025	0.0049			
Biomass		4.8970	2.0119	0.2565	2.2099	0.0225	0.0000	0.1677	0.2565	0.1381	0.0016	0.0000
Dry Biomass (Without Ash)		4.5008	2.0119	0.2565	2.2099	0.0225	0.0000	0.1677	0.2565	0.1381	0.0016	0.0000
H2O (moisture)	7.50%	0.3671										
Ash (dry basis)	0.64%	0.028909953										
Out												
Flue Gas		30.91172582	2.166712	0.237128	7.636792	20.87109	0	0.180559	0.237128	0.477299	1.490792	0
CO2	13.23%	4.089137681	1.115219	0	2.973918	0	0	0.092935		0.18587		
CO	7.94%	2.453482597	1.051493	0	1.40199	0	0	0.087624		0.087624		
H2O	6.90%	2.134152883	0	0.237128	1.897025	0	0		0.2371	0.118564		
N2	67.52%	20.87109427	0	0	0	20.87109	0				1.4908	
O2	4.41%	1.363858391	0	0	1.363858	0	0			0.0852		
Flue Ash		0.0428497										
Bio-oil		1.52	0.318743	0.036239	0.170112	0.000473	0.010504	0.0266	0.1273	0.0562	0.0000	0.0003
Pyrolysis oil (17.5 MJ/kg) (D.B.)		0.700264	0.318743	0.036239	0.170112	0.000473	0.010504	0.0266	0.0362	0.0106	0.0000	0.0003
Reaction water	0.00%	0		0	0				0.0000	0.0000		
Non-reaction water	53.93%	0.819736		0.091082	0.728654				0.0911	0.0455		
Biochar		0.0512	0.026056	0.001123	0.011486	0.000585		0.0022	0.0011	0.0007	0.0000	0.0000
Dry Biochar (Without Ash)		0.038164928	0.026056	0.001002	0.010522	0.000585	0	0.0022	0.0010	0.0007	0.0000	0.0000
H2O (moisture)	0.0211774	0.001084283		0.00012	0.000964				0.0001	0.0001		
Ash (dry basis)	0.2384639	0.012209352										